UNIVERSIDADE ESTADUAL DE CAMPINAS
Faculdade de Engenharia Química

Daniel Santos Fernandes

Modelagem e simulação do coprocessamento de bio-óleo de pirólise rápida de eucalipto com petróleos brasileiros

Modeling and simulation of eucalyptus fast pyrolysis bio-oil coprocessing with Brazilian crude oils

Campinas
2025

Daniel Santos Fernandes

Modeling and simulation of eucalyptus fast pyrolysis bio-oil coprocessing with Brazilian crude oils

Modelagem e simulação do coprocessamento de bio-óleo de pirólise rápida de eucalipto com petróleos brasileiros

Dissertation presented to the School of Chemical Engineering
of the State University of Campinas in partial fulfillment
of the requirements for the degree of Master in Chemical Engineering.

Dissertação apresentada à Faculdade de Engenharia Química da
Universidade Estadual de Campinas como parte dos requisitos exigidos
para obtenção do título de Mestre em Engenharia Química.

Orientador/Supervisor: Leonardo Vasconcelos Fregolente

ESTE TRABALHO CORRESPONDE À VERSÃO FINAL
DA DISSERTAÇÃO DE MESTRADO DEFENDIDA PELO
ALUNO DANIEL SANTOS FERNANDES, e ORIENTADA PELO
PROF. DR. LEONARDO VASCONCELOS FREGOLENTE.

Campinas
2025

Ficha catalográfica
Universidade Estadual de Campinas (UNICAMP)
Biblioteca da Área de Engenharia e Arquitetura
Rose Meire da Silva - CRB 8/5974

F391m

Fernandes, Daniel Santos, 1995-
Modeling and simulation of eucalyptus fast pyrolysis bio-oil coprocessing with Brazilian crude oils / Daniel Santos Fernandes. – Campinas, SP : [s.n.], 2025.

Orientador: Leonardo Vasconcelos Fregolente.
Dissertação (mestrado) – Universidade Estadual de Campinas (UNICAMP), Faculdade de Engenharia Química.

1. Bio-óleo. 2. Modelagem. 3. Aspen Plus. 4. Eucalipto. 5. Destilação. 6. Coprocessamento. 7. Créditos de carbono. 8. Descarbonização. I. Fregolente, Leonardo Vasconcelos, 1980-. II. Universidade Estadual de Campinas (UNICAMP). Faculdade de Engenharia Química. III. Título.

Informações complementares

Título em outro idioma: Modelagem e simulação do coprocessamento de bio-óleo de pirólise rápida de eucalipto com petróleos brasileiros
Palavras-chave em inglês:
Bio-oil
Modeling
Aspen Plus
Eucalyptus
Distillation
Coprocessing
Carbon credits
Decarbonization
Área de concentração: Engenharia Química
Titulação: Mestre em Engenharia Química
Banca examinadora:
Leonardo Vasconcelos Fregolente [Orientador]
Diogo Ardaillon Simões
Luís Cutz
Wai Nam Chan
Data de defesa: 27-02-2025
Programa de Pós-Graduação: Engenharia Química

Objetivos de Desenvolvimento Sustentável (ODS)
ODS: 7. Energia acessível e limpa
ODS: 12. Consumo e produção responsáveis

Identificação e informações acadêmicas do(a) aluno(a)
- ORCID do autor: https://orcid.org/0000-0002-3737-6154
- Currículo Lattes do autor: https://lattes.cnpq.br/8813883732161032

Prof. Dr. Leonardo Vasconcelos Fregolente

Prof. Dr. Diogo Ardaillon Simões

Prof. Dr. Luis Cutz

Prof. Dr. Wai Nam Chan

A ata de defesa com as respectivas assinaturas dos membros encontra-se no SIGA/Sistema Fluxo de Dissertações/Teses e na Secretaria do Programa da Unidade.

Dedication

I dedicate this work to my parents, my sister and most loved ones, who had been of incomparable support and understanding throughout undergraduate and graduate years. All that is good in me, began with them.

I also dedicate it to my closest friends who, through conversations and leisure moments, helped me stay on course during hard times and provided me with insights in moments of doubt.

To my advisor Leonardo Vasconcelos Fregolente, who was always collaborative in the way he could during all steps of the development of this work, and also patient when unexpected events of my personal life delayed the goals progress.

To all professors from my school of chemical engineering for providing me the challenges which served as path to discovery of the infinite knowledge of engineering.

Lastly, I dedicate this work to the hope of a better, more sustainable and more technological world, ultimate goal to those who have the blessing of understanding.

"(...) For even the very wise cannot see all ends (...) all we have to decide is what to do with the time that is given us.", Gandalf the Grey, J.R.R. Tolkien, The Fellowship of the Ring

Acknowledgements

This work was developed with the support of the Faculty of Chemical Engineering from the State University of Campinas (UNICAMP), Brazil, including professors and personnel, as well as the dependencies. This work had software academic licenses supplied by AspenTech® (Aspen Plus®/Aspen HYSYS®) and Microsoft® (MS Excel®).

No private or public companies financial support was used in the development of this work.

Resumo

Segundo a International Energy Agency (IEA), a demanda global por energia crescerá entre 0,5% até 2035, com rápida taxa de aumento relacionada aos biocombustíveis e energias mais limpas como um todo, e manutenção das demandas por petróleo bruto. Dentro desse cenário de busca por menores emissões, o coprocessamento de matérias-primas de fonte renovável dentro das refinarias, aproveitando a infraestrutura existente, é uma solução tecnológica para transição energética mais limpa estrategicamente valorizada e em contínuo desenvolvimento atualmente. O eucalipto, produzido em grandes volumes no território brasileiro, é uma biomassa promissora para a fabricação de bio-óleo de pirólise rápida (FPBO), produto de poder calorífico e relação H/C próximos a 15 MJ/kg e 1.40, respectivamente, valores superiores a alguns tipos de carvão vegetal e lenha. Apesar de apresentar características desfavoráveis ao coprocessamento em refinarias de petróleo (como densidade, viscosidade e teor de água maiores que o óleo fóssil), o bio-óleo pode ser introduzido como matéria-prima em algumas unidades específicas de refinarias para adicionar conteúdo renovável às frações do petróleo para produzir combustíveis como óleo combustível, diesel, querosene de aviação e gasolina. Essa rota pode favorecer a sustentabilidade da cadeia e o aumento da receita com créditos de descarbonização por meio do programa RenovaBio. Assim, este trabalho teve como objetivo desenvolver um novo método para modelagem matemática de FPBO e sua simulação de coprocessamento com petróleo em uma unidade de destilação, utilizando um modelo integrado dos softwares Visual Basic e Aspen Plus®. Um segundo objetivo deste trabalho foi avaliar os impactos gerados no EBITDA pelo aumento dos gastos com utilidades devido ao coprocessamento e a receita adicional com créditos de carbono. Os resultados preliminares mostram que a modelagem do bio-óleo por meio de *surrogate components* pode ser realizada com um nível satisfatório de precisão, estimando valores de propriedades dentro de um erro médio de 20% em relação aos dados da literatura para densidade e curva de destilação. Em experimentos simulados, o FBPO de eucalipto foi coprocessado a 10 vol% com petróleo do pré-sal brasileiro em unidades de destilação atmosférica e a vácuo, gerando produtos com até 13% em peso de conteúdo renovável, especialmente em faixas de combustíveis usados para transporte. No entanto, a separação de fases em unidades de dessalinização é um grande gargalo que torna essa rota de coprocessamento virtualmente inviável tecnicamente. Os impactos econômicos da refinaria foram avaliados parcialmente, identificando potenciais economias devido ao baixo preço mínimo de venda do bio-óleo e ao aumento da receita com créditos de carbono (CBIOs). No entanto, esses impactos positivos são compensados principalmente pelo aumento nos custos de energia e hidrogênio.

Palavras-chave: Bio-óleo, Modelagem, Aspen Plus®, Eucalipto, Destilação, Coprocessamento, Créditos de Carbono, Descarbonização

Abstract

According to the International Energy Agency (IEA), global energy demand will grow between 0.5% by 2035, with rapid increase rate related to biofuels and cleaner energy as a whole, and maintenance of crude oil demands. Within this scenario of seeking lower emissions, the coprocessing of raw materials of renewable source within the refineries, taking advantage of the existing infrastructure, is a technological solution for cleaner energy transition strategically valued and in continuous development today. The eucalyptus, produced in large volumes in the Brazilian territory, is a promising biomass for the manufacture of fast pyrolysis bio-oil (FPBO), a product of calorific value and H/C ratio close to 15 MJ / kg and 1.40, respectively, values higher than some types of charcoal and firewood. Despite having unfavorable characteristics for co-processing in oil refineries (such as density, viscosity and water content higher than fossil oil), bio-oil can be introduced as feedstock in some specific refinery units to add renewable content to petroleum fractions to produce fuels such as fuel oil, diesel, aviation kerosene and gasoline. This route may favor the sustainability of the chain and the increasing revenue from decarbonization credits through RenovaBio program. Thus, this work aimed at developing a new method for mathematical modeling of FPBO and its coprocessing simulation with crude oil in a distillation unit, using an integrated model of Visual Basic and Aspen Plus® software. A second objective of this work was to assess impacts generated in EBITDA by the increase in utilities spend due to coprocessing and the additional revenue from carbon credits. Preliminary results show that bio-oil modeling through surrogate components can be performed with a satisfactory level of accuracy, estimating property values within an average error of 20% in relation to literature data for density and distillation curve. In simulated experiments, eucalyptus FBPO was coprocessed at 10 vol% with Brazilian pre-salt crude oil in atmospheric and vacuum distillation units, yielding products with up to 13 wt.% renewable content, especially in transport fuels ranges. However, phase separation in desalting units is a major bottleneck that makes this coprocessing route virtually unfeasible technically. Refinery economics impacts were evaluated partially, identifying potential savings due to low minimum selling price of bio-oil and increased revenue from carbon credits (CBIOs), However, these positive impacts are offset mainly by increase in energy and hydrogen costs.

Keywords: Bio-oil, Modeling, Aspen Plus®, Eucalyptus, Distillation, Coprocessing, Carbon Credits, Decarbonization

List of Figures

List of Tables

List of Abbreviations and Symbols

Symbol	Description	UOM
A, B, T0	Parameters of Riazi (2005) correlation for distillation curve prediction	-
AGO	Atmospheric Gasoil	-
a_h, b_h, d_h	Heat capacity-temperature group contribution equation parameters.	-
A_{ji}	Quantity of CHONS in each selected component j, for each chemical group i.	-
API	API Gravity (American Petroleum Institute Gravity)	°API
A_{res}, B_{res}	General weight parameters for composed weighted least-squares method	-
a_{res}, b_{res}	Singular weight parameters for weighted least-squares method	-
ATR	Atmospheric Residue	-
A_{visc}, B_{visc}	Viscosity-Temperature group contribution equation parameters.	
bbl	1 barrel (unit of measure)	0.1589873 m^3
BP_i	Cubic average boiling point (at 1 atm) calculated for chemical group i	°C
BP_m	Boiling Point (at 1 atm) for component m	°C
CAPM	Capital Asset Pricing Model rate	%
CBIO	Brazilian Carbon Credits (1 tonCO_2 equivalent)	USD.tonCO_2^{-1}
CDU	Crude distillation unit	-
CI	Correlation Index	-
$c_{j,i}$	Contribution of selected component j in group i	%
$c_{j,lignin}$	Contribution of selected lignin derived components j in lignin group	%
Cp	Heat capacity estimated by Ruzicka method.	J.mol^{-1}
DSL	Diesel	-
EBITDA	Earnings before interest, taxes, depreciations and amortizations	$
FBP	Final boiling point	°C
FCC	Fluid Catalytic Cracking Unit	-
H/C	Mass ratio of H to C atoms	-
HC	Hydrocracking unit	-
HDT	Hydrotreatment unit	-
HHV	Higher heating value	MJ/kg
HVGO	Heavy Vacuum Gasoil	-
IBP	Initial boiling point	°C
KER	Kerosene	-
LHV	Lower Heating Value	MJ/kg
LPG	Liquefied Petroleum Gas	-
LVGO	Light Vacuum Gasoil	-
MABP	Mass Average Boiling Point	°C
MSE	Mean Squared Error	-
MW	Molecular weight	kg.$kmol^{-1}$
MW_i	Simple average molecular weight calculated for chemical group i	kg.$kmol^{-1}$
MW_m	Molecular weight for component m	-
NAPH	Lighe Naphtha	-
NEEA	Energy-Environmental Efficiency Score for RenovaBio Program	g_{CO2}.MJ^{-1}
O/C	Mass ratio of O to C atoms	-
Q_k, A_w	Combinatorial group contribution and individual group molecular surfaces	m^2.$kmol^{-1}$
R	Universal Gas Constant (R = 8.3145)	m^3.Pa.K^{-1}.mol^{-1}
r_f, r_m	Risk free and market associated expected return rates	%
R_k, V_w	Combinatorial group contribution individual group molecular volumes	m^3.$kmol^{-1}$
SG	Speficic gravity	-
$Structure_{ji}$	Chemical structure for selected component j in chemical group i	-
TAN	Total Acid Number	mg_{KOH}.kg^{-1}
$T_{ASTM\ D\ 86}$	Distilled temperature measure by ASTM D 86 Method	°C
T_{br}, T_r	Reduced boiling and system temperatures	-
T_c, P_c, V_c, Zc	Critical temperature, pressure, volume and compressibility factor.	°C, Pa, m^3
T_{TBP}	Distilled temperature measure by True Boiling Point Method (TBP)	°C
UOP/Watson K	Watson Factor/UOP Factor	-

VABP	Volume Average Boiling Point	°C
V_b	Le Bas molar volume	$m^3.mol^{-1}$
VCR	Vacuum Residue	-
VDU	Vacuum distillation unit	-
$w_{j,lignin}$	Mass fraction of selected lignin derived compounds j in mixture.	-
w_{ji}	Mass fraction of selected bio-oil surrogate compounds j in group i	-
X_i	Cumulative average mass fraction of m components from chemical group i	-
$x_{n,m,i}$	Mass fraction for component m, from chemical group i, obtained from source n	-
X_{si}	Standardized (0 to 1) avg. mass fraction of component m from chemical group i	-
Y_{ci}	Average mass fraction for chemical group i, corrected for heavy components	-
Y_i	Average mass fraction for chemical group i	-
$y_{n,i}$	Estimated mass fraction for chemical group i, obtained from source n	-
α, β	Parameter of Dhulesia (1984) correlation for invert distillation curve prediction	-
$\alpha_{BR,}$ β	Country-associated and sector-associated risk multipliers	%
γ^c, γ^r	Activity coefficient from UNIFAC method (combinatorial and residual)	-
Γ_k, X_k	Residual group contribution activity and fraction in the system	-
θ_i, Φ_i	Volume and Surface combinatorial factor	-
λ	Thermal conductivity estimated by Sato-Riedel correlation.	$J.m^{-1}.s^{-1}$
μ	Dynamic viscosity	Pa.s
μ_i*,μ_i	Single component and mixture dynamic viscosities by Andrade's Equation.	Pa.s
ν	Kinematic viscosity	$m^2.s^{-1}$
ν_k, n_g	Specific groups present in molecule and number of molecules in the system	-
ρ	Density	$kg.m^{-3}$
τ^{bm}	Residual binary interaction factor and interaction parameter bm.	-

Summary

1. Introduction

1.1. The energetic transition

Biofuels production around the globe increased 36% from 108 to 151 Mm^3, between 2011 and 2020 (Torroba, 2021), having Brazil as a key protagonist of that growth, with production jumping from 31.6 to 42.9 Mm^3 (35.6%) (between 2014 and 2023) (ANP, 2024). According to the Energetic Research Company (EPE - Brazil), there is a clear trend of bioenergy global demand growth for the next decade, especially in industrial and transport sectors, including biofuels (EPE, 2020).

After the COVID-19 pandemic between 2020 and 2022, an increase in energetic demand as a whole was expected in the following years, however, a slower rate of energy demand increase was observed, contrasting with cleaner energy demand increase (including biofuels). This was expected, as there are several policies promoting renewable fuels, in particular biomass, being improved and incentivized worldwide. (IEA, 2024)

The main obstacle to adopt renewable sources of energy, however, is Brent/WTI price, as it is cheaper than bio-fuels. Currently being negotiated between 60 to 80 USD/bbl, when crude oil prices rise, biofuels become more competitive, also facilitating higher capex projects investments with environmental goals (INEA, 2016; Bennaceur e Bendob 2017; OPEC, 2020; NREL,2015).

European policies promoting sustainable energy, for example, the Horizon 2020 BECOOL partnership firmed with the Brazilian Ministry of Science, Technology, Innovations and Communications (MCTIC) (EURAXESS, 2017; BECOOL 2020), demonstrate that ESG is generating real strategies, not only financial movements. ESG initiatives are estimated to attract up to 100 trillion USD in investments until 2030 (BNP Paribas, 2019),

This strategic partnership shows the acknowledgement of Brazil's undeniable potential for biofuels, supported by climate and land extension advantages, altogether with concise and direct policies, which is partially not seen in Europe.

These obstacles, coupled with lower electricity prices and the dilemma between land availability for food versus land availability for fuel, lead the continent towards electrification solutions for GHG mitigation in the past years, putting biofuels as a second option (like 1G Ethanol, for example). In spite of that, several blending obligations had been imposed by European biofuels commissions, resulting in higher volumes of biofuels used each year, posing as an interesting market for Brazil and pushing coprocessing as a relevant option. (Danielis *et al*., 2021).

1.2. Biofuels in Brazil and Decarbonization Credits (CBIOs)

In synergy with the complexity of the European scenario, North America's oil dominance and discredit for global warming impacts (Hamilton *et al*., 2018) challenges the approval of higher blending ratios, remaining in the ranges to 5-10% ethanol in gasoline and 1-5% biodiesel in fossil diesel (Wolinetz, 2020; EIA, 2021).

Regarding Asia, the major consumer of energy in the world (mainly due to China and India), the ratios are even lower, in the range of 2-3% for ethanol and <1% for biodiesel. India has already proposed increasing these ratios up to 20% and 5%, respectively, until 2030 (USDA, 2021-1). Conversely, although there are goals of ethanol production set by the Chinese government until the same year, no policies are been stated by the moment to ensure higher blending percentages. (USDA, 2021-2).

In Brazil, the National Petroleum, Natural Gas and Biofuels Agency (ANP) holds a policy for 27% blend in volume of bioethanol in gasoline (minimum of 18% and expandable to up to 35%) and 14% blend in volume of biodiesel in diesel (up to 20% by 2030) (ANP, 2024). This represents about approximately 8 to 10% of Brazilian total energy matrix, and 20 to 25% of the transport fuel matrix.

Fortifying and modernizing the sector, ANP with partnership with the Brazilian Agricultural Research Enterprise (EMBRAPA) has developed the program RenovaBio (RenovaBio 2017, 2018), which focuses on three main strategies: I) Annual carbon intensity reduction targets (CO_2/MJ) for a minimum period of ten years; II) Certification of biofuels by efficiency in reducing GHG emissions; III) Decarbonization Credits (CBIOs) (USDA, 2021-3).

Whether the first two strategies focus on building the commitment to the environmental goals and auditing results, the third incentivizes the whole biofuels production chain. Through this model, producers of biofuels can generate and sell carbon credits, while distributors purchase those credits to meet environmental targets, through the stocks market. (RenovaBio, 2017).

Until now, the program has proven to be a model to be followed, with more than 24 million CBIOs sold at an average price of $5.79, each equivalent to 1 metric ton of CO_2 not emitted (B3, 2021). This additional source of income, allied with the fact that approximately only 0.8% of Brazil's land is used to produce bioethanol (the main biofuel of the country), encourages companies

to develop not only bioethanol and biodiesel, but also other biofuels and bioproducts from different raw materials, adding value and reducing carbon footprint along the whole chain.

1.3. Co-processing and Fast pyrolysis bio-oil

Acknowledging that fossil routes will still be the main source for production of fuels and chemicals for the next 10 to 15 years (Climate Action Tracker, 2021), the most logical strategy to achieve environmental targets is to change steps of production, for example blending biofuels with fossil fuels, as mentioned, or even including renewable raw materials or intermediaries inside the oil refining chain to be part of the final product, which is commonly called coprocessing.

In the case of fossil fuels and chemicals, coprocessing represents mixing a raw material or intermediate product to crude oil or its fractions inside the refinery. Furthermore, this mixture can be submitted to just one or to several transformation steps, for example, coprocessing since the early stages of distillation of the crude oil or the later thermal and reactive modifications phases such as fluid catalytic cracking, hydrotreating, etc. (Cruz *et al*., 2019).

Most of the strategies of coprocessing are still under development (Yáñez, 2020). Three of them are already under use and being improved: I) Blending of vegetable oil into diesel fractions to be hydrotreated or blending of hydrotreated vegetable oil (HVO) directly into the diesel pool; II) Coprocessing hydrothermal liquefaction (HTL) oil with vacuum gasoil in fluid catalytic cracking units (FCC), to recover fractions of gasoline, kerosene, diesel and fuel oil; III) Coprocessing fast pyrolysis bio-oil (FPBO) also with vacuum gasoil in fluid catalytic cracking (Pinho *et al*. 2017). While HVO is similar to C12-C25 from the diesel pool and biodiesel production process is well known, HTL and FPBO are still challenges to engineering.

Hydrothermal liquefaction is a thermochemical process of decomposition hydrocarbon mixture into a less complex and more stable mixture in the presence of a solvent, often water or ethanol. The oil generated is composed mainly of phenols, esters, furans and alcohols in the range of C2-C20, yet to be separated from the solvent used. On advantage, since HTL uses wet solvents, is the only technology economically feasible to process wet biomass for example. However, since the process is carried out at high temperatures and pressures (250 to 450 °C, 100 to 350 bar), there are technological and economical barriers involving its application, with most of the results still on bench scale (Castello, 2018).

Fast pyrolysis is the thermal – and sometimes catalytic – decomposition of organic matter,

usually under absence of oxygen, in a short period of time of 1 to 10 seconds. This process can be fed with lignocellulosic biomass (which is composed by cellulose, hemicellulose and lignin) or recycled hydrocarbons, such as used tires and plastic waste, as demonstrated in China (Uzoejinwa, 2018). Depending on the temperature and pressure used, the mix of products generated differ. Mild temperatures and pressures (300 to 500 °C, 5 to 10 bar) usually generates 5 to 35% syngas (gaseous mixture rich in CO and H2, usually used for energy generation), 10 to 35% biochar (porous charcoal, also usually used for energy generation) and 40-70% bio-oil (Uddin *et al*., 2018).

Fast pyrolysis bio-oil, FPBO, is a highly polar, unstable and mostly water-soluble mixture of hydrocarbons. Each raw material used in the process produces a different composition of bio-oil, also altering its physical and chemical properties (Bridgwater, 2012). When lignocellulosic biomass is used, a more oxygenated, acidic and reactive bio-oil is generated, proven to be feasibly coprocessed in FCC in controlled injected fractions (Pinho *et al*. 2015, 2017), although its stability challenges. (INEA Residue2Heat, 2016; IEA Bioenergy Task 34, 2020).

This trade-off between quality and costs, regarding a technology that does not include solvents or severe conditions and can flexibly use several types of biomasses (Lindfors *et al*. 2015), is the key financial aspect on why FPBO already has been produced in commercial scale by companies like Ensyn, from Canada and BTG Biofuels from Netherlands (Stefanidis *et al.* 2017; ALI et al. 2018; WU et al. 2019). The applications of the bio-oil produced in these companies is focused on feedstock for FCC, co-processing with VGO, and fuel for industrial boilers, blended with similar viscosity fuel oil (Pinho *et al*. 2017), and the raw material used are both hardwood (such as maple or eucalyptus) or softwood (such as cedar or pine) (Ensyn, 2022).

Another route for coprocessing is inserting bio-oil with crude oil, in the early stages of the refinery. This approach has not been explored in detail, due to complex sugars and lignin derivates presence in bio-oil that tend to polymerize during heating, causing structural problems in furnaces and distillation columns (Van Dyk *et al*., 2019). Most studies focus on molecular distillation to create value out of each chemical group in its composition (Wang *et al*., 2015). However, there are no practical or simulated studies, exposing these challenges of coprocessing bio-oil and crude in distillation, leaving an open space to verify its potentials of generating every product of a refinery with a percentage of renewable feedstock.

1.4. Feedstock and Composition

According to Brazilian Tree Institute (IBÁ, 2024), in 2023 there was 10.23 mi ha of planted forestry in Brazil, with 7.83 mi ha accounting for Eucalyptus trees (77%) and 1.92 mi ha Pinus trees (18%) (the rest 5% are distributed among other types of trees of commercial use), representing along with soybean and sugarcane the most important possible renewable feedstocks to biofuels and biochemicals.

However, it is estimated that only 60 to 70% of the whole eucalyptus tree is actually dedicated to pulp & paper and other applications, as 30 to 40% are forestry residues that remain on the extraction area, acting as soil protection and nutrition, but this percentage is more than the 12 to 20% that is actually needed, according to literature (Al-Kaisi; Yin, 2005). The same is seen regarding the other feedstocks cited, with different proportions.

With the climate and land advantages in Brazil, and with feedstock availability, supply chain and operations for bio-oil plant have already been fairly simulated, showing good investments returns. Nevertheless, these simulations often rely on yield and conversion estimates from literature, and elevated risk of investment due to many uncertainties (Iglesias *et al*., 2021).

To reduce this uncertainty, several models of pyrolysis have been built, but most relying on a specific technologies or bench-scale tests, reducing the scope of the scenarios simulated (Onarheim *et al*., 2015). On other hand, bio-oil composition modeling, due to its complexity, is often not detailed enough to simulate downstream precise processes, such as distillation or even FCC co-processing. Several authors have the approach of defining surrogate compositions, key components bio-oil components reported in literature to improve accuracy, but due to scarcity of literature data, the same outcome of generality limitation is reached (Wang *et al*., 2014; Lee *et al*., 2016; Pourzolfaghar *et al*., 2018; Patil *et al*., 2019).

2. Objectives

2.1 Objectives

The main objective of this work is to develop a new method of eucalyptus bio-oil composition modeling, reliable to literature data and flexible to be applied to different feedstocks and to simulate yield of biofuels achieved in the processes investigated.

Having this method developed, the work also aims to simulate the coprocessing of the modelled bio-oil with Brazilian crude oils, in the distillation sections of the refinery, evaluating the impacts on operational and financial parameters, and the quantification of renewable products in

each fraction distilled.

2.2 Main Activities

The sequence of activities performed in this work to achieve the objectives planned are as follows:

- Create a database of reported literature's eucalyptus bio-oil, including mass fractions, chemical groups (acids, phenols, etc.) percentages, chemical structure, molecular weight and boiling point of each component.
- Create a database of possible heavy eucalyptus bio-oil components not present in the literature, including mass fractions, chemical groups percentages, chemical structure, molecular weight and boiling point of each component.
- Build an integrated Microsoft Visual Basic for Applications® and Aspen Plus® algorithm to optimize composition based on commonly reported parameters (H/C, O/C, density, distillation curve).
- Build a database of Brazilian crude oils from literature.
- Adequately insert eucalyptus bio-oil composition in Aspen Plus®, accounting for thermodynamic method corrections (UNIFAC). The same for Brazilian crude oils.
- Build Aspen Plus® atmospheric and vacuum distillation units and simulate coprocessing of bio-oil with Brazilian crude oils.
- Simulate in Microsoft Excel® the minimum selling price of eucalyptus bio-oil.
- Evaluate operational (temperature, pressure, flow, fractions) and financials (utilities and raw materials costs) parameters changes with and without coprocessing, including carbon credits.

2.3 Cronogram

This work is part of the Integrated Education Program (PIF) from the School of Chemical Engineering of the State University of Campinas (FEQ-UNICAMP), in which the candidate starts its graduate studies in the last undergraduate year. The timeline of the project can be seen in Figure 2.1.

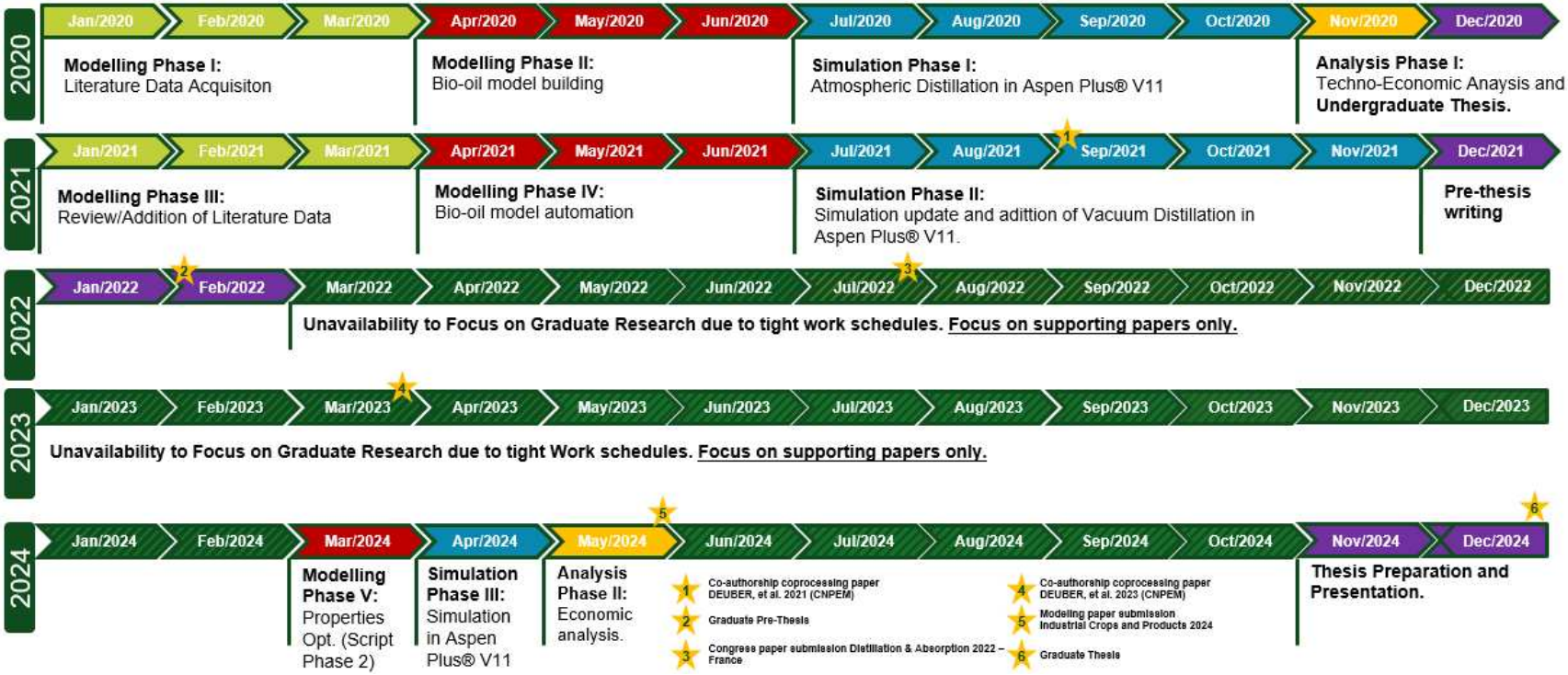

Figure 2.1. Work timeline with main achievements and due dates

3. Literature Review

3.1 Crude Oil Characteristics and Processing

3.1.1 Brazilian Crude Oil Production

Brazil's crude oil production rose from 823 Mbbl in 2014 to 1241 Mbbl in 2023, approximately 51%, while natural gas had its production increased approximately 71% (31.8 to 54.7 MMm^3) in the same period. Still, Brazil has to consume its oil reserves and import oil to supply in-country consumption and exports (ANP, 2024).

The upstream sector growth had leveraged several oil field auctions to 3rd party field explorers. Between 2010 and 2020, Brazil's government won only in bonuses, excluding royalties and taxes, approximately R$ 63.3 billion (R$ 36.2 billion in transfer of rights regime auctions (pre-salt and new fields), R$ 16.9 billion in exceeding reserves – marginal accumulations – shared production, R$ 10 billion in exploration concessions and R$ 200 million in permanent offers – well reactivation and production) (MME, 2021) (FGV, 2014).

Most of the investments made are in pre-salt fields in the Santos basin, although the geological formation extends to Campos and Espirito Santo basins. The ultra-deep-water fields present in this region contain mostly medium oils, with low sulfur and nitrogen contents, strategic parameters for refining (Petrobras, 2021).

The Figure 3.1 shows a map of the oil fields explored in the pre-salt polygon, both by exploration concessions and partition sharing regimes. In 2023, 76% of crude oil produced in Brazil was from Santos basin and 20% from Campos basin, with 100% and 81% of these totals from pre-salt, respectively (ANP, 2024).

According to ANP, approximately 97% of processed material in Brazilian refineries is national oil, where more than 75% is originated in pre-salt fields. These facts add an advantage to the proximity of the polygon from important port regions of the country, attracting internal investments (ABRALOG, 2019; ANP, 2024).

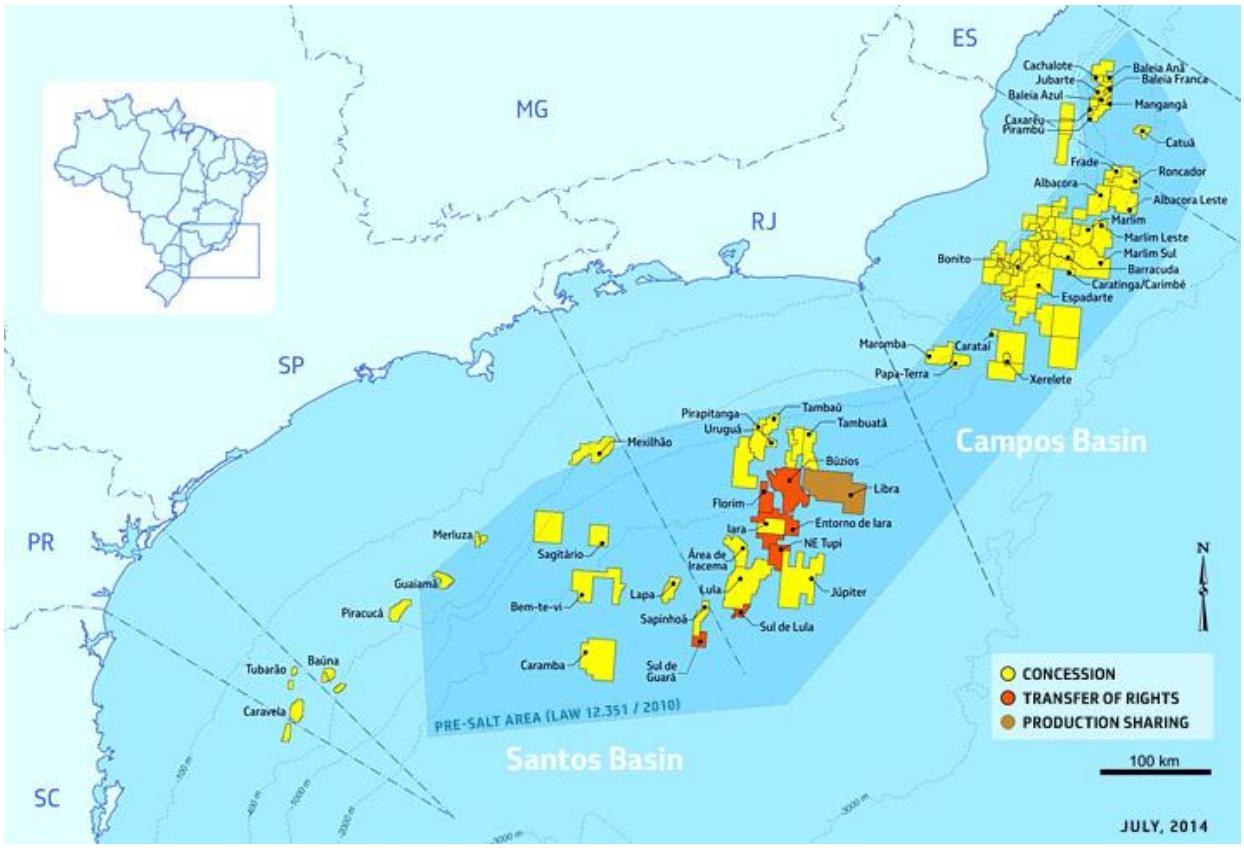

Figure 3.1. Map of explored fields in the pre-salt polygon (Petrobras, 2014)

3.1.2 Crude Oil Characterization and Methods

As seen, pre-salt oil is the role-model Brazilian crude oil: a light-medium density oil, with low sulfur (0.04 to 1.97 wt.%) and nitrogen contents (0.002 to 0.722 wt.%), interesting aspect regarding environmental concerns (Vanini *et al*., 2020; França *et al*., 2021; EPA, 2021).

In terms of refining, lighter oils are more easily refined, since no cracking is needed to produced fuels or light chemicals. In these cases, after distillation of oil, most of the distillate is flown through hydrotreating and then finishing steps of fuel production. Heavy oils, alternatively, have larger fractions that need to undergo the bottom barrel upgrading process, the thermal and catalytic cracking of complex hydrocarbons, increasing complexity and costs (Coker, 2018). Figure 3.2 shows a general design of a refinery.

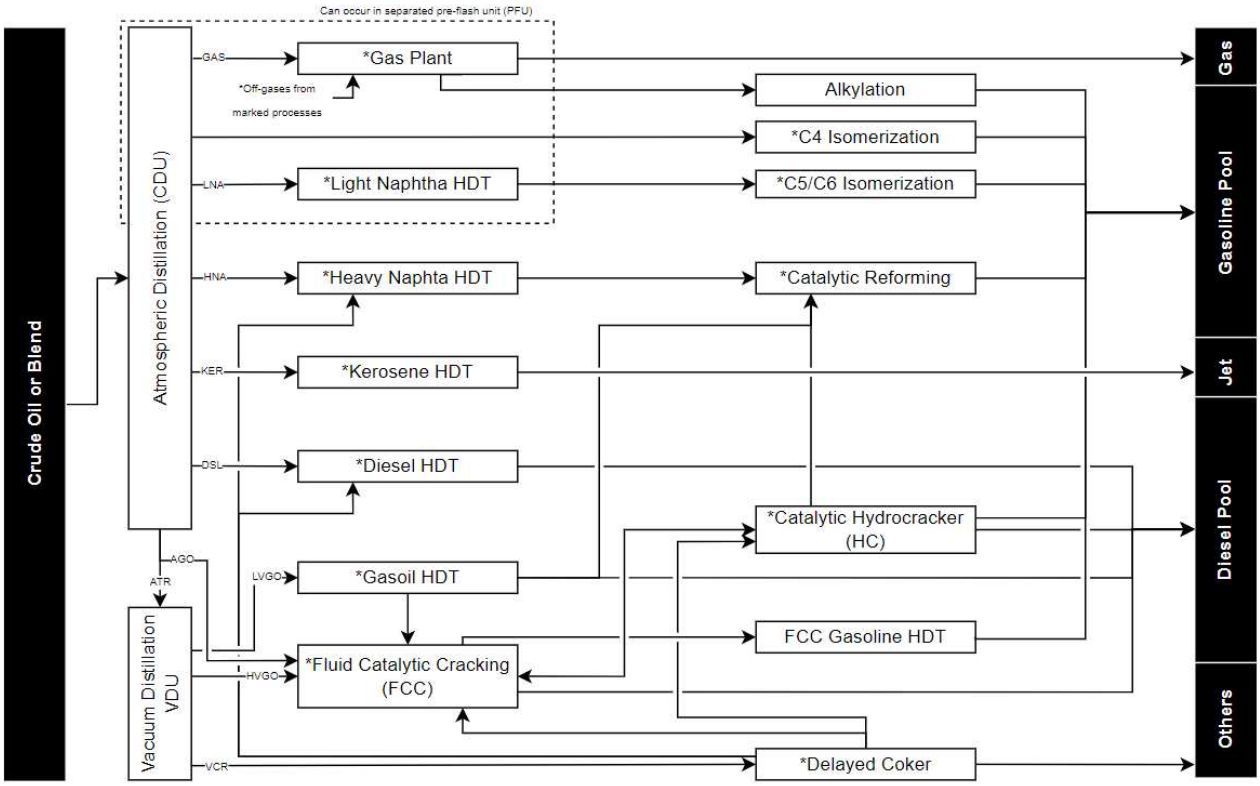

Figure 3.2. Typical refinery block flow diagram (own authorship)

In the refinery procurement process, several oils from different regions are investigated in terms of price and quality, to attend each fuel or chemical production goals. Due to geological aspects that impacts oil bulk properties, oil blend are constantly refined to increase production and efficiency.

In Brazil, pre-salt oil is blended with non-pre-salt oil and many others to meet required standards. Table 3.1 shows details of the Tupi filed crude oil (former Lula field) and many others worldwide, explaining differences distillation temperatures, heteroatoms contents, chemical structure and transport properties, properties explained later in this section.

To price and to evaluate technical quality of fields and oils, market and engineering use oils assays, a set of compiled relevant oil properties for fulfill drilling, transport and refining operations.

Table 3.1. Comparison between Tupi field crude oil (former Lula field) and other worldwide (Aspen HYSYS® Database)

Parameter/Crude Oil	Tupi (Lula) 2011 (BR)	Arabian Light 2012 (SA)	Brent 2014 (UK)	Eagle Ford 2015 (US)	Ural Novorossisk 2014 (RU)	West Hackberry 2015 (US)
IBP (°F) [%vol]	92.57 [5,0]	80,11 [6,42]	61,07 [5,0]	28,45 [6,39]	80,09 [5,25]	68.40 [5,0]
FBP (°F) [%vol]	513.29 [95,0]	550,08 [79,91]	691,98 [95,0]	549,76 [95,78]	550,17 [76,56]	741.57 [95,0]
°API	29.66	34.01	38.08	52.82	32.10	33.33
Sulfur %wt	0.283	1.874	0.404	0.040	1.368	1.545
Nitrogen %wt	0.198	0.077	0.109	0.010	0.233	0.112
TAN (mgKOH/g)	0.299	0.058	0.112	0.028	0.146	-
Viscosity (cSt) 20 °C	9.420	7.659	4.797	1.753	11.347	7.150
Paraffins (%vol)	40 – 50*	34.83	35.94	56.23	22.80	-
Naphthenes (%vol)	-	25.76	35.03	36.59	50.30	2.99
Aromatics (%vol)	27.90	39.41	-	7.17	26.89	39.49
Naphtalenes (%vol)	13.30	6.22	-	-	-	-
Asphaltens (%wt)	0.496	1.274	0.278	0.053	1.278	1.515

*Data not informed in Aspen HYSYS®, acquired from public sources.

Usually, assays contain chemical data, elemental analysis (C, H, O, N, S, metals), water content, wax content and the total acid number (TAN). Many assays also display hydrocarbons characterization (usually the PNA proportions: paraffinic, naphthenic and aromatic) and the light gases dissolved in oil, the light-ends. As for physical data such as API gravity (or °API), specific density, molecular weight, kinematic viscosity, Reid vapor pressure (RVP), boiling points at given volume vaporized (distillation curves) and pour point (Coker, 2018).

Initial and final boiling point (IBP and TBP), the temperatures which 0 and 100% of oil's volume is vaporized, determine the range of products that oil can produce. The cut temperatures, as are commonly referred, are the initial and final boiling points for each petroleum product generated, for example kerosene fraction which has IBP and FBP of approximately 193 and 271 °C, respectively Table 3.2 shows some of the commonly used ranges.

Table 3.2. Cut temperatures commonly used in refineries (adapted from EIA, 2012)

Fraction	IBP (°C)	FBP (°C)
LPG (Liquefied Petroleum Gas)	-	32
Light Naphtha	32	85
Heavy Naphtha	85	193
Kerosene	193	271
Diesel	271	427
Atmospheric Gasoil (AGO)	427	566

Atmospheric Residue (ATR)	566	-

The cuts showed are one of the many variations used worldwide, different in each country mainly due to legislation and certifications of standard quality. Also, these ranges can vary between refineries that produce the same petroleum derivates with different crude oils and process efficiencies. Figure 3.3 shows a distillation curve of crude oil and several petroleum products' curves, showing the approximate percentage in volume of each product retrieved, for example, kerosene fraction between 21% and 47%, an approximate total of 26% in the crude oil.

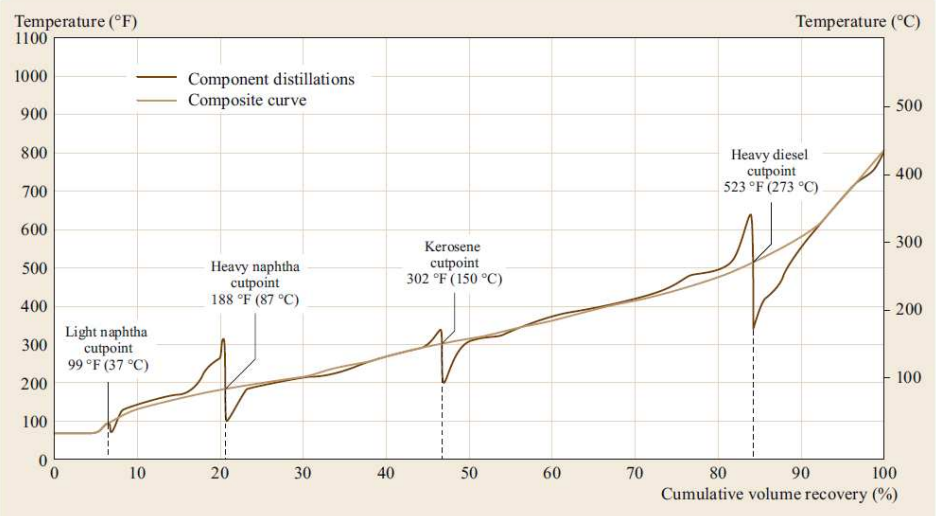

Figure 3.3. Typical Distillation Curve and Temperature Cuts (Hsu; Robinson, 2017)

In Brazil, the National Petroleum, Natural Gas and Biofuels Agency (ANP) regulates the specifications of petroleum products that are sold to foreign companies and to final customer. Some of these products and its parameters are showed in Table 3.3.

Table 3.3. Specification of petroleum products in Brazil (ANP, 2024)

Parameter	LPG	Gasoline C	Kerosene (QAV-1)	Diesel S10
Reid Vapor Pressure (RVP) 37.8°C (kPa)	1430	Máx. 69.0	-	-
Butanes max. (%vol)	-	-	-	-
Pentanes max. (%vol)	2.0	-	-	-
Total Sulfur (ppm wt)	140	50.0	Max. 3000	Max. 10
Density (kg/m3)	-	715.0	771.3 - 836.6	815.0 - 850.0
T10%vol (°C)	-	Min. 65.0	Max. 205.0	180.0
T50%vol (°C)	-	Max. 80.0	-	245.0 - 295.0
T90%vol (°C)	-	190.0	-	-
FBP (°C)	-	215.0	300.0	370.0
MON (Octanes)	-	82.0	-	-
RON (Octanes)	-	93.0	-	-
Benzene (%vol)	-	1.0	-	-
Aromatics (%vol)	-	35.0	25.0	-

Flash Point (°C)	-	-	Min. 38.0	Min. 38.0
Freeze Point (°C)	-	-	Max. - 47.0	
Viscosity (mm^2/s)	-	-	Max. 8.0 (20 °C)	2.0 - 4.5 (40 °C)
Cetane Number	-	-	-	Min. 48
Water (ppm wt)	-	-	-	Max. 200

3.1.2.1 K Factor and Compositional Analysis

As mentioned, each oil has its geological formation characteristics modifying bulk properties important to generate products of interest. Geological differences, the cause of these differences, change molecules' structures into more paraffinic, naphthenic or aromatic aspects, as well as polymers formations. Figure 3.4 shows an example of each type of molecules.

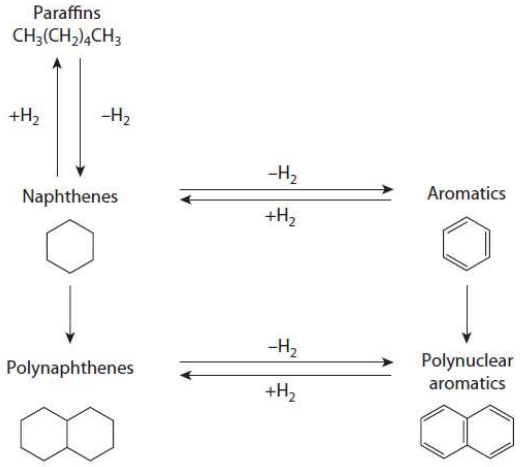

Figure 3.4. Naphthenic, Paraffinic and Aromatic examples of compounds (Speight, 2014)

These molecular characteristics influence directly on processing properties like density, viscosity and boiling point, from both crude oil and its distillates (Figure 3.5). Molecular differences also indicate different contents of heteroatoms, impacting catalytic processes such as hydrotreating and fluid catalytic cracking.

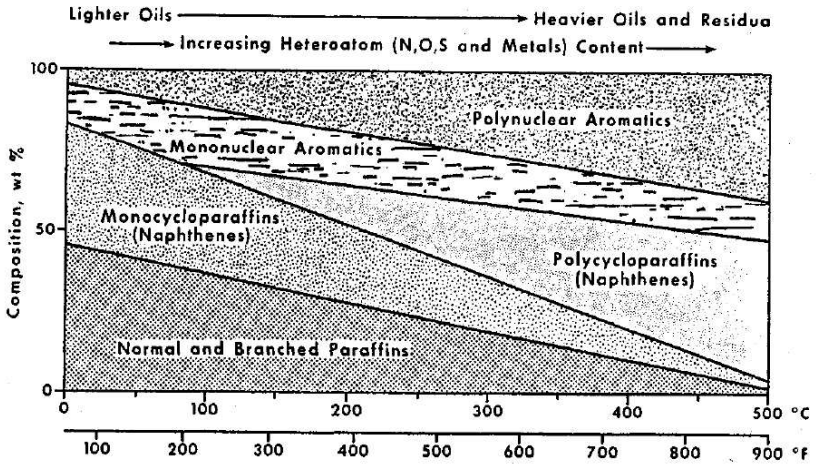

Figure 3.5. Changes in petroleum characteristics due to molecular structure (Speight, 1998)

However, the molecular characteristic analysis is complex and costly, often carried out by GC-MS or GC-FID. When possible, it is substituted by indicators like correlation index (CI) (Equation 3A) and characterization factor K (or Watson factor) (Equation 3B), both relying on mass/volume average boiling point (MABP/VABP) and specific gravity (SG) on inverse proportion.

Highly paraffinic oils usually have $12.5 < K < 13$ and $0 < CI < 15$, naphthenic oils $10.5 < K < 12.5$ and $15 < CI < 50$ and aromatic oils $K < 12.5$ and $CI > 50$. Oils with $K < 10$ and $CI > 70$ are usually heavy oils or bitumen, with higher fractions of poly-structures SPEIGHT (2015).

$$CI = 473.7\,SG - 456.8 + \frac{48640}{MABP[K]} \tag{3A}$$

$$K = \sqrt[3]{\frac{MABP[°R]}{SG}} \tag{3B}$$

Due to the advances in petroleum characterization research, more precise methods of research have been developed to provide more accurate classifications and even quantify chemical structures present. Hosseinifar and Shahverdi (2021) have developed an empirical model that predicts paraffinic, naphthenic and aromatic contents, also through bulk properties like average boiling point, specific density and refractive index, achieving errors below 5.5% while other commonly used predicting models can present errors above 15%.

Besides commonly found PNA (paraffin, naphthene, aromatic) classifications, other classifications can also be reported in reservoirs or crude oils characterization, such as PONA (PNA + olefins), PIONA (PNA + olefin and isoparaffinic), SARA (saturates, aromatics, resins and asphaltenes) and the elemental analysis, which measures total amounts of C, H, O, N, S and metals.

(Riazi, 2005).

The elemental analysis is one of the most important characterizations of crude oil. Hydrotreating crude fractions to produce gasoline, kerosene, diesel and many other products focuses on removing instaurations, reducing aromatic content and remove heteroatoms from the molecules (Treese *et al*., 2015). O, N and S, are converted in H_2O, NH3 and H_2S in the hydrotreating process, but can poison Mo, W, Ni and Co catalysts in the process, as well as other metals like Ni, V, Cd and Pb. Deactivation is dangerous to operational and financial stability of refineries (Bartholomew; Farrauto, 2006).

Elemental analysis is usually carried out in GC-TCD (gas chromatography with thermal conductivity detection) after crude oil is combusted and reduced, generating CO_2 (measuring C – ASTM D3178), CO (measuring O – ASTM E385), H_2O (measuring H – ASTM D1018), N_2 (measuring N – ASTM3179) and SO_2 (measuring S – ASTM D4294). The list of ASTM methods for each element is extensive. Important ratios are calculated from the results of these analysis, H/C and O/C for example, often used to distinguish more energetic fractions than others, due to higher H/C or lower O/C, among other applications. Figure 3.6 shows several types of hydrocarbons compared (Speight, 2014).

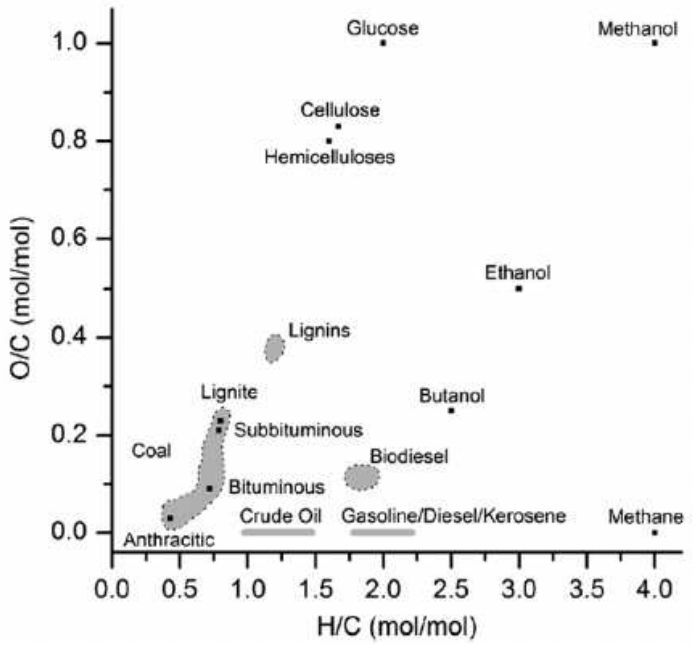

Figure 3.6. Van Krevelen diagram comparing several hydrocarbons by H/C and O/C ratios (reproduced from Rinaldi and Schüth (2009))

As for transition metal traces, various ASTM methods are proposed for each, not having a

single test to differently analyze each metal. However, total metals analysis can be measured by crude ash acid dilution and analysis in atomic absorption spectrometry (AAS) or inductively coupled plasma spectrometry (ICPS) (Speight, 2014). Transition metals are more commonly found in crude oils with higher contents of asphaltenes, in which its higher electronic availability for ligands favors polyaromatics formations (Abdel-Raouf, 2012).

In Brazil's pre-salt oil fields, due to the high presence of brine, uncommon equilibria are formed, impacting drilling, transporting and also refining. Drexler *et al*. (2020) reported that, due to higher alkaline metals such as Na, Ca, Mg, K, Ba and Sr identified in elemental analysis methods, surface tension variations between crude oil and brine are more susceptible to CO_2 presence, affecting extraction operation and, potentially, costs.

3.1.2.2 Water Content and Total Acid Number (TAN)

Another set of important parameters related to oil's characteristics and processability are water content and the total acid number.

Water content usually is measured by ASTM D1744, ASTMD377 and ASTM D4928 (Karl Fischer titration methods), and is an indicator of efficiency in the water-oil separation stages in early-refining. In this settling process, surface-active electrical emulsion breakers are added to crude to provide phase separation, as the presence of water in later stages of the process can cause severe equipment damage. Besides, water is indicated to enhance the mineralization of oil (i.e. degradation of oil) (Speight, 2015). For crude oils, water contents below 0.5% are considered satisfactory, as for petroleum products the ranges are even lower (Fregolente *et al*., 2012; Gonçalves *et al*., 2019; Gatiboni, 2020; Enders, 2019).

Also measured by titration, the Total Acid Number (TAN) accounts the totality of acids in crude oil. Also called neutralization number, it is measured in mg_{KOH}/g_{oil} during the titration process, with a normal range of 0.05 to 6.0 mg_{KOH}/g_{oil}, increasing for heavier crudes due the higher presence of naphthenes (specifically naphthenic acids). More acidic crudes are more corrosive to refinery equipment, demanding blends with lighter crudes or investments in anti-corrosive chemicals and/or equipment.

In Brazil's pre-salt oils, due to the higher content of salts and alkali-metals as mentioned in 3.1.2.1, crude oil TAN measurements can be severely altered, as showed by Fernandes *et al*. (2022), specially for light crudes, potentially causing financial losses, since acidic crudes are

usually negotiated by 80% of non-acidic crude's price.

3.1.2.3 API Gravity, Molecular Weight and Viscosity

Besides chemical characterization properties mentioned, many important physical properties are also measured and used to characterize crude oil. The most used crude parameter listed is the API gravity measured in API degrees (°API). This property derivates from specific density (density of the fluid divided by density of water at the same condition) as expressed in Equation 3C.

$$°API = \frac{141.5}{SG_{15.6\,°C}} - 131.5 \quad (3C)$$

Several ASTM methods were developed for evaluate the density from a variety of petroleum products. ASTM D70 documents the general density measurement method, while ASTM D5002 covers density, °API and specific density analysis methods for crude samples, usually present in oil assays.

Due to its simplicity, °API is also used for oil characterizations, similarly to Watson factor but in terms of density. In this case, 45 < °API < 65 represents petroleum products, 35 < °API < 45 light oils, 20 < °API < 35 medium oils, 10 < °API < 20 heavy oils, °API < 10 extra heavy oil or bitumen. (Riazi, 2005).

As density is temperature-dependent, °API reported correspond only to the referred condition, requiring development of different correlations between density and temperature for different °API ranges. One of these correlations was determined by Alomair *et al*. (2016) for 376 heavy oil fractions. ASTM D1298 is the standard method to develop such correlations.

In Brazil, pre-salt fields like Tupi have medium-light oils, with °API between 27 and 30, with medium-low contents of sulfur, nitrogen and metals, while post-salt fields heavy oils in Campos Basin are reported to have °API between 13 to 17 and high viscosity (Bruhn *et al*., 2017). This superior quality is one of the reasons for high investments in the pre-salt polygon.

API or specific gravity, paired with the mean average boiling point (in Kelvin), can be used to obtain molecular weight (MW) as shown in Equation 3D (Pedersen *et al*., 1989). Molecular weight determination methods are usually costly, such as freeze point depression osmometry or gel permeation chromatography, these correlations were developed to mitigate cost and time delay, as the parameter is often used in other estimations and predictions (Coker, 2018).

$$MW = 42.965\left[e^{(2.097\,10^{-4}T_b - 7.78712SG + 2.08476\,10^{-3}T_bSG)}\right]MABP^{1.26007}SG^{4.98308} \quad (3D)$$

Crude oil impacts directly efficiency and costs also due to viscosity. In assays, kinematic viscosity is often supplied in cSt and sometimes in Saybolt Furol/Universal Seconds (SFS/SUS). The first can be determined by several ASTM methods such as ASTM D445 and ASTM D4486, using glass capillary kinematic viscosimeters. While the second group is determined by a specific method ASTM D88, but correlations for conversion to kinematic viscosity are also documented by ASTM D2161 (Speight 2015).

Kinematic viscosity ν, in cSt or mm^2/s, is not the actual force to flow crude oil through certain distance, that is the dynamic viscosity μ in Pa.s or g/cm.s, related to density ρ as shown in equation 3E.

$$\nu \left[\frac{mm^2}{s}\right] 10^{-4} = \frac{\mu\left[\frac{g}{cm.s}\right]}{\rho\left[\frac{g}{cm^3}\right]} \tag{3E}$$

As stated for density before, dynamic viscosity also is temperature-dependent, requiring specific correlations for different °API ranges. Alomair *et al.* (2016), as commented before, also developed viscosity correlations based on 376 heavy oil fractions.

As for pre-salt oil in Brazil, there is few available literatures on specific characteristics of crude's viscosity after extraction. Elias and Trevisan (2016) analyzed pre-salt's oil from Campos Basin, but do not report any anomaly compared to any sweet light oil already analyzed. Mangili and Ahón (2019), however, identified that pre-salt's oil could be more susceptible to swelling due to high CO_2 pressure inside reservoirs, affecting dramatically precision of well-known correlations for viscosity.

3.1.2.4 Distillation Curve

There are many types of distillation methods to evaluate boiling points. The most common methods are the true boiling point (TBP), the ASTM D 86 and the chromatography simulated distillation methods. All of them retrieve the temperature at which a determined percentage of oil is vaporized (in volume), for example, T50 – temperature at which 50 %vol of oil is vaporized.

ASTM D 86 is the most common method followed in refineries, distilling crude without refluxes. It provides T0, T5, T10, T20, T30, T40, T50, T60, T70, T80, T90, T95 and T100, being T0 and T100 the least accurate, which makes many refiners report only the T5 to T95, or even shorter ranges for heavy crudes.

Although ASTM D 86 is a quick and simple method suitable for day-to-day operations, it

is not precise, which leads oil producers to include true boiling point (TBP) method results in assays. This procedure vaporizes crude oil in a distillation column with 15 to 100 theoretical stages and high reflux rates, registering the true boiling point of fractions collected. In practice, often the same percentage points from ASTM D86 are used, but virtually any number of fractions can be collected. For example, for wide boiling point crudes, the standard points are recommended, on the other hand for petroleum fractions that produce several different products, an analysis with a curve with a larger number of cuts can help improve yields.

There are several correlations between ASTM D 86 and TBP temperatures, for example the Riazi-Daubert method (Equation 3F), where a_{ASTM}, b_{ASTM} and c_{ASTM} are correlated parameters for the conversion showed in Table 3.4. For this conversion, is assumed that T100 is the same on each method and parameter c is set as null (Riazi, 2005). Conversion models between ASTM D86 and other methods such, as simulated distillation or equilibrium curves, are also available, these being necessary the inclusion of specific density for each fraction.

$$T_{TBP,i} = a_{ASTM}\left[T_{ASTM\ D86,i}\right]^{b_{ASTM}} SG^{c_{ASTM}} \tag{3F}$$

Table 3.4. Correlation parameters for ASTM D86 to TBP conversion (Riazi, 2005)

%vol	a_{ASTM}	b_{ASTM}	c_{ASTM}	ASTM D 86 range (°C)
0	0.9177	1.0019	0.0000	20-320
10	0.5564	1.0900	0.0000	35-305
30	0.7617	1.0425	0.0000	50-315
50	0.9013	1.0176	0.0000	55-320
70	0.8821	1.0226	0.0000	65-330
90	0.9552	1.0110	0.0000	75-345
95	0.8177	1.0355	0.0000	75-400

The last and more complex method is the chromatography simulated distillation. In this method, GC-FID (gas chromatography with flame ionization detector) is usually applied, passing vaporized fractions of a sample through a retention column. Lighter components are retained first, while heavy components take more time to vaporized and be capture by the column. The intensity of energy generated by the flame ionization of each compound captured in the column generate different heights' peak signals, which area represent the mass percentage of the compound in the mixture (Riazi, 2005).

Although this method is costly and of complex operation, advances in research focused in detailing petroleum composition has been made. This relationship could improve refineries logistics and operations, for example in chemicals and utilities use regarding the content of a

specific type of compound. Coutinho *et al.* (2022), showed this impact between chromatography analyzed compounds and bulk properties for several samples of pre-salt oil.

When just some of temperature data is available, several methods have been proposed to estimate the remaining points, many software propose equations to fit available data. Riazi (1989) proposed a distribution model showed in Equation 3G, where the three parameters $A_{Predict}$, $B_{Predict}$ and $T0_{Predict}$ are determined by available experimental data through linearization or direct fitting through additional software such as Microsoft Excel® Solver®. This equation can also be used predict density or specific density distributions over distillation curves (Riazi, 1989).

$$\frac{T[K]-T_0}{T_0} = \left[\frac{A}{B}\ln\left(\frac{1}{1-x[\%vol]}\right)\right]^{\frac{1}{B}} \tag{3G}$$

In the case of uncertain measurement of cuts, average boiling point calculation for each fraction is performed using Equation 3H. In the case, either volume average boiling point (VABP) and mass average boiling point (MABP) can be calculated using the gamma Γ(B) parameter. For the complete curve estimation, generalized average temperature is shown in Equation 3I. Both equations 3H and 3I can also be applied to predict density or specific density.

$$\begin{pmatrix} T^*_{avg} = \left(\frac{A}{B}\right)^{\frac{1}{B}}\Gamma\left(1+\frac{1}{B}\right) \\ T_{avg} = T_0\left(1+T^*_{avg}\right) \\ \Gamma\left(1+\frac{1}{B}\right) = 0.992814 - 0.504242B^{-1} + 0.696215B^{-2} - 0.272936B^{3} + 0.088362B^{-4} \end{pmatrix} \tag{3H}$$

$$T_{avg} = \frac{(T_{10}+T_{30}+T_{50}+T_{70}+T_{90})}{5} \tag{3I}$$

It can be seen that equation 3G is a logistic equation, with asymptote on x = 1. Several different types of equations have been investigated to evaluate petroleum properties, most logistic or exponential expressions (Al-Assady, 2009). Nonetheless, all have small but consistent precision limitations regarding T0 and T00.

For engineering development and operations planning, expressions in which the property (temperature) is the dependent variable are not always the best solution. A method proposed for inversion of these equations was first presented by Dhulesia (1984), resulting in volume or mass fractions in terms of the reduced properties (T*) and two parameters α and β (Equation 3J). These inversions give refineries a rough estimate of yield of each cut, which can better lead to efficiency optimizations. Obviously, precise data conversion and fitting are essential to use these equations.

(Fu *et al*. 2018).

$$vol\% = \left(1 - e^{1\left(\frac{T^*}{\alpha}\right)^{\beta}}\right), T^* = \frac{T - IBP_{fraction}}{FBP_{fraction} - IBP_{fraction}} \; in\; °C \; or \; K \tag{3J}$$

3.2 Fast Pyrolysis Bio-oil

3.2.1 Fast Pyrolysis Process and Feedstock

Fast Pyrolysis Bio-Oil is one the three products in fast pyrolysis process. This thermochemical and, sometimes catalytic (Lazaridis *et al*., 2018), decomposition of biomass is carried out in mild-high temperatures (300 – 600 °C), low pressures (1 – 10 bar) and, in most cases, in absence of air. It is a fast process (1 – 5 seconds), with yield of 40 to 70% of bio-oil generated, as well as 5 to 40% of syngas (mainly H_2 and CO) and 10 to 35% biochar (Uddin *et al*., 2018) (Figure 3.7).

Figure 3.7. Fast pyrolysis products: biochar (left, with biomass to its right) (Hamilton, 2007), bio-oil (center) (Iowa State University) and syngas burning flames (right) (Hwang *et al*., 2013)

The process depends highly upon biomass and technology used, as shown by Protásio *et al*. (2020) and Gholizadeh *et al*. (2019). Several pyrolysis reactors have been tested in pilot scale and few in commercial scale. (Uddin *et al*., 2018). Recent study of Tang *et al*. (2021), extensively analyzed literature data to predict pyrolysis products yields given different biomass properties and process properties (Leng *et al*., 2021).

In Brazil, there are four main potential agricultural feedstocks for pyrolysis implementation: I) sugarcane bagasse/trash; II) corn straw/trash; III) soybean straw/trash; IV) eucalyptus residue. These agricultural residues are currently used either for energy generation in boilers (specially sugarcane and corn, due to ethanol production, and eucalyptus, due to the kraft process), or left at extraction site for soil enrichment or cattle feeding. Theoretically, the use of this residue for energy could be lowered with the use of renewable energy (e.g.: wind, solar), increasing the availability

of biomass for fuels.

According to the Energetic Research Company - SIEnergy (EPE-SIEnergia), which measures the urban and agricultural waste with potential to generate energy, between 2011 and 2020, agriculture alone still presented 3.8 Mton of potential biomass energy wasted (SIEnergy - EPE, 2022). This fact was also observed by Araújo *et al*. (2019). Although this value is low compared to total agricultural production, it indicates that there is room for other uses, even not changing the current practices for each type of crop.

On top of the list of the energy waste, cattle pasture residues are the biggest source (81% of total) (i.e.: pasture residual forage), followed by agriculture with 11.5% (includes sugarcane, corn, soybean, etc.), forestry with 4.5% and food/urban waste with 2.5%.

As already mentioned, agricultural wastes are mainly being used in energy generation (steam boilers). As for food/urban waste, management of these residues is costly and too susceptible to composition changes, so the main route for energy generation is incineration, with potential development of biodigestion routes (Dos Santos *et al*., 2019). Cattle pasture residues share additional management challenges, usually tied to large land extensions, which impact on the feasibility to collect it for energy use.

Lastly, in the Brazilian forestry sector, eucalyptus cultures leave up to 30 to 40% of total tree as residues (branches and leaves). This percentage is higher than 12 to 20% reported as satisfactory to this end (Al-Kaisi; Yin, 2005).

Moreover, according to Brazilian Trees Institute (IBÁ, 2024), eucalyptus planted area has grown approx. 43% (5.5 Mha to 7.8Mha) from 2013 to 2023, remaining as 78% of total planted area. With 21 Mton cellulose production, estimating wood density as 500 kg/m^3 and 30 to 50 m^3/ha/year productivity (Rocha *et al*., 2019) and dry basis yield of 55% cellulose/wood (Penín *et al*., 2020), a value of only 30 to 40% of total planted area is used for cellulose (2/3 of sector's revenue).

This value is fairly consistent with chemical analysis of eucalyptus, reporting approximately 40 to 50% of cellulose in wood (Poke; Raymond, 2006), leaving approximately 20 to 30% to hemicellulose and lignin in eucalyptus composition, flexible sources of value generation.

While biochemical routes of valorization are more commonly used for sugarcane and corn (bioethanol production by fermentation), chemical routes of conversion are more suitable for soybean (biodiesel – FAME production) and more specially eucalyptus, for cellulose and lignin

separation (Santos *et al*., 2021) (Braz; Mariano, 2018). In all of these routes, value is generated from conversion of biomass to final product.

However, for the thermochemical route, the route of choice is co-generation of energy in boilers. Although this energy is important for pulp & paper industry (Pereira *et al*., 2018), great amount of energy is lost in the process since is not incorporated in the final product, as it could be through gasification or pyrolysis technologies, also generating energy through power cycles (Jong *et al*., 2015; Solarte-Toro *et al*., 2021).

Iglesias *et al*. (2021) have shown that using eucalyptus residue FPBO production, in São Paulo state in Brazil, is feasible and profitable. Rodrigues (2018) and Pighinelli *et al*. (2014) concluded that eucalyptus and eucalyptus residue are more suitable for pyrolysis compared to sugarcane bagasse, focusing on greater oil yield.

3.2.2 Bio-oil Chemical Characterization and Methods

Eucalyptus, as mentioned, is composed of 40 to 50% cellulose, 20 to 30% hemicellulose and 20 to 30% lignin. Most of cellulose is extracted for selling, while hemicellulose and lignin are usually used for cogeneration or for applications still in development such as the lignin market. (Horst, 2013). Figure 3.8 shows the chemical structure of lignin-cellulosic materials.

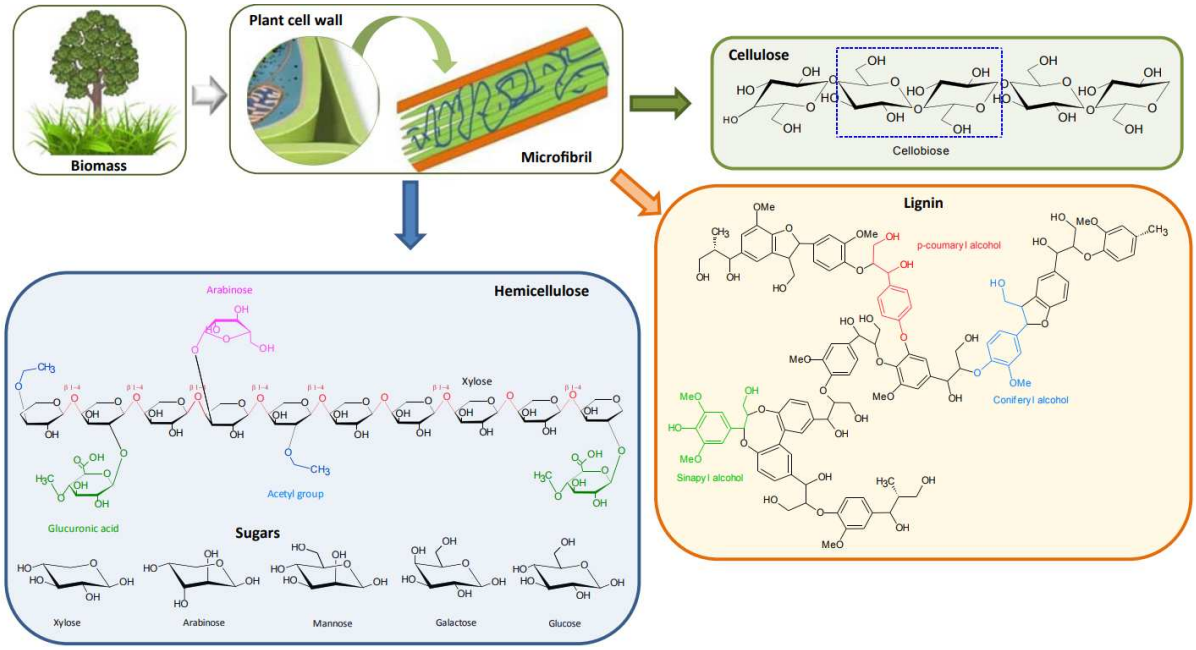

Figure 3.8. Cellulose, Hemicellulose and Lignin chemical structures (Mussatto, 2016)

During fast pyrolysis for bio-oil production, the three chemical structures undergo parallel routes of decomposition involving dehydrogenation, decarboxylation and dehydration, making kinetic modeling extremely complex (Shen *et al*., 2015). Figures 3.9 to 3.12 shows some of these routes usually proposed to model bio-oil production.

As seen in Figure 3.9, the main products generated from cellulose are aldehydes, ketones and alcohols, such as hydroxyacetaldehyde (C3), hydroxyacetone (C3), furfural (C5), furfuryl alcohol (C5) and 5-hydroxymethylfurfural (C5), mainly by dehydration reactions. Besides the compounds with lower carbon numbers, depolymerization of complex sugars can generate levoglucosan (C6) and disaccharides like cellobiose (C12) and highly reactive monosaccharides such as glucopyranoses (C6) and arabinopyranoses (C5) (Shen; Gu, 2009).

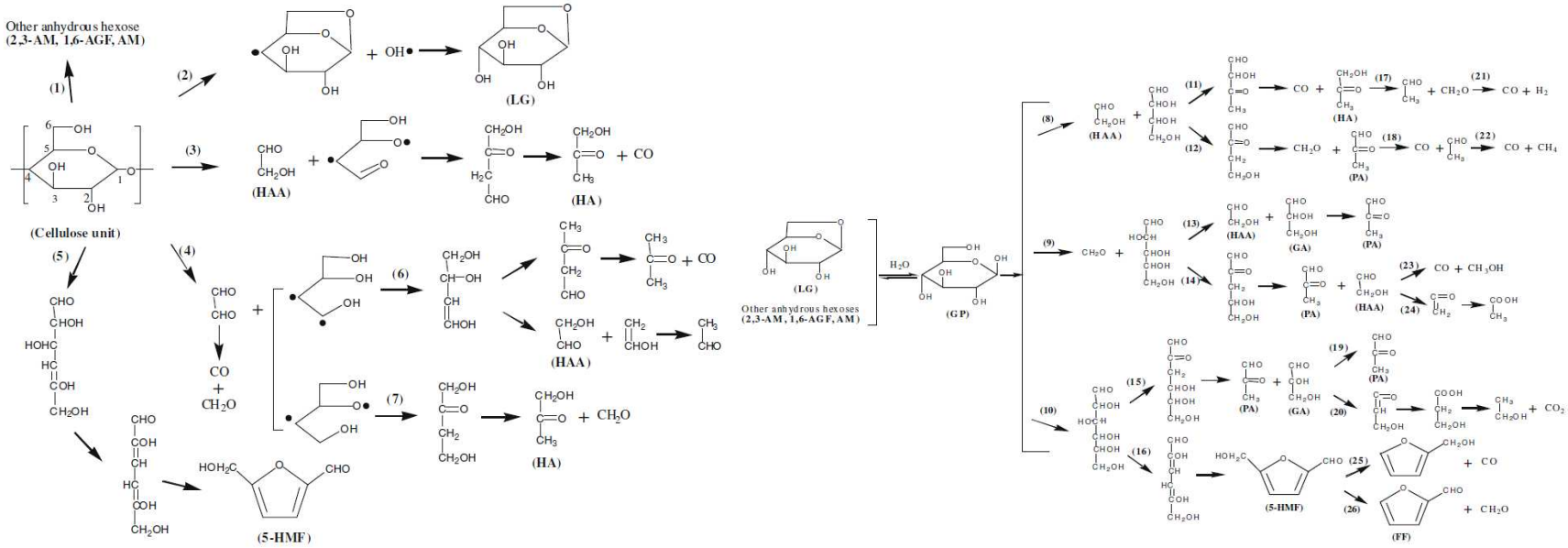

Figure 3.9. Primary (left) and secondary (right) routes of cellulose pyrolysis (Shen; Gu, 2009)

Legend: (1 – isomerization to other anhydrous hexoses; 2 – levoglucosan production (LG) (transglicosylation); 3 & 4->7 – hydroxyacetone production (HA), with and without hydroxyacetaldehyde formation (HAA); 5 - 5-hydroxymetilfurfural production by dehydration (5-HMF); 4->6 – HAA production; 8->11 – HA (17) or gases (21) production from HAA, aldehydes and ketones, due to LG conversion to glucopyranose (GP); 8->12 - pyruvaldehyde (PA), aldehydes (18) or gases (22) production from GP; 9->13 – PA production from glyceraldehyde (GA) and HA, due to GP decomposition; 9->14– light oxygenated compounds production from HA e PA, due GP decomposition: CO and methanol (23) or ketones e acids (24); 10->15 – PA and GA (19) or light oxygenates + gases (20) production from hexoses; 10->16 – 5-HMF (16), furfuryl alcohol (25) and furfural (FF) (26) production from dehydration.

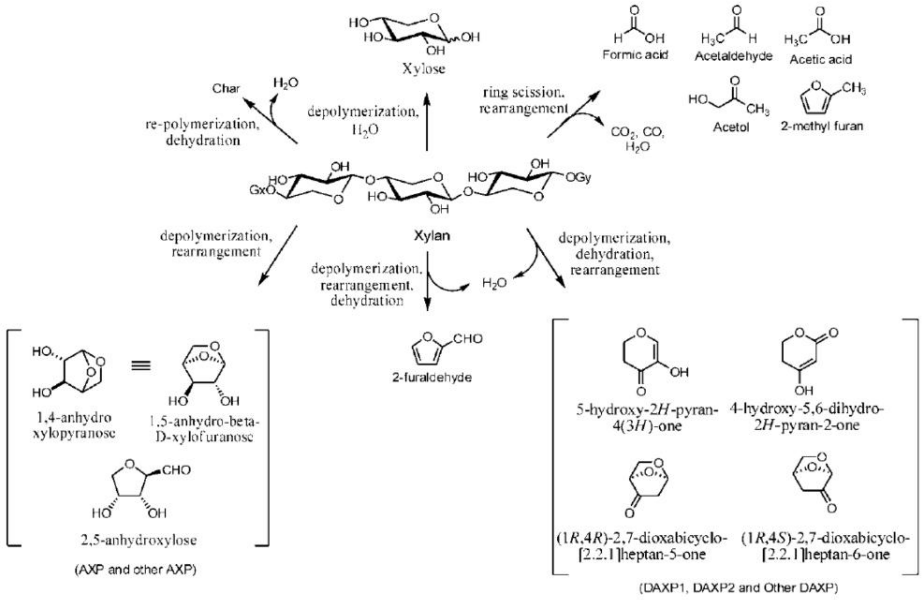

Figure 3.10. Proposed thermodecomposition reactions of xylan, one of hemicellulose's substructures (Patwardhan *et al*., 2011)

Decomposition of hemicellulose, seen in Figures 3.10 and 3.11, is much less know than cellulose, due to complexity of hemicellulose's structure and wider ranges of decomposition (while decomposes to anhydrosugars mostly at 300 °C, hemicellulose starts to decompose at lower temperatures) (Suciu *et al*., 2019).

Nonetheless, several reaction paths are proposed for hemicellulose pyrolysis, showing formation of several lower carbon acids, aldehydes and furans such as formic acid (C1), acetic acid (C2), acetaldehyde (C2), acetol (C2), furaldehydes (C5) and methyl furans (C5). Anhydrosugars are also generated, driven by xylan structure depolymerization and dehydration. Among particular compounds generated by hemicellulose pyrolysis are ketones, specifically forming pyranones by anhydrosugars ring dehydration and also cyclopentanones, by ring opening, dehydration and re-cyclization (Husain *et al*., 2019) (Dussan *et al*., 2017).

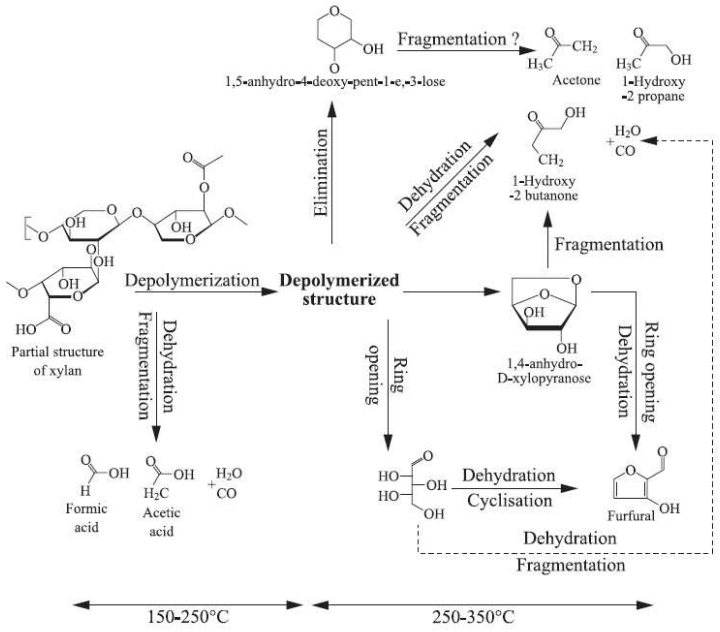

Figure 3.11. Proposed temperature ranges for thermodecomposition of xylan, one of hemicellulose's main sub-structures (Dufour, 2016)

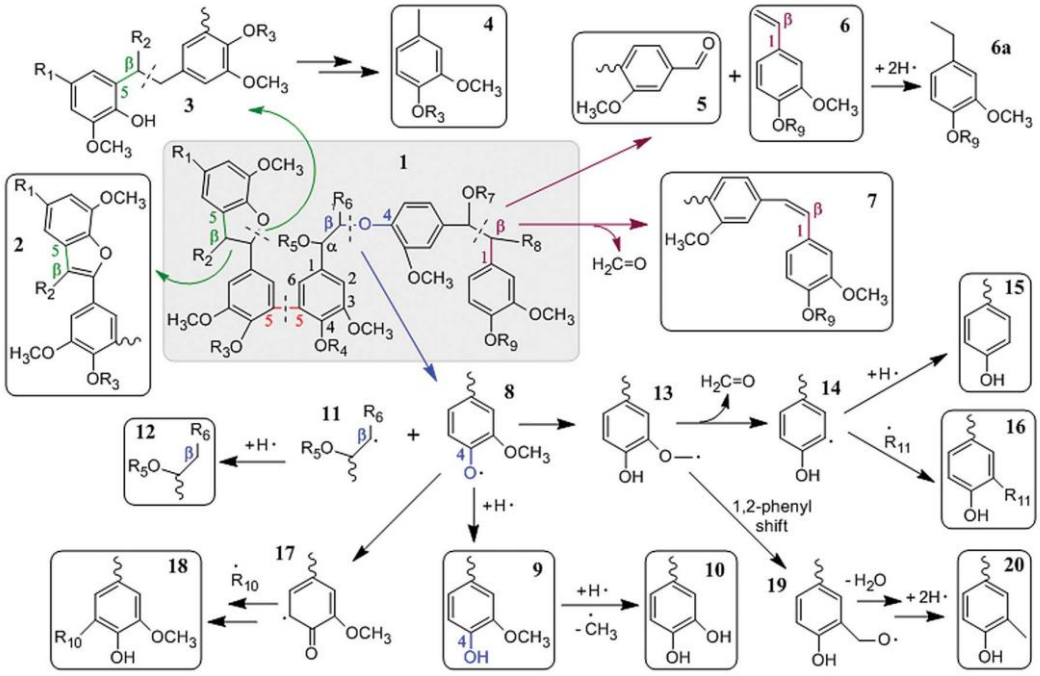

Figure 3.12. Proposed thermodecomposition reactions of lignin during fast pyrolysis (adapted from Kosa *et al*. (2011); explained based on Wang *et al*., (2018))

Legend: 1 – proposed structure of lignin; 2 – relatively stable products from β-5 carbon (2-phenylcoumaran or dehydroabietic acid, for example); 3 – α-C clivage products (pinoresinol for example); 4 – methyl guaiacols from thermal decomposition; 5 – methoxy benzaldehydes from β-1 carbon; 6 – dimethoxy styrenes from β-1 carbon; 6a – reduced vinyl ethyl-guaiacols; 7 – stilbenes from thermal decarboxylation; 8 – phenoxy radicals from β-4 carbon; 9 – guaiacols; 10 – catechols from demethylation; 11, 13, 14, 17, 19 – transient radicals; 12 – oxygenated aliphatics (esters, ethers, etc.); 15 – phenols from decarboxylation; 16, 18 – condensation phenolic compounds; 20 – cresols from demethylation.

Lastly, the most complex biomass structure is lignin. Figure 3.12 shows higher boiling point lignin derivate compounds such as 2-phenylcoumaran and stilbenes (> C10), benzaldehydes (C6 – C10) and phenolics (phenols, guaiacols, catechols, cresols etc.) (C6-C10) the most important chemical group in bio-oil, reaching mass fractions between 40 and 60% of total composition in wood biomass (Pelucchi *et al*., 2019). Most of lignin decomposition reactions occur at high temperatures (> 400 °C), fact which leads to several intermediates still present in final FPBO (HUSAIN et al., 2019) (Kosa *et al*., 2011).

As seen, bio-oil is a complex mixture, with virtually all chemical groups in its composition (Table 3.5). The resource available to model and work with the mixture has been surrogate components: model components most often identified in bio-oil samples analyzed. This approach is proven to be a quick approach for catalyst development research (Wang *et al*., 2014; Lee *et al*., 2016; Pourzolfaghar *et al*., 2018; Patil *et al*., 2019).

Table 3.5. Typical molecules in Bio-oil (Pires *et al*., 2019)

Chemical Group	Usual %wt.
Water	19 – 30
Pyrolytic Lignin	15 – 27
Hybrid Oligomers	11 – 18
C2-C4 light molecules (ketones, acids, aldehydes)	10 – 22
Anhydrosugars	10 – 20
Humins	3 – 7
Mono-Phenols	1 – 5
Mono-Furans	0 – 1

However, most of these models use only one or two surrogate compounds per chemical group, also not taking into account molecular weight nor boiling point in the selection process. This fact limits the method applicability regarding complex engineering simulations, elevating the risk associated with any projections made (Sader *et al*., 2019). Further improvements of this method are presented in this work, after careful review of several literature references (Patel *et al*., 2021; Iglesias *et al*., 2021; Scown *et al*., 2021; Singh *et al*., 2020; Heidari *et al*., 2019; Pimenta *et al*., 2018).

Only in the last decade, research groups began to publish compositional analysis through what is considered the state-of-the-art technology for bio-oil characterization: two-dimensional gas chromatography (GC x GC) (Staš *et al*. 2021; Hertzog *et al*., 2021).

Unlike common gas chromatography, the method uses two chromatographic columns where only targeted chemicals, composed by targeted chemical groups, are transferred from one

column to another during the analytical process. This variation of the method is called heart-cutting GC x GC, and implied the use of two separate detectors, merging outcome results at process conclusion.

Another variation, the comprehensive GC x GC, applies no separation of the sample, injecting it completely from one column to another by flow modulator. The method requires only one detector; however, some publications separate the effluent into more than one detector (Auersvald, 2021). The goal, achieved by both methods, is to provide greater level of details into gaseous chromatographic analysis, as normal GC peak would overlap due to variety of components in bio-oil.

Eucalyptus bio-oil has been analyzed by Brazilian research groups, initially by more simple and quick methods involving only one GC-qMS analysis coupled with principal components analysis (PCA), with low level of composition detailing (Lazzari *et al*., 2018).

Recent research, in the decade 2010 to 2019, provided research community with optimized GC×GC/TOF-MS analysis (time-of-flight mass spectrometry) (Figure 3.13) (Farrapeira *et al*., 2021), acknowledging the presence of several bio-oil compounds and chemical groups, including potential applications as polymeric matrix for biomaterials (Araújo *et al*., 2010) and potential hazards due the presence of polycyclic aromatic hydrocarbons (PAH) (Torri, 2013; Faccini *et al*., 2013).

However, two-dimensional chromatography still needs standards to quantify components in bio-oil. Since FPBO has over 200 different components, advances are still needed for complete compositional models of bio-oil. In the other hand, some studies rely on patterns to bypass the necessity of standards, achieving quantification of most commonly found chemicals. This approach merges both surrogate composition and GC x GC method.

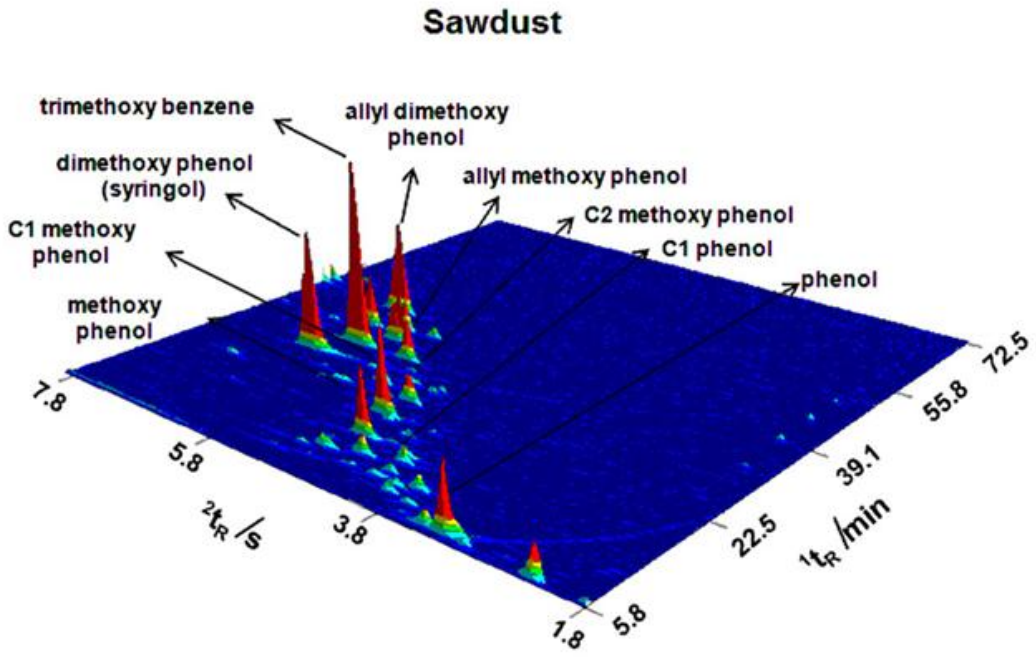

Figure 3.13. Example of GC x GC-TOFMS for eucalyptus sawdust (Faccini *et al*., 2013)

3.2.3 Bio-oil Physical Characterization, Methods and Standards

Since chemical characterization still needs advances, physical characterization cannot proceed on molecular level. Besides, the presence of polar and non-polar groups, coupled with the high oxygen-reactive components presence turns bio-oil into an unstable mixture, that undergo aging and phase separation processes.

Table 3.6 shows a review of challenges, causes and consequences of many bio-oil characteristics. Also, Yang *et al*. (2015) presents a review article containing many aspects surrounding bio-oil aging and the methods to evaluate its stability overtime.

Table 3.6. Characteristics, causes e consequences of Bio-oil (adapted from Bridgwater (2012) and Oasmaa *et al*. (2012))

Characteristic	Causes	Consequences
Acidity (low pH)	Organic acids from biopolymers degradation.	Pipeline and Equipment Corrosion.
Aging	Extension of polymerization and decomposition secondary reactions.	Slow elevation of viscosity and potential phase separation.
Alkaly-Metals Presence	High presence of ash in feedstock and incomplete solids separation.	Catalyst poisoning, solids deposition in combustion, equipment erosion, corrosion and damaging, slag formation (metal oxides mixture).
Biochar presence	Solids incomplete separation.	Bio-oil aging, particles sedimentation, filter plugging, poisoning of catalysts and motors.
Chlorine presence	Contamination or high chlorine in raw material.	Catalyst poisoning.
Dark color	Biopolymers cracking and biochar presence.	Materials colors' change when in contact (e.g. resins).
Raw material contaminants.	Inadequate sourcing.	Particulate material in final product, possible aging catalyst.
Low distillability	Reactive mixture of biomass decomposition products.	Unviability of bio-oil distillation in high percentages. High reactivity below 100 °C and high decomposition above 100° C
High Viscosity	Inherent to composition.	Elevation of equipment head loss, impacting price. Low atomization in spray ejectors.
Low H/C	Low H/C in biomass.	Complex *upgrading*.
Uncompatibility to certain materials	Presence of phenolics and aromatics	Pipelines elbows and sealants damaging.
Low miscibility to hydrocarbons	High presence of oxygenated (elevates polarity).	Difficult mixture to add to fuels or petroleum fractions.
Nitrogen presence	Contamination or high N presence in raw material.	Strong odor, catalyst poisoning, NOx exhaust in combustion.
Oxygen presence	Highly oxigenated biomass.	Low stability and miscibility to hydrocarbons.
Phase separation	High humidity and ash in biomass, incomplete solids separation.	Phase separation (organic and aqueous) or multiple phase separation, inefficient mixture, handling and storing.
Strong odor	Aldehydes or other VOC from hemicellulose decomposition.	Although non-toxic, odor can cause plant location complexities.
Mixed solids presence	Particulate from fluid beds, biomass contamination and biochar.	Equipment sedimentation, erosion, corrosion and plugging.
Variable molecular composition	Fast depolymerization and cooling of pyrolysis products.	Composition susceptible to aging and properties changes, complex product standardization.
Sulfur presence	Contamination or high S presence in raw material.	Intense catalyst poisoning.
Temperature sensitiveness	Incomplete decomposition reactions.	Possible phase separation above 60 °C and irreversible above 100 °C. Irreversible viscosity increase above 60 °C. Possible phase separation above 60° C.
Toxicity	Several low-toxicity compounds present.	Low toxicity to humans and null ecotoxicity.
Variable Viscosity	Bio-oil's composition	High viscosity to elevated temperature, increased by aging.
Water presence	Humidity in raw material, pyrolysis or upgrading reactions product.	Complex effects on viscosity and stability. Reduced heating value, elevated density, elevated pH. Negative effects on catalysts.

Researchers from Finland's Technology Center (VTT) proposed bio-oil standards (Table 3.7), similar to petroleum fractions standards, reducing uncertainty of the fluid's properties. The focus application of their work was to enable commercial use of bio-oil in diesel boilers, for energy generation.

This sequence of standards is the most complete found in literature, later adopted by ASTM International, as the current international standards for bio-oil by ASTM D7544-12 (ASTM International, 2017). Moreover, ASTM in partnership with NREL is developing new standards and methods specific for bio-oil, e.g. carbonyl content determination by potentiometric titration, one

of the chemical groups responsible for bio-oil instability (Black; Ferrell, 2020) (ASTM International, 2020).

Table 3.7. Bio-oil International Standards, according to ASTM D7544 (Oasmaa *et al*., 2015; Oasmaa *et al*., 2012; Oasmaa; Peacocke, 2010)

Property	Grade G	Grade D
Gross Heat of Combustion, min. (MJ/kg)	15	15
Water, max. (wt%)	30	30
Pyrolysis Solids, max. (wt.%)	2,5	0.25
Kinematic Viscosity 40 °C, max. (mm^2/s)	125	125
Density 20 °C (kg/dm^3)	1.1 – 1.3	1.1 – 1.3
Sulfur, max. (wt%)	0.05	0.05
Ash, max. (wt%)	0.25	0.15
pH	Not informed	Not informed
Flash Point, min. (°C)	45	45
Pour Point, max. (°C)	-9	-9

However, the modified petroleum analysis methods, e.g. modified ASTM (international) or Brazilian (national) methods, are the majority of the available procedures, providing only a satisfactory result until further technological advances are achieved (Guedes *et al*., 2010). Table 3.8 shows a set of adapted petroleum standard procedures.

As seen, there is no standard method for distillation of bio-oil. Boucher *et al*., (2000) and then Yuan *et al*. (2021) distilled bio-oil until solid residue formation, showing low distillation temperature ranges and vaporized yields (e.g. < 40% in mass). Wang *et al*. (2015) submitted biocrude to molecular distillation, achieving 67% in mass of total bio-oil, aiming for complex lignin compounds extraction.

Krutof and Hawboldt (2020) presented a hybrid method, empirical and mathematical, to predict bio-oil distillation curves, specifically for higher boiling points. Through ASTM D86 method, mass fraction of bio-oil vaporized was 55% and 72% for atmospheric and vacuum conditions, respectively.

As seen, all of these methods do not provide heavier compounds distillation ranges, even in vacuum conditions. Also, when simulation assisted, the methods showed deviations above 20 °C from experimental data, accompanied by out-of-range properties values as well, exposing the technical difficulty in the process.

Table 3.8. Bio-oil Standard Physical and Chemical Parameters and Modified Standard Petroleum Characterization Methods (adapted from Lehto *et al*., 2014; Baldassin, 2015; Oasmaa *et al*., 2015; Oasmaa *et al*., 2012; Oasmaa; Peacocke, 2010; NREL; ASTM)

Parameter	UOM	Characterization Method
Higher Heating Value (HHV)	MJ/kg	DIN51900, ASTM D240,
Lower Heating Value (LHV)	MJ/kg	DIN51900, ASTM D240, ASTM D5291
Water	wt%	ASTM E203, NBR 15531,
pH	-	ASTM E70
Total Acid Number – TAN	$mg_{KOH}/g_{bio\text{-}oil}$	ASTM D664, NBR 14448, NBR 14543, NBR 14248
Kinematic Viscosity 40 °C	mm^2/s	EN ISO 3104, ASTM D445, NBR 10441, NBR 15983
Density 15 °C	kg/dm^3	EN ISO 12185, ASTM D4052, NBR 7148, NBR 7148
Pour Point	°C	EN ISO 3016, ASTM D97, NBR 11349, NBR 15468
Flash Point	°C	EN ISO 2719, ASTM D93B, NBR 7974, NBR 14598
Sustained Combustibility	-	EN ISO 9038
Micro (MCR) and Conradson Carbon Residue (*CCR*)	wt%	ASTM D4530, ASTM D189, NBR 14318, NBR 15586
Solids	wt%	ASTM D7579, NBR 14647
C	wt% d.b.[a]	ASTM D5291
H	wt% d.b.[a]	ASTM D5291
N	wt% d.b.[a]	ASTM D5291
S	wt% d.b.[a]	EN ISO 20846, ASTM D4294, ASTM D5453, NBR 16371, NBR 14533, NBR 15546
O	wt% d.b.[a]	By difference from the methods above
Ash	wt% d.b.[a]	EN ISO 6245, ASTM D482, NBR 9842
Na, K, Ca, Mg	wt% d.b.[a]	EN ISO 16476, NBR 16480-1, NBR 16480-2
Cl	ppm	NBR 16432

[a]*d.b. = dry basis*

3.3 Simulations and Optimization Methods

3.3.1 Simulation Coprocessing Methods and Designs

Simulations of petroleum fractions always has been more a statistical procedure than a mathematical one. Due to the incapacity of modeling each component present in the fluid, assumptions are made to build the simulation the closest to real possible. In the process, usually average properties and surrogate components (as mentioned in section 3.2.2) are used to estimate each property of the whole mixture, through thermodynamics calculations.

Often used to account for that uncertainty, the strategy of creating pseudocomponents is well known in petroleum research (Riazi, 2005). In the strategy, a set of limited hydrocarbons with well-known boiling point and properties, represent the whole mixture in a certain degree of precision.

Each cut of crude oil distillation curve can be represented by several pseudocomponents, while this number must be reasonable according to which petroleum fraction is being represented. Coker (2018) presented rules of thumb for number of pseudocomponents estimation, depending upon the section of distillation curve considered (Table 3.9), decreasing the number of pseudocomponents at higher temperatures.

Table 3.9. Rule of Thumb to determine number of pseudocomponents (Coker, 2018)

Curve section (IBP – FBP) (°C)	Interval Size (°C)	Example number using boundaries
T < 200	10	21[a]
200 < T < 400	15	14
400 < T < 600	20	11
600 < T	30	8[b]

[a]IBP = 0 °C
[b]FBP = 810 °C

Also, each component is selected based on normal true boiling point, the weight or volume average temperature over the interval defined. For example, a section from 75 °C to 85°C, with equally distributed fraction, normal boiling point is 80 °C, where benzene can be selected as pseudocomponents (Figure 3.14).

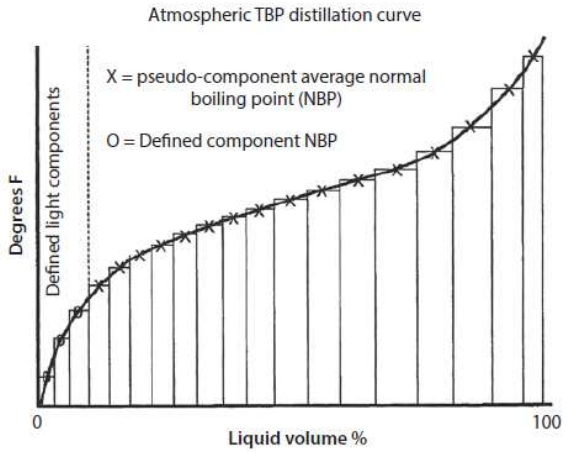

Figure 3.14. Distillation curve segmentation for pseudocomponents selection (Coker, 2018)

The selection can be more judicious, as shown by Riazi (2005), using characterization properties of each segment, obtained by chromatographic analysis. According to the author, the more specific the petroleum fraction more specific pseudocomponents are need for precision, e.g. bitumen with high aromatics and polyaromatics content requires several different aromatic pseudocomponents, with specific characteristics.

Simulation software like Aspen HYSYS®, Aspen Plus®, PRO/II®, UniSim®, ChemCAD®, DWSim®, COCO® and many others, when supplied by distillation curves and density, generate a set of pseudocomponents to calculate other of the fluid's properties (Danilov *et al*., 2021; Haydary, 2018).

The bio-oil, and sometimes biomass (Chen *et al*., 2017), surrogate composition, is a version of the pseudocomponents method where distillation curve is not available. In this case, as already stated, chemical similarities are often the component selection criteria and, for obvious reasons, the modified version provides substantially less precision. However, several authors use surrogate composition for property estimation and modeling, and also to model coprocessing, sometimes with improvements from analytical data (Andrade *et al*., 2018; Fonts *et al*., 2021; Fonseca *et al*., 2019; Krutof; Hamboldt, 2020; Cruz *et al*., 2017).

It is important to note that, even in the rare occasions when bio-oil distillation curve is known or partially known, its direct use as input for pseudocomponents calculation in simulations is not advisable. The reason for this is that commercial simulation software methods to use distillation curves usually consider that a hydrocarbon mixture is being processed, and not a mixture with

complex oxygenated compounds present. These oxygenated compounds play a critical role in the fluid's properties and need to be addressed properly with thermodynamic interactions.

3.3.2 Thermodynamic Properties Models and Estimation

After proper identification of components or pseudocomponents present in the mixture, property estimation is performed starting from available data. For most of petroleum fractions, known hydrocarbons or pseudo-hydrocarbons usually have empirical equilibrium binary interaction and physical properties' correlations parameters, e.g. Aspen HYSYS® databanks.

However, for bio-oil's pseudocomponents, only chemical structures, molecular weights and, in some cases, boiling points are available. Fonts *et al*. (2021) presented an extensive method for estimation of several properties.

For this work, Aspen Plus® was selected for simulation of co-processing, therefore literature review is focused on the software and relevant properties.

To estimate missing binary interaction parameters and properties, Aspen Plus® uses the Property Constant Estimation System (PCES), a set of several equations with basic chemical inputs, e.g. chemical structure and chemical groups/group composition members.

Equations 3K to 3M (alphabetical order) is the UNIFAC method present in Aspen Database.

$$\ln \gamma = \ln \gamma_i^c + \ln \gamma_i^r \tag{3K}$$

$$\ln \gamma_i^c = \ln\left(\frac{\Phi_i}{x_i}\right) + 1 - \frac{\Phi_i}{x_i} - \frac{Z}{2}\left[\ln \frac{\Phi_i}{\theta_i} + 1 - \frac{\Phi_i}{\theta_i}\right] \tag{3L}$$

$$\Phi_i = \frac{x_i r_i}{\sum_j^{nc} x_j r_j} \qquad \theta_i = \frac{x_i \frac{z}{2} q_i}{\sum_j^{nc} x_j \frac{z}{2} q_j}$$

$$r_i = \sum_k^{ng} \nu_{ki} R_k \qquad q_i = \sum_k^{ng} \nu_{ki} Q_k$$

$$R_k = \frac{V_{wk}}{15.17}, \qquad Q_k = \frac{A_{wk}}{2.5 .10^9}$$

$$\ln \gamma_i^r = \sum_k^{ng} \nu_{ki}\left[\ln \Gamma_k - \ln \Gamma_k^i\right] \tag{3M}$$

$$\ln \Gamma_k = Q_k\left(1 - \ln \sum_m^{ng} \theta_m \tau_{mk} - \sum_m^{ng} \frac{\theta_m \tau_{km}}{\sum_n^{ng} \theta_m \tau_{nm}}\right)$$

$$\theta_k = \frac{X_k \frac{z}{2} Q_k}{\sum_m^{ng} X_k \frac{z}{2} Q_k} \quad \tau_{nm} = e^{-\frac{b_{nm}}{T}} \quad X_k = \frac{\sum_j^{nc} \nu_{kj} x_j}{\sum_j^{nc} \sum_j^{ng} \nu_{mj} x_j}$$

In the equations above, γ is the activity coefficient, separated between combinatorial effect (γ^c) (entropic effects due to the shapes of the molecules) and residual effects (γ^r) (interactions between molecules in the mixture).

In the combinatorial part, Φ_i accounts for the molecular volume and θ_i to surface volume. These variables are calculated with number of groups of type k in molecule i (v_{ki}), the total number of groups in their mixture ng. Also, the number of the components in the mixture is defined by nc and orientation of the molecules (z = 10) is an adjusted constant of the method.

The groups volumes R_k and surfaces Q_k are two of the parameters in the UNIFAC method. For the estimation of these Bondi (1964) proposed a method using van der Waals volume and surface areas V_w and A_w of the group of atoms (Figure 3.15). When these parameters are not present in Aspen Plus® Property Databank, retrieved from Poling *et al*. (2001), the software uses the references method for estimation, since it depends solely on atomic radius and molecules structures.

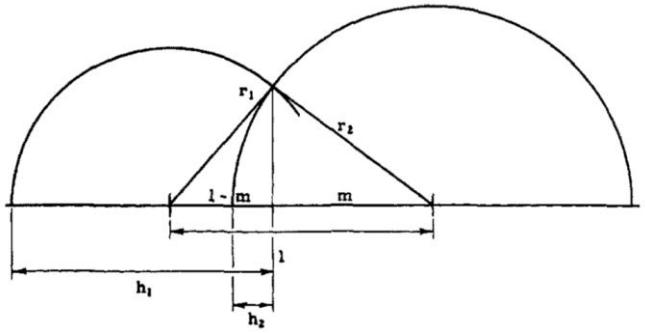

r_1, r_2 = van der Waals radii
l = covalent bond distance
m = auxiliary parameter
h_1, h_2 = height of sphere segments

$$m = \frac{r_2^2 - r_1^2 + l^2}{2l}; \quad h_1 = r_1 + l - m; \quad h_2 = r_2 - m$$

$$V_1^1 = \pi h_1^2 \left(r_1 - \frac{h_1}{3}\right); \quad \Delta V_{2-1} = \pi h_2^2 \left(r_2 - \frac{h_2}{3}\right); \quad V_2 = \frac{4\pi}{3} r_2^3$$

Example:
van der Waals volume of diatomic molecule:

$$V_W = N_A \left[V_1^1 + V_2 - \Delta V_{2-1}\right] \text{ cm}^3/\text{mole}$$

where $N_A = 6.02 \times 10^{23}$ molecules/mole
and r's are given in Angstrom units

Volume of center atom = Total volume of atom
Surface area = $2\pi rh$

Figure 3.15. Method of Calculation of van der Waals Volume and Surface Areas (Bondi, 1964)

In the residual part, Γ_k is the activity of the group at the mixture composition and Γ^i_k in a system only composed of referred molecules i. X_k is the group mole fraction of group k in the mixture. Lastly, the interaction parameter between groups b_{mn} can only be obtained by experimental data.

Aspen Plus® does not estimate this parameter, the user must select one the interactions already reported in the literature, present in Aspen Databank. However, new pairs of groups had been reported in the literature since 1975, as the UNIFAC method has been modified for several different specific applications (DDBST, 2022).

Similarly to UNIFAC, for the estimation of missing molar volumes (and consequently mass densities), Aspen Plus® uses Rackket equation (Mjalli *et al*., 2015), which compressibility parameter Z_c is estimated by Le Bas molar volume additive method V_b (Poling *et al*., 2001) (Equation 3N),

using input chemical structure. Critical temperature and pressure are also estimated using structure through several PCES methods.

$$V_s = \frac{RT_c}{P_c} Z_c^{\left[1+\left(1-\frac{T}{T_c}\right)^{\frac{2}{7}}\right]}, Z_c = \frac{P_c V_c}{RT_c}, V_c = 0.9V_b \quad (3N)$$

For dynamic viscosity, Aspen Plus® uses Andrade's equation (Andrade, 1934-1) (Andrade, 1934-2) (Equations 3O and 3P), which pure component liquid viscosity is calculated by Orrick-Erbar group contribution model, using pure component liquid density (ρ) and two tabulated structure-related group parameters (A_{visc} and B_{visc}) (Poling *et al*., 2001). The binary interaction parameters (k_{ij} and m_{ij}) are null by default, when no experimental data is available.

$$\ln \mu^l = \sum_i x_i \ln \mu_i^{*,l} + \sum_i \sum_j \left(k_{ij} x_i x_j + m_{ij} x_i^2 x_j^2\right), k_{ij} = a_{ij} + \frac{b_{ij}}{T}, m_{ij} = c_{ij} + \frac{d_{ij}}{T} \quad (3O)$$

$$\ln \frac{\mu_i^{*,l}}{\rho MW} = A + \frac{B}{T} \quad (3P)$$

For heat capacity estimation, Aspen Plus® uses Ruzicka group contribution method (Poling *et al*., 2001) (Equation 3Q). The model uses three parameters (a_h, b_h and d_h) estimated from chemical groups quantities (ν) present in the structure of each component and R is the universal gas constant.

$$C_p = R\left[A_h + \frac{B_h T}{100} + D_h \left(\frac{T}{100}\right)^2\right], A_h = \sum_{i=1}^{k} \nu_i a_{h_i}, B_h = \sum_{i=1}^{k} \nu_i b_{h_i}, D_h = \sum_{i=1}^{k} \nu_i d_{h_i} \quad (3Q)$$

Lastly, for thermal conductivity estimation, Aspen Plus® uses the Sato-Riedel correlation (Equation 3R), which uses only critical (T_c) and boiling (T_b) reduced temperatures, and molecular weight.

$$\lambda_i^{*,l} = \frac{1.1053152}{MW_i^{\frac{1}{2}}} \left(\frac{3+20(1-T_{ri})^{\left(\frac{2}{3}\right)}}{3+20(1-T_{bri})^{\left(\frac{2}{3}\right)}}\right), T_{bri} = \frac{T_{bi}}{T_{ci}}, T_{ri} = \frac{T}{T_{ci}} \quad (3R)$$

3.3.3 Optimization algorithms

The equations described in section 3.3.2. are theoretical with empirical constants as inputs. Therefore, each output dependent variable changes with independent variables variation, e.g. composition, temperature and pressure.

To develop these types of correlations, a single objective optimization (SOO) is set, e.g. minimize (experimental property value – theoretical property value)^2, with the single addition of restrictions, as shown in Equation 3S, where f(x) are the ordinary main dependent variables objective functions and x are the independent variables with limited possible boundary values.

$$\begin{gathered} min \\ f_m(x),\ \ m = 1, 2 \dots M \\ subject\ to \\ x_{lower} \leq x_i \leq x_{upper},\ \ i = 1, 2 \dots I \end{gathered} \tag{3S}$$

Regarding experimental or empirical results, the same empirical constants may be applied, however independent variables must be uncovered, often with a certain degree of correlation between each other. One example is the relation between distillation curves and density distribution, both affected by composition variations, as seen in section 2.1.2.

In this cases, multi-objective optimizations (MOO) are required. Equation 3T shows a general form of multi-objective optimization, where f(x) are the ordinary main dependent variables desired, g(x) and h(x) are ordinary secondary dependent variables also affected by the independent variable x, with limited possible boundary values. Microsoft Excel® Solver® is an example of constrained multi-objective optimization algorithm (Frank; Wolfe, 1956).

$$\begin{gathered} min \\ f_m(x),\ \ m = 1, 2 \dots M \\ subject\ to \\ g_j(x) \geq 0,\ \ j = 1, 2 \dots J \\ h_k(x) \geq 0,\ \ k = 1, 2 \dots K \\ x_{lower} \leq x_i \leq x_{upper},\ \ i = 1, 2 \dots I \end{gathered} \tag{3T}$$

Common approach for the objective functions is the least-squares methods (LS), in which the squared difference the squared differences between observed and theoretical properties (sum of residuals R) is minimized. Equation 3U shows the general form of the least-squares method, where y is the vector of properties mentioned calculated in each condition x_i and β is the vector of coefficients to be determined, e.g. temperature, pressure and composition.

$$\min\{R = \sum_{i=1}^{n} r_i^2 = \sum_{i=1}^{n} |y_i - y(x_i, \beta)|^2\} \tag{3U}$$

However, simple least-squares approach does not account for interference between co-dependent variables. For example, a composition x_i that not only affects property $y_i(x_j)$ but also $y_{i+1}(x_j)$, e.g. composition fraction of phenol (x_j) affecting not only T10 (y_i) but also density (y_{i+1}) at that specific fraction.

In these cases, to three options are available: multi-objective optimization methods including (but not limited to) weighted sum least-squares (weights are different for each variable for each property), evolutionary/genetic algorithms or neural networks.

Neural networks have already been used for pyrolysis applications, but the disadvantage is

that correlations are not very well determined, having the model to be trained prior to each execution (Chen *et al*., 2018). Another problem is that is well-known that neural networks depend on a large quantity of data to generate reliable results which, in this application, is almost impossible to have.

Evolutionary, like particle swarm optimization (PSO), and genetic algorithms (GA) are the state-of-the-art in sequential and rule-determined optimization methods, also applied to neural networks bio-oil yield predictions (Ullah *et al*. 2021; Rangaiah; Bonilla-PetriciocleT, 2013). But as mentioned, system rules or operators that decide whether or not proceed with certain sequential solution to the next calculation is time-consuming and extremely complex regarding bio-oil composition.

Lastly, weighted sum multi-objective optimization through least-squares or weighted least-squares is a modification of the common least-squares to account for two impacts, seen in Equation 3V): i) weighted least-squares including the weight of each component residue on total dependent variable residue (a_{res}, b_{res}, c_{res} … etc.); ii) weighted sum including the weight of dependent variable residue on total residue objective function residue (A_{res}, $B_{res,}$ C_{res} … etc.). Equation 3V show the example of the method for a total residual including 2 terms, however, a general approach with several terms can be applied.

$$\min\{R_{Total} = \boldsymbol{A_{res}} a_{res_i} |y_i - y(x_i, \beta)|^2 + \boldsymbol{B_{res}} b_{res_i} |z_i - z(x_i, \gamma)|^2\} \quad (3V)$$

The disadvantage of this method, although its simplicity, is the challenge of tuning the weights assigned to each component in the mixture. Since literature data is scarce in the case of this work, this method was not prioritized and traditional least-squares method was used.

3.4 Biofuels Certification and Carbon Credits

3.4.1 Biofuels Certification Policy

Notorious rise in consumption of petrochemicals and fuels, coupled with higher demands for sustainable raw materials, creates a growth scenario for biofuels and green chemicals. (Bloomberg, 2019; 2020). In Brazil, between 2014 and 2023, production of biofuels increased: bioethanol 28.2 to 35.4 Mm^3 (+25.4%) and biodiesel 3.4 to 7.5 Mm^3 (+119.9%) (ANP, 2024).

Coupled with this environment, the ESG (Environment, Social and Governance) trend is focused on bioeconomy development through biofuels, biochemicals, and CO_2 capturing/mitigation technologies. Carbon Credits are one of CO_2 mitigation strategies that showed important progress, particularly in Brazil, with CBIO, which is a carbon currency created specifically for producers and

users of biofuels.

The RenovaBio program (responsible for CBIO) aims for annual carbon intensity reduction targets, also generating extra revenue source for the companies associated (RenovaBio, 2018; ANP, 2024) (Figure 3.16).

To create reducers, the program provides the legal and technical basis of biofuels certification, for producers to benefit from carbon credits market negotiation on sell-side. To validate the targets, the program applies mitigation targets to voluntary distributors, also benefited from the negotiation on buy-side (Guimarães, 2021).

The RenovaCalc calculates a value of emissions to each production process analyzed, evaluating the CO_2 or CO_{2eq} generated on each stage of the process. It takes into account the yield of renewables, raw materials amounts and sources, inbound and outbound freight distances, and also some of the raw materials and biofuels' properties.

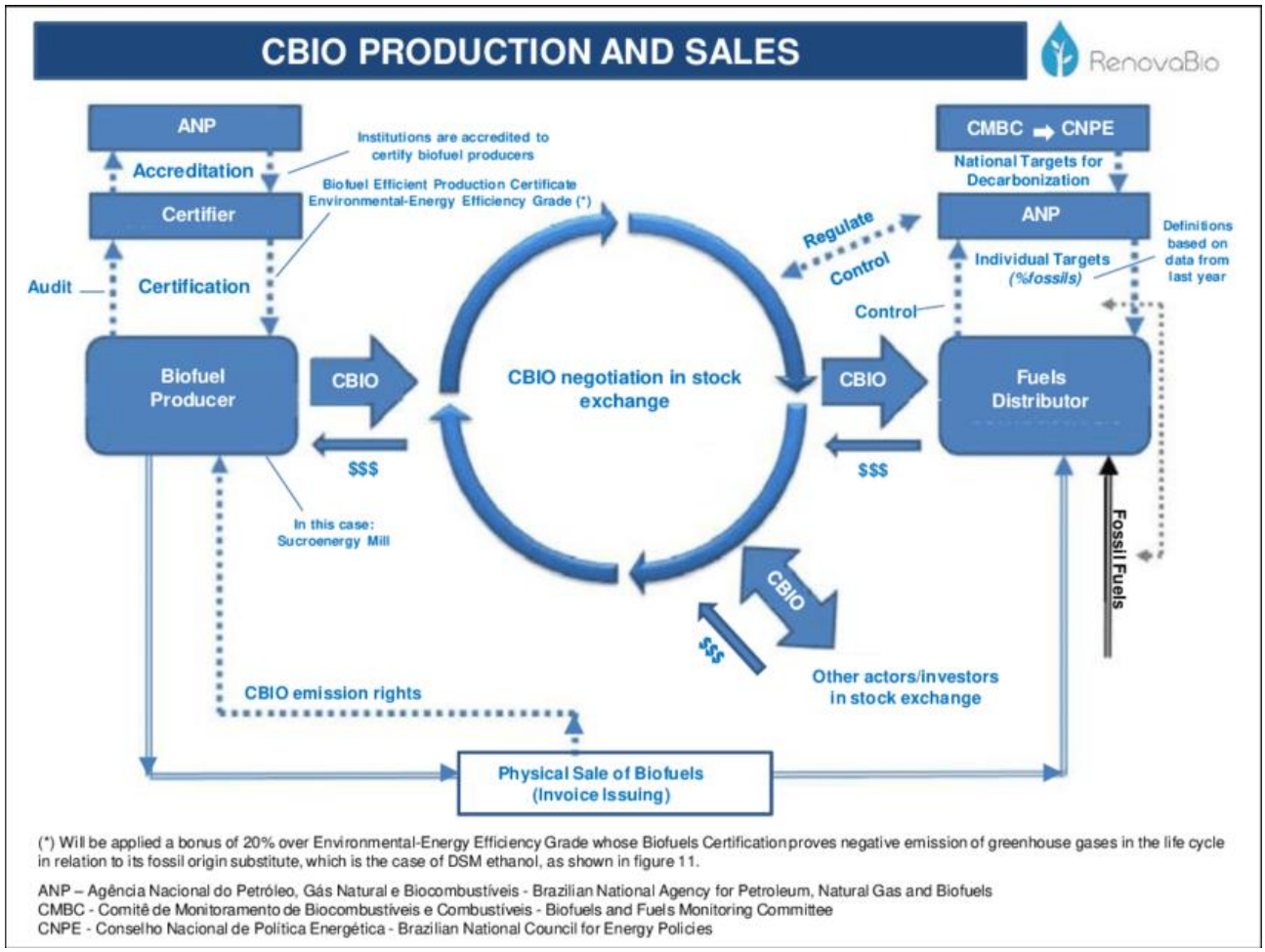

Figure 3.16. Flowchart of RenovaBio program mechanism through CBIOs (Olivério *et al*., 2019)

The result of the calculation is the gCO_{2eq}/MJ emitted by the production of the alternative fuel divided by its lower heating value, which is then compared to the value of the main substituent fossil fuel, to determine the certification score labeled Energy-Environmental Efficiency Score (NEEA, in Portuguese) (Equation 3W).

$$NEEA = \left(\frac{gCO_{2eq}}{MJ}\right)_{Fossil} - \left(\frac{gCO_{2eq}}{MJ}\right)_{Renewable} \quad (3W)$$

This score is initially estimated by the own producer of biofuels, supported by model spreadsheets supplied by ANP. Currently, there are models for biogas, ethanol 1G/1G2G/2G from sugarcane, ethanol 1G from corn, ethanol 1G from sugarcane/corn, biodiesel and HVO. However, the certification is made by RenovaBio agency, audited by 3rd party companies.

Lastly, to effectively generate an extra revenue source, the score is applied to the volume of biofuels sold, with standard lower heating value (MJ/kg) and density (kg/m^3) (Equation 3X) to calculate $tonCO_2$ = 1 CBIO mitigated, available to be sold (by the producers) and bought (by the distributors) in the stocks market (Salina *et al*., 2019).

$$Revenue_{CBIO} = Price\left(\frac{\$}{ton_{CO_2}}\right) CBIO\left(ton_{CO_2}\right) = Price\left(\frac{\$}{ton_{CO_2}}\right) \frac{NEEA\left(\frac{gCO_{2eq}}{MJ}\right) LHV\left(\frac{MJ}{kg}\right) \rho\left(\frac{kg}{m^3}\right) Volume(m^3)}{10^6} \quad (3X)$$

Negotiation prices for CBIO variated between 9 to 10 US$ in 2020 and 6 – 7 US$ in 2021, due to foreign exchange complications. However, due to international pressures on climate change mitigation measures, CBIO achieved 11 US$ in 2022 and its forecast is to increase in quantity and value. (Castro, 2020).

There are two main types of carbon pricing: implicit and explicit. Implicit pricing represents regulatory impositions of technological and governance advances to reduce emissions. Higher taxes over fossil fuels are an example of this method, which is not as effective as the explicit pricing, due to its lower legal and technological flexibility.

The explicit method, however, states clear goals and taxations, but with flexibility on how companies would achieve targets, being often rewarded with opportunities in the market with the action taken. There are two main types of explicit pricing: carbon taxation and the emission trading scheme (ETS) (EPE, 2020).

In the carbon taxation method, a regulatory agency applies an emission fee per a certain amount of GHG liberated in units of, for example, US$ per $tonCO_2e$. This strategy encourages companies to achieve technological improvements with clear definition of taxes, not targeting

specific products or industries. Although the method has political obstacles related to tax creation and the efficiency on the application of the fee paid, there are 35 countries already using this scheme, including Canada, France and Germany (The World Bank, 2022; EPE, 2020).

In the emission trading schemes (ETS), a more modern approach, a structured and certified carbon market is established, with regulators, buyers and sellers. This type of carbon pricing provides opportunities for companies to develop new sources revenue generation and are used in 30 regions, including China, most of European countries and some regions of the US. The two main type of structures are the baseline-and-credit and the cap-and-trade.

In the baseline-and-credit scheme, a regulator proposes a rate of descent for GHG emissions in a determined timeframe (baseline). Companies that achieve even lower emissions than the baseline proposed, are rewarded with carbon credits to be sold to the market, especially to other companies that struggle to meet the targets. In the cap-and-trade scheme, a regulator fixes a maximum level of emissions (cap) and auction or distribute emissions permits to trespass that level. These permits are negotiated by companies in the regulated market.

The main obstacles for ETS adoption are regarding market volatility and technological cost predictability. However, although carbon credits market is volatile, containment methods, for example hedge funds, can be applied, the same way as commodities trading. Also, cost uncertainty regarding technological investment is partially mitigated by distribution of carbon credits free of charge (Guimarães, 2021).

The RenovaBio program, as described, is a hybrid ETS method from the strategies above, where the carbon credits are produced by biofuels industries and sold in the open market (sell-side). The distributors that have emission baselines to be followed by these credits (buy-side), also benefiting from market dynamic.

Still, RenovaBio program is in development, comprising the biofuels sector, specifically the distributors and direct bioethanol (1G and 2G), biodiesel and biogas producers. Another clean energy generation methods are still not contemplated, due to complexity of certification and technologies to be yet improved, as is the case of coprocessing renewable feedstocks in refineries, including bio-oil and others (EPE, 2020).

However, after pressures from Petrobras (Brazilian state oil company), a new law has been approved in 2021, to acknowledge HVO diesel and kerosene as advanced renewable fuels, opening possibilities of improvements of RenovaBio (Brazil's Chamber of Deputies, 2021).

3.4.2 Biofuels integration into Refineries

With the recognition of only specific coprocessed fuels as advanced biofuels, the effective design of operations and supply chain to achieve maximum CO_2 mitigation in these products is important. Routes of direct integration with existing refineries are extensively assessed in literature (Michailos; Bridgwater, 2019; Yáñez *et al*., 2020; Talmadge *et al*. 2020; Young, 2019; Wu *et al*., 2019; Wu *et al*., 2020). The main opportunities are identified in Figure 3.17; however, each has its own challenges regarding compatibility of petroleum fractions and biocrudes.

Atmospheric and vacuum distillation insertion poses challenges regarding the presence of oxygenated, complex, unstable chemical structures present in many types of bio-oils, with the increased risk of deploying into several streams of the refining unit. Also, some non-volatile molecules such as sugars and lignin derivates can be unsuitable for distillation (Van Dyk *et al*., 2019).

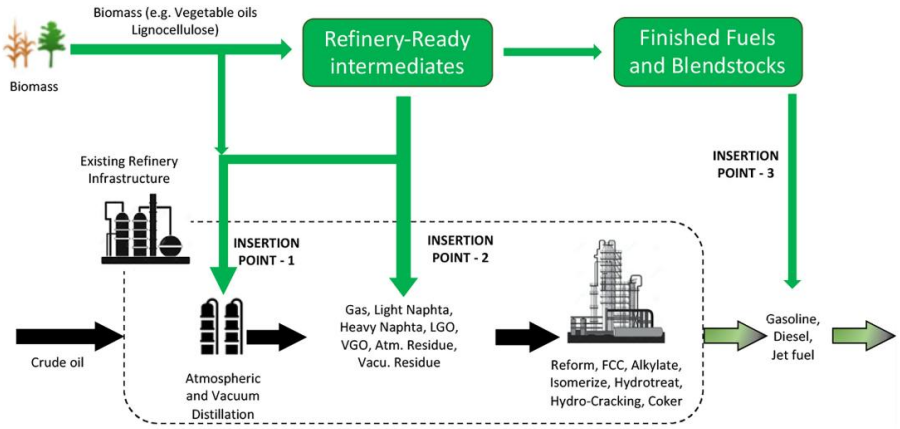

Figure 3.17. Potential insertion points for biomass coprocessing in oil refineries (adapted from Yáñez *et al*., 2020; Van Dyk *et al*., 2019; PNNL, 2014)

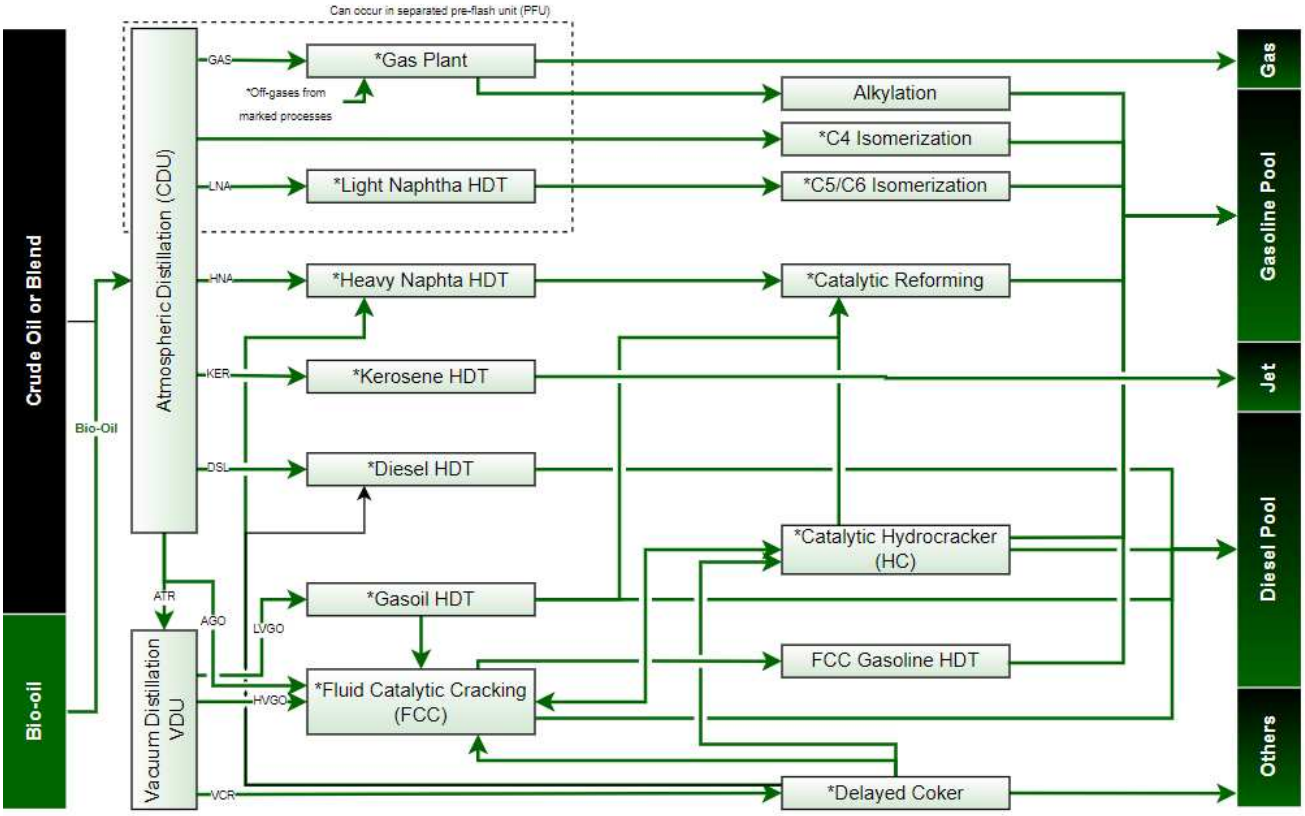

Figure 3.18. Typical refinery process flow diagram with renewable feed stock integration in atmospheric distillation units

However, there are few experiments in literature, specifically with small percentages blends with crude oil, which could have its solubility improved by property-similar crudes, addition of steam in furnace passes (crucial point of polymerization) (Van Dyk *et al*., 2019) or addition of emulsifiers (Leng *et al*., 2018). The impacts of this strategy can be seen in Figure 3.18, virtually producing advanced biofuels in any output stream.

As for blending biocrudes and finished fuels, challenges regarding fuel properties variations discourage this insertion option. The high oxygen and aromatic content in biocrudes change final blends, elevate cost and technological complexity to meet quality standards (Yáñez *et al*., 2020).

Lastly, insertion of biocrudes in petroleum intermediates has less challenges than the other options. In this case, the blend is proposed be placed in streams prior hydrotreating units (HT), hydrocracking units (HC), fluid catalytic cracking units (FCC) and gasification units. Gasification units are not in scope of this work, leaving to the reader more appropriate literature.

For hydrotreating and hydrocracking units (Figure 3.19 and 3.20), deactivation of catalysts due to high oxygen content and coking are the main challenge, elevating operational and cost complexity (French *et al*., 2011; Cruz *et al*., 2019; Benés *et al*., 2019).

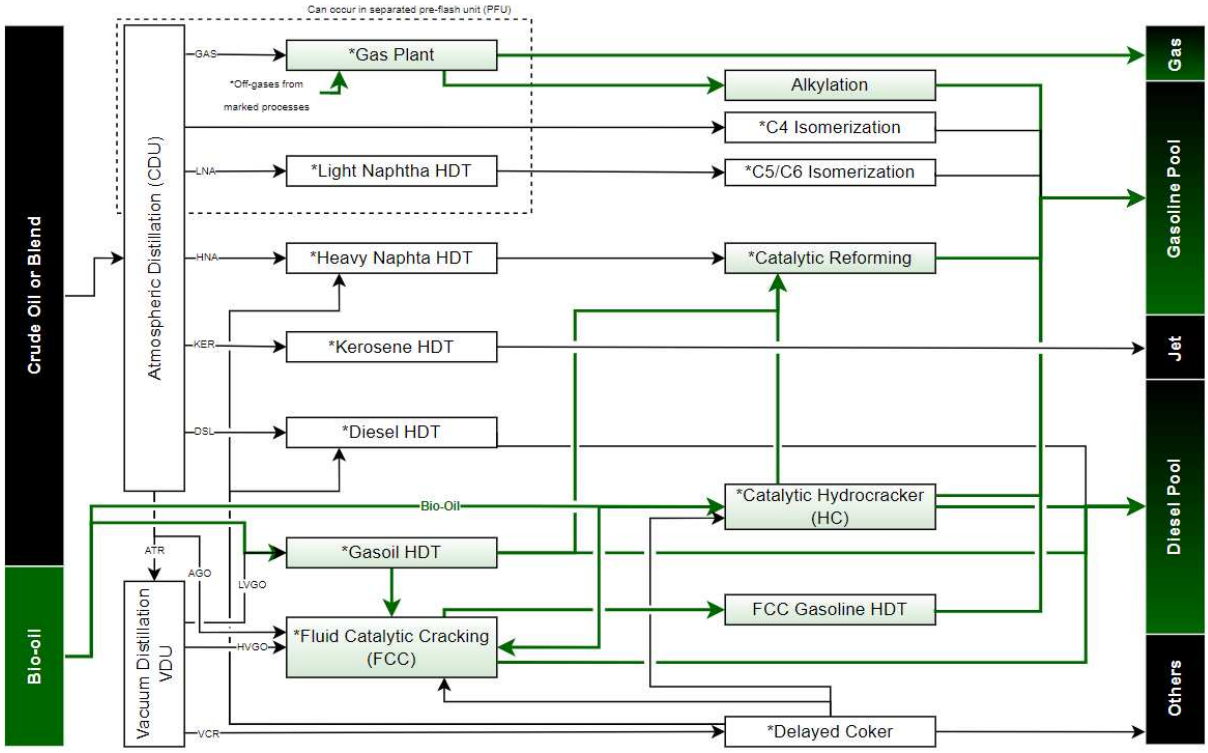

Figure 3.19. Typical refinery process flow diagram with renewable feed stock integration in heavy HT and HC units

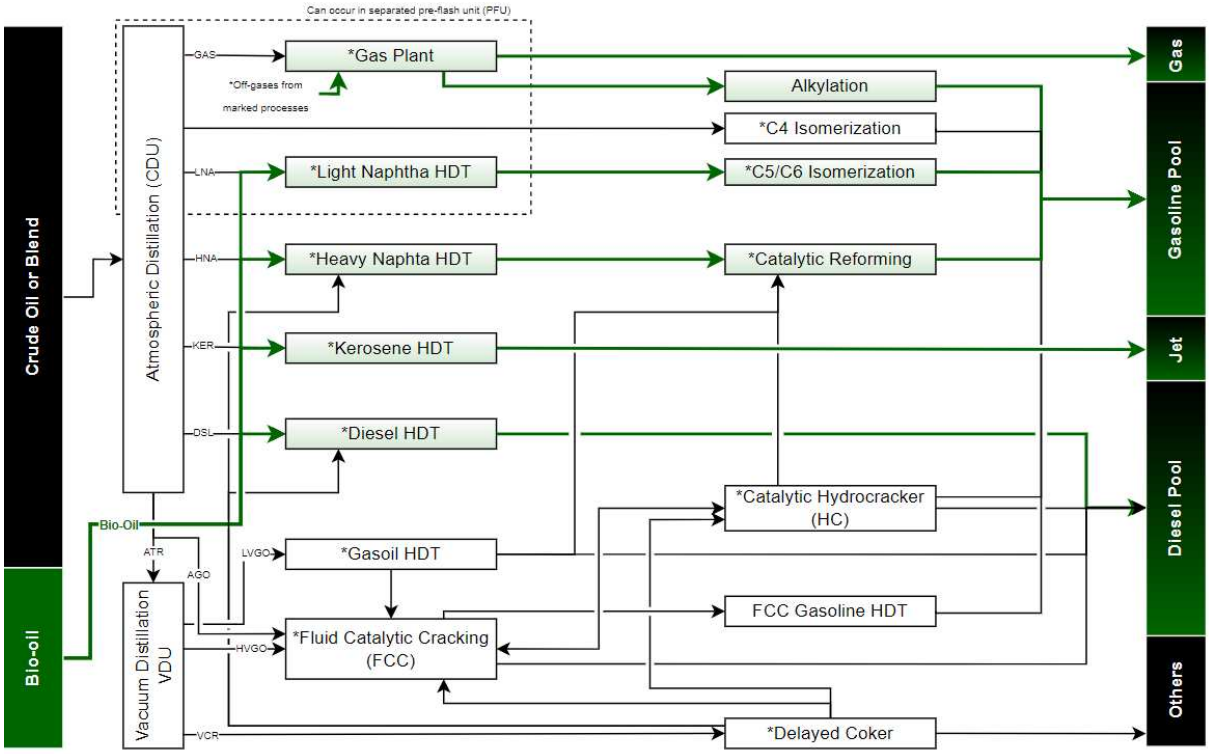

Figure 3.20. Typical refinery process flow diagram with renewable feed stock integration in mild HT and HC units

Since catalysts are regenerated on-site for FCC, this technology is the most promising for heavier biocrudes such as FPBO (Figure 3.21), blended with vacuum gasoil (20/80 %vol), as shown by Pinho *et al*. (2017).

Catalyst is reported to handle up to 50 wt.% of bio-oil in vacuum gasoil, however aromatics content was severely increased. Also, the main concern is that only 30% of the biogenic carbon from the input was recovered in the products (most of it going to coke) (Pinho *et al*., 2022).

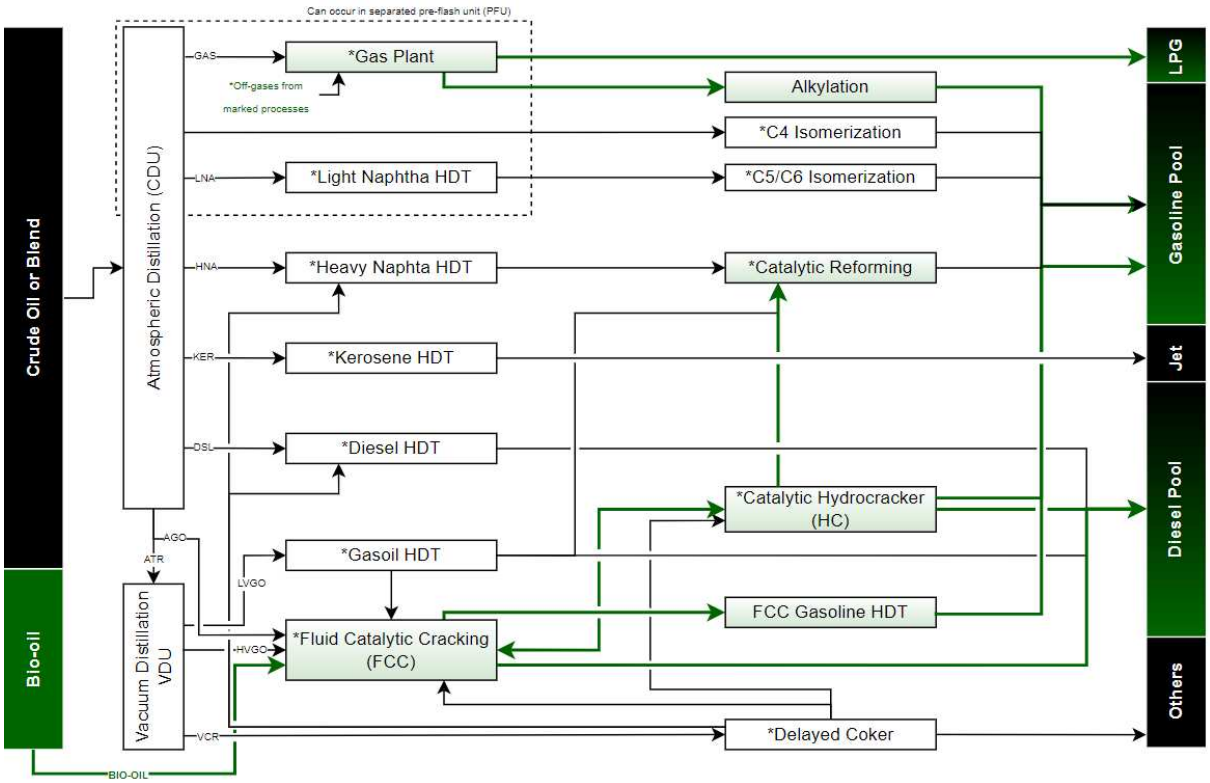

Figure 3.21. Typical refinery process flow diagram with renewable feed stock integration in FCC

4. Materials and Methods

4.1 Fast Pyrolysis Bio-oil Modeling

4.1.1 Bio-óleo Composition Modeling

The logical structure to model bio-oil composition was constructed as depicted in the logic flow diagram in Figure 4.1. The model consisted in 3 main manual inputs (2 types of literature data and the chemical structures available) and 3 sequential optimization algorithms (contribution parameters optimizer, mass composition optimizer and property optimizer). Also, the model integrated Aspen Plus® with Microsoft Excel® Visual Basic for Applications® which, apart from manual inputs and configurations, automates the composition proposal completely.

All terms in Figure 4.1 are explained in the topics below, however, a list of each symbology used is offered below to facilitate understanding:

Table 4.1. List of symbols present in Figure 3.1

Symbol	Description
A_{ji}	Quantity of C, H, O, N, S in each selected component j, for each chemical group i.
BP_i	Cubic average boiling point (°C) (at 1 atm) calculated for chemical group i
BP_m	Boiling Point (°C) (at 1 atm) for component m
$c_{j,i}$	Contribution (in %) of selected component j in group i
$c_{j,lignin}$	Contribution (in %) of selected lignin derived components j in lignin derived compounds group
H/C	Mass ratio of H to C atoms
MW_i	Simple average molecular weight calculated for chemical group i
MW_m	Molecular weight for component m
O/C	Mass ratio of O to C atoms
p_{ji}	Physical-chemical properties
$Structure_{ji}$	Chemical structure for selected component j in chemical group i
T0 to T100	Retrieved fraction (in vol%) from true boiling point simulated distillation curve
$w_{j,lignin}$	Mass fraction of selected lignin derived compounds j in bio-oil surrogate mixture.
w_{ji}	Mass fraction of selected bio-oil surrogate compounds j in group i
X_i	Cumulative average mass fraction of m components from chemical group i
$x_{n,m,i}$	Estimated mass fraction for component m, from chemical group i, obtained from source n
X_{si}	Standardized (0 to 1) average mass fraction of component m from chemical group i
Y_{ci}	Average mass fraction for chemical group i, corrected for heavy components presence
Y_i	Average mass fraction for chemical group i
$y_{n,i}$	Estimated mass fraction for chemical group i, obtained from source n
ρ, μ, k, c_p	Density, kinematic viscosity, thermal conductivity and heat capacity simulated at standard conditions

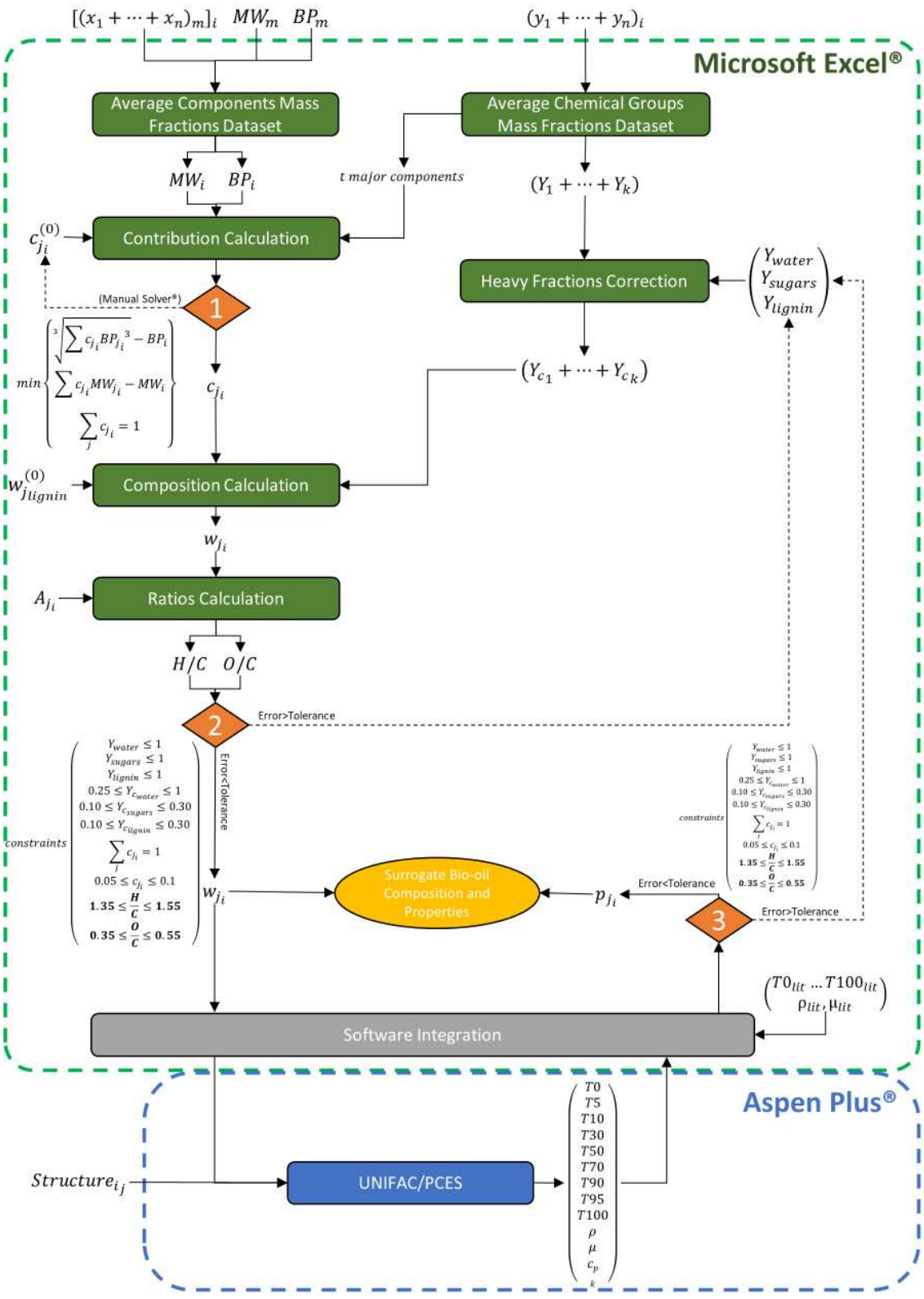

Figure 4.1 – Logic Flow Diagram of Bio-oil Modeling (own authorship)

4.1.1.1 Average Components Mass Fractions Dataset

As shown in figure 4.1, a dataset containing reported bio-oil composition from literature was populated. The scarce data retrieved was composed from GC-MS relative composition data, with additional research of each component molecular weight and boiling point. The dataset 1 structure is depicted in Table 4.2 and calculations in equations 4A and 4B.

Table 4.2. Example of average components mass fractions dataset (dataset 1)

i	m	Component	Formula	Group	MW	BP (°C)	Source 1 (x) (wt.%)	Source n (x) (wt.%)	Mass fraction X in i (wt.%) *	Std Mass fraction X_s in i (wt.%) **
1	0	Acetic Acid	C2H4O2	Acids	60.05	117.90	4.65	…	3.975	98.75%
1	1	Propanoic Acid	C3H6O2	Acids	74.08	141.20	0.1	…	4.025	1.25%
…	…	…	…	…	…	…	…	…	…	…
2	0	Phenol	C6H6O	Phenol	94.11	181.70	0.87	…	2.49	33.2%
2	1	Syringol	C8H10O3	Phenol	154.16	261.00	4.9	…	6.12	48.4%
2	2	Hydroquinone	C6H6O2	Phenol	110.11	286.00	0.0	…	7.50	18.4%
…	…	…	…	…	…	…	…	…	…	…

$$X_i = \sum X_{m_i} = \sum \left\{ X_{m-1_i} + \left[\left[\frac{(x_1 + \cdots + x_n)}{n} \right]_m \right]_i \right\} \tag{4A}$$

$$X_{s_i} = \sum X_{s_{m_i}} = \sum \left\{ \left[\left[\frac{(x_1 + \cdots + x_n)}{n} \right]_m \right]_i * \frac{100}{X_i} \right\} \tag{4B}$$

$$X_{-1} = 0, i = 1, 2 \ldots k \; groups, m = 0, 1 \ldots l \; components \; in \; group$$

Chemical formula and structure, molecular weight and boiling point were retrieved from public databases including the US National Center for Biotechnology Information free PubChem Repository (National Center for Biotechnology Information - PubChem), the Royal Society of Chemistry free open database ChemSpider (Royal Society of Chemistry, ChemSpider) and the US National Institute of Standards and Technology (NIST) free database (U.S Department of Commerce, NIST).

From standardized wt.% calculated, each chemical group received an average molecular weight MW_i and boiling point BP_i, calculated using each component m present in each group i as shown in Equations 4C and 4D.

$$MW_i = \sum_{m=0}^{m=l} MW_m * X_{s_{m_i}} \tag{4C}$$

$$BP_i = \sqrt[3]{\sum_{m=0}^{m=l} BP_m^3 * X_{s_{m_i}}} \tag{4D}$$

$$i = 1, 2 \ldots k \; groups, m = 0, 1 \ldots l \; components \; in \; group$$

4.1.1.2 Average Chemical Groups Mass Fractions Dataset

Due to scarcity of literature pieces including GC-MS data, a second dataset was built, including bio-oil chemical groups estimated mass fractions, which are more easily estimated through FTIR analysis and, in some cases, GC-MS also. This dataset also included the components most commonly found in eucalyptus bio-oil, selected to represent each group through the calculations shown in the next section. An example of the dataset 2 is shown in Table 4.3 and equations 4E.

Table 4.3. Example of average chemical groups mass fraction dataset (dataset 2)

Group i	Source 1 (y_s) (wt.%)	Source 2 (y_s) (wt.%)	Source n (y_s) (wt.%)	Group Mass Fraction (Y) (wt.%) *	1st Component	2nd Component	3rd Component
Acids	4.84	15.73	…	10.29	Acetic Acid	Propanoic Acid	-
Phenols	26.25	15.28	…	20.76	Phenol	Syringol	Hydroquinone
…	…	…	…	…	…	…	…

$$Y_i = \left[\frac{(y_{s_1}+\cdots+y_{s_n})}{n}\right] = \left[\frac{(y_1+\cdots+y_n)*100}{n\sum_1 y_n}\right] \quad (4E)$$

$$i = 1, 2 \ldots k \ groups$$

4.1.1.3 Heavy Components Dataset and Adjustment

Since most of literature data does not include heavy components in bio-oil composition analysis, due to the limitations of chromatography equipment, to completely model the fluid it was needed to estimate components most likely to be found when boiling it at higher temperatures.

These components are mostly complex sugars and lignin derivatives, accounting for about 40% of total composition. This adjustment was made obtaining the corrected mass fractions (Y_c) are obtained as depicted in Equation 4F.

$$Y_{c\,i} = \left[\frac{\frac{Y_i*100}{\sum_1 Y_i}}{n+1}\right] \quad (4F)$$

$$i = 1, 2 \ldots k+1 \ groups$$

PNNL research group (2013) data was used as reference to propose the components to be included (Appendix A1), as well as the analysis of lignin and cellulose decomposition reaction paths seen in section 3.2.

In this phase, percentages of water, sugars and lignin derivates are set as inputs for the composition algorithm, as later explained in 4.1.1.6.

4.1.1.4 Components Selection and Contribution Parameter Optimizer Algorithm

Each component most commonly reported selected in dataset 2 had its contribution (c) in its respective chemical group calculated by solving the mass balance between the average molecular weight from dataset 1 in each chemical group i and the mass fraction of the j components in the group mixture, as well as achieve similar boiling point, as shown in Equation 4G.

$$f(T,BP) = min\begin{Bmatrix} \sqrt[3]{\sum c_{j_i} {BP_{j_i}}^3} - BP_i \\ \sum c_{j_i} MW_{j_i} - MW_i \\ \sum_j c_{j_i} = 1 \end{Bmatrix} \quad (4G)$$

$$i = 1, 2 \dots\ k+1\ groups$$

$$j = 1, 2 \dots\ t\ components\ selected$$

$${c_{i}}_{j}^{(0)} = 0.5\ (initial\ guess)$$

This calculation did not include heavy components, which were set as constraints in the composition algorithm, later explained in 4.1.1.6.

4.1.1.5 Mass Composition and Ratios Optimizer

Composition (w) of each component was then calculated using each component contribution and group corrected fraction, as shown in Equation 4H.

$$w_{j_i} = c_{j_i} Y_{c_i} \quad (4H)$$

$$i = 1, 2 \dots k+1\ groups$$

$$j = 1, 2 \dots t\ componentes\ selected$$

Once composition was calculated, each component chemical formula was used to compose the ratios calculation, using each mol of atoms, as shown in Equation 4I.

$$A = \sum w_{j_i} \# A_{j_i} \quad (4I)$$

$$A = C, H, O, N, S\ (mol)$$

$$i = 1, 2 \dots k+1\ groups$$

$$j = 1, 2 \dots t\ components\ selected$$

4.1.1.6 Mass Composition Optimizer Constraints

To achieve the desired properties for bio-oil, a set of constraints were imposed to the algorithm (Table 4.4). Assumptions were made to assure the composition calculated would be the most precise possible, according to literature data.

The water, sugars and heavy fractions constraints were assumed with the intent of prevent local maximum and minimums convergence, including values that would "explode" the optimization function. As for the corrected fractions constraints, values close to reported in literature were selected: 25-35% water, 10-30% sugars and 10-30% lignin derivates. The term "convergence", adopted in this work refers to the minimum verbalization of the calculation, as this optimization problem is clearly over-specified and multiple solutions are possible.

Table 4.4. Constraints applied to Composition Algorithm (Morgan *et al*., 2016; Joubert *et al*., 2011; Oasmaa; Peacocke, 2001; Merckel, 2014)

Variable Name	Variable	Type	Min.	Max.	Value
Water mass fraction	Y_{water}	Input	-	100%	-
Sugars mass fraction	Y_{sugars}	Input	-	100%	-
Lignin Derivate mass fraction	$Y_{lignin\ (heavy\ fractions)}$	Input	-	100%	-
Water corrected fraction	$Y_{c,water}$	Constraint	25%	35%	-
Sugars corrected fraction	$Y_{c,sugars}$	Constraint	10%	30%	-
Lignin corrected fraction	$Y_{c,lignin\ (heavy\ fractions)}$	Constraint	10%	30%	-
Lignin Components (heavy)	$Sum(c_{lignin,j})$	Constraint	-	-	100%
Each component mass fraction	$C_{lignin,j}$	Input	5%	10%	-
H/C	-	Constraint	1.35	1.55	-
O/C	-	Constraint	0.35	0.55	-

Heavy components were not calculated with methods shown in 4.1.1.2 to 4.1.1.5, a direct selecting approach estimation approach was used, shown in Table 4.5. A most-likely origin for each component, prior to pyrolysis process, is also shown.

Table 4.5. Heavy components selected

Component	Origin	Origination Route	Ref.
Phenol, 2,6-dimethoxy-4-(3-hydroxyprop-1-enyl)-	Lignin	Ether Cleavage	Kawamoto (2017)
Phenol, 2-methoxy-4-(3-hydroxy-1-propenyl)-	Lignin	Ether Cleavage	Kawamoto (2017)
Phenol, 4-(3-hydroxy-1-propenyl)-	Lignin	Ether Cleavage	Kawamoto (2017)
Stilbene, 3,5-dimethoxy-	Lignin	Condensation Reactions	Kuroda *et al.* (2007); Nakamura *et al*., (2007)
Dehydroabietic Acid	Lignin	Natural Synthesis;	Trapp and Croteau (2001)
Benzofuran, di-	Lignin	Cyclization of phenols	Kawamoto (2017)
Phenyl Coumaran Compounds (Pseudocomponent)	Lignin	-	Pnnl (2014)
β-O-4 Compounds (Pseudocomponent)	Lignin	-	Pnnl (2014)
Benzofuran, 2-phenyl-2,3-dihydro-1-	Lignin	Primary Pyrolysis Reactions	Kawamoto (2017)
Pinoresinol	Lignin	Coniferyl Alcohols Dimerization	Barceló *et al*. (2004)

4.1.2 Composition Simulation in Aspen Plus® and Property Optimizer

Bio-oil surrogate composition optimized in terms of H/O and O/C by the algorithm was then feed into the Aspen Plus® simulation to be optimized in terms of physical properties, more specifically distillation curve.

Different from literature (Krutof; Hawboldt, 2020; Khan; Adewuyi, 2019), this work used UNIFAC as thermodynamic method, as shown in section 3.3. The selection of the method was based primarily on the fact that bio-oil is a very complex non-ideal liquid mixture, with polar and non-polar components (Bridgwater, 2012), not being suitable the use of equations of state (EoS) method. In addition to this, the scope of this work is the simulation of the distillation units, assuming pressures below 10 atm, not relying on highly non-ideal gas phase with complex dissolution interactions.

The critical aspect of selection, however, is that the mixture is composed by several cellulose, hemicellulose and lignin decomposition products, such as complex sugars and lignin intermediates, most of it absent or incomplete in Aspen Property Databanks. In these cases, the software already standardly uses UNIFAC to estimate missing properties and parameters, using the chemical structure of the component through Property Constant Estimation System (PCES), also shown in section 3.3. In this sense, unifying the method used simplifies the simulation. Besides equilibrium data, several important properties such vapor pressure, density, viscosity and heat capacity were missing for bio-oil components and were estimated methods shown in section 3.3.

A dynamic integration with Microsoft Excel® Visual Basic for Application®, was built on Software Integration (Figure 4.1) present in Appendix A1.

The Software Integration was set to input each mass composition into a single stream created in Aspen Plus®. Also, 11 temperature sensors were included in this stream, to retrieve all distillation curve points generated by Aspen (T0, T5, T10, T30, T50, T70, T90, T95, T100) and 4 property analyzers of interest: density (ρ), viscosity (μ), heat capacity (c_p) and thermal conductivity (k). During the optimization cycles, the results from each run were matched to the respective input composition and listed in Excel.

With physical-chemical properties calculated by Aspen, the composition was once again optimized, but in this step the targets of the optimizer are defined as the properties of the biocrude (literature values in this work – new lab results in future works). The optimizer compares the property estimated by Aspen Plus® for a determined biocrude composition with the reference value and, if the error is higher than a determined tolerance, it adjusts the composition with an arbitrary parameter, running the entire optimization cycle again (the 3 sequential optimizers).

Each optimization cycle's results are written to Excel, as a log for each run, to verify if the solution error was getting closer to a minimum. The error metric in this case was defined as the minimum square error (MSE) (Equation 3U) for both H/C and O/C ratios, and physical-chemical

properties. The entire code for the optimizer and software integration can be seen in Appendix A2.

4.2 Brazilian Crude Oils Modeling

Crude oils were selected mainly from Santos and Campos basins, in Brazilian territory. The process was carried out by two methods: direct access to Aspen Database and literature (web scrapping).

The first method used several assays available in Aspen HYSYS®, containing distillation curves, densities, light-ends compositions, sulfur, nitrogen and metal contents, besides molecular characteristics, for example labeling the oil as naphthenic, aromatic or paraffinic. This database contained information prior to 2015.

The second method, more complex, was searching oil companies' sources for assays, including Petrobras, ExxonMobil, Total Energies, Shell, Trident Energy, PetroRio, and many others. These assays were included in Aspen Plus®, automatically generating a set of pseudocomponents ranging from PC36 (pseudocomponents with boiling point of 36°C) to up PC1000. All fields from the assays used and its sources are depicted in Table 4.6.

Table 4.6. Brazilian crude oils from Santos and Campos basins (sorted by year)

Field	Year	Basin	Characteristic (API°)	Assay Source
Marlim	1997	Campos	Heavy (20.7)	Aspen HYSYS®
Albacore Leste	2009	Campos	Heavy (20.7)	Aspen HYSYS®
Polvo	2009	Campos	Heavy (20.8)	Aspen HYSYS®
Roncador (Light)	2011	Campos	Medium (28.1)	Equinor
Tupi (former Lula)	2011	Santos	Medium (29.7)	Aspen HYSYS®
Frade	2012	Campos	Medium (25.4)	Aspen HYSYS®
Peregrino	2013	Campos	Heavy (14.1)	Aspen HYSYS®
Roncador (Heavy)	2014	Campos	Heavy (19.9)	Equinor
Tubarão Martelo	2014	Campos	Heavy (21.0)	PetroRio
Iracema	2015	Santos	Light (36.5)	Aspen HYSYS®
Sapinhoá	2015	Santos	Light (41.1)	Aspen HYSYS®
Lapa	2018	Santos	Medium (22.7)	Total Energies
Mero	2019	Santos	Medium (28.9)	Total Energies
Sururu	2020	Santos	Medium (28.5)	Total Energies
Atapu	2021	Santos	Medium (28.4)	Total Energies
Tubarão Martelo	2021	Campos	Heavy (20.3)	PetroRio
Sepia	2022	Santos	Medium (27.2)	Total Energies
Frade	2022	Campos	Heavy (20.8)	PetroRio
Albacora Leste	2023	Campos	Heavy (21.2)	PetroRio
Peregrino	2024	Campos	Heavy (14.3)	Equinor

4.3 Coprocessing Simulation

A crude distillation unit (CDU) and vacuum distillation unit (VDU) were built in Aspen Plus®. The design of these unit operations (and the simulation as a whole) was simplified as much as possible (compared to a real refining operation), as detailed engineering is not the focus of this work. Given this, four assumptions were taken:

1) Catalytic units were not simulated (HDT, HC, delayed coking, etc.);
2) A single equipment *design* was chosen for all simulation scenarios;
3) Pipes head losses and equipment internals were ignored;
4) Only steady-state processes were simulated.

The following equipment (listed with TAGs and Aspen Plus® models used):

- Blending Tank (TK-#01) (model: MIXER);
- Desalters (DS-#01) (model: DECANT);
- Reciprocating Pumps (P-#01) (model: PUMP):
  - P-#01: TK-### to DS-###;
  - P-#02: DS-### to CDU-###;
  - P-#03: CDU-### to VDU-###;
- Heat Exchangers (Heat Train) (E-###) (model: HEAT-X):
  - E-#01/2: integration CDU LPG and blend;
  - E-#03: integration CDU top pumparound and blend;
  - E-#04: integration CDU NAPH and desalted blend;
  - E-#05/6: integration CDU KER and desalted blend;
  - E-#07: integration CDU middle pumparound and desalted blend;
  - E-#08/9: integration CDU DSL and desalted blend;
  - E-#10: integration CDU bottom pumparound and desalted blend;
  - E-#11: integration CDU AGO/VDU LVGO and desalted blend;
  - E-#12: integration VDU top pumparound and ATR;
  - E-#13: integration VDU HVGO and ATR;
  - E-#14: integration VDU middle pumparound and ATR;
  - E-#15: integration VDU VCR and ATR;
- Crude Distillation Unit (CDU-#01) (model: PETROFRAC)
- Vacuum Distillation Unit (VDU-#01) (model: PETROFRAC)

Specifications for each equipment are listed below (Tables 4.7 to 4.10). It is important to note

that usual cut temperatures of T5% and T95% (true boiling point analysis) were used to analyze those quality parameters, to simplify convergence complexity.

Table 4.7. Pumps and Desalters specifications sheet

Parameter/TAG	P-#01	P-#02	P-#03	TK-#01	DS-#01
Output Pressure (kgf/cm^2)	10	14	15	-	-
Operation Pressure (kgf/cm^2)	-	-	-	1.25	3
Operation Temperature (°C)	-	-	-	-	125
Wash Water (%vol feed+water)	-	-	-	-	5
Electrical Eff. (%)	95	95	95	-	-
Mechanical Eff. (%)	70	70	70	-	-

Table 4.8. Heat Exchangers specification sheet

Parameter/TAG	E-#01/2	E-#03	E-#04	E-#05/6	E-#07	E-#08/9
Head Loss (kgf/cm^2)	2	2	2	2	2	2
Output Temp. (°C)	25-50	50-75	100-125	100-150	125-175	175-200
Cold Stream	Blend	Blend	Blend[a]	Blend[b]	Blend[b]	Blend[b]
Hot Stream	LPG	CDU-TPA#	NAPH	KER	CDU-MPA#	DSL
	E-#010	**E-#011**	**E-#012**	**E-#013**	**E-#014**	**E-#015**
Head Loss (kgf/cm^2)	2	2	4	4	4	4
Output Temp. (°C)	200-225	225-250	400-410	410-420	420-440	440-450
Cold Stream	Blend[b]	Blend[b]	Blend[c]	Blend[c]	Blend[c]	Blend[c]
Hot Stream	CDU-BPA#	AGO/LVGO	VDU-TPA#	HVGO	VDU-MPA#	VCR

[a]Degassed Blend
[b]Blend without LPG and Light Naphtha fractions
[c]Blend without LPG, LNaphtha, HNaphtha, Kerosene, Diesel and Atmospheric Gasoil fractions

Table 4.9. CDU and VDU Units' Specifications Sheet

Parameter/TAG	CDU-#01	VDU-#01
Number of Stages	35	9
Feed Stage	21	8
Bottom Steam Feed Stage	25	9
Condenser Pressure (kgf/cm^2)	1.25	0.100
Top Pressure (kgf/cm^2)	1.50	0.125
Bottom Pressure (kgf/cm^2)	2.20	0.150
Furnace Pressure (kgf/cm^2)	2.20	0.125
Furnace Temperature (°C)	*(DSP*)*	*(DSP*)*
Overflash (%)	5	2.5
Condenser	Partial V/L	Partial V
Condenser Temperature (°C)	93	*(DSP*)*
Distillate Flow (kbbl/day)	CDUGAS+NAPH	VDUGAS
Bottom Steam Ratio (ton/kbbl) [lb/bbl]	9.08 [20]	4.54 [10]
Bottom Steam Temperature (°C)	400	600
Bottom Steam Pressure (kgf/cm^2)	25	45

*DSP stands for Design Specs (the solving solution of Aspen Plus

Table 4.10. CDU and VDU additional specification sheet

Parameter/TAG	CDU-#01	VDU-#01
Stripper Flow C-S-KER (kbbl/day)	KER + *(DSP*)*	-
Stripper Flow C-S-DSL (kbbl/day)	DSL + *(DSP*)*	-
Stripper Flow C-S-AGO (kbbl/day)	AGO + *(DSP*)*	-
Stripper Flow V-S-LVGO (kbbl/day)	-	LVGO + *(DSP*)*
Stripper Flow V-S-HVGO (kbbl/day)	-	HVGO + *(DSP*)*
N Stages C-S-KER	5	-
N Stages C-S-DSL	5	-
N Stages C-S-AGO	5	-
N Stages V-S-LVGO	-	5
N Stages V-S-HVGO	-	5
Draw Stage C-S-KER	8	-
Pumpback Stage C-S-KER	6	-
Draw Stage C-S-DSL	15	-
Pumpback Stage C-S-DSL	13	-
Draw Stage C-S-AGO	20	-
Pumpback Stage C-S-AGO	18	-
Draw Stage V-S-LVGO	-	6
Pumpback Stage V-S-LVGO	-	4
Draw Stage V-S-HVGO	-	8
Pumpback Stage V-S-HVGO	-	6
Steam Flow C-S-KER (ton/kbbl) [lb/bbl]	4,54 [10]	-
Steam Temperature C-S-KER (°C)	275	-
Steam Pressure C-S-KER (kgf/cm^2)	3	-
Steam Flow C-S-DSL (ton/kbbl) [lb/bbl]	4,54 [10]	-
Steam Temperature C-S-DSL (°C)	375	-
Steam Pressure C-S-DSL (kgf/cm^2)	10	-
Steam Flow C-S-AGO (ton/kbbl) [lb/bbl]	4,54 [10]	-
Steam Temperature C-S-AGO (°C)	400	-
Steam Pressure C-S-AGO (kgf/cm^2)	25	-
Steam Flow V-S-LVGO (ton/kbbl) [lb/bbl]	-	4,54 [10]
Steam Temperature V-S-LVGO (°C)	-	475
Steam Pressure V-S-LVGO (kgf/cm^2)	-	30
Steam Flow V-S-HVGO (ton/kbbl) [lb/bbl]	-	4,54 [10]
Steam Temperature V-S-HVGO (°C)	-	550
Steam Pressure V-S-HVGO (kgf/cm^2)	-	40
Draw Stage C-P-TPA	8	-
Pumpback Stage C-P-TPA	6	-
Flow C-P-TPA (kbbl)	KER	-
ΔTemperature C-P-TPA (°C)	-25	-
Draw Stage C-P-MPA	15	-
Pumpback Stage C-P-MPA	13	-
Flow C-P-MPA (kbbl)	DSL	-
ΔTemperature C-P-MPA (°C)	-25	-
Draw Stage C-P-BPA	20	-
Pumpback Stage C-P-BPA	18	-
Flow C-P-BPA (kbbl)	AGO	-
ΔTemperature C-P-BPA (°C)	-50	-
Draw Stage V-P-TPA	-	3
Pumpback Stage V-P-TPA	-	5
Flow V-P-TPA (kbbl)	-	LVGO
ΔTemperature V-P-TPA (°C)	-	-25
Draw Stage V-P-MPA	-	7
Pumpback Stage V-P-MPA	-	5
Flow V-P-MPA (kbbl)	-	HVGO
ΔTemperature V-P-MPA (°C)	-	-50

To better estimate mass balance for each column, feed streams true boiling point distillation curves generated by Aspen Plus® were fitted into modified logistic equations (Equation 4L and 4M). By knowing each cut temperature desired and the parameters for the stream, approximate flow could be determined. The method is similar to the ones described in section 3.1 (Riazi, 2005).

$$\%vol = \frac{A_1 - A_2}{1+\left(\frac{T}{T_0}\right)^{A_3}} + A_2 \tag{4L}$$

$$\%vol = \frac{B_1}{1+e^{-B_2(T-T_0)}} \tag{4M}$$

The first equation is more accurate for curve tails adjustment, due to reduced temperature powered by a smoothness factor. The second equation is more suitable to middle distillates adjustment, as exponential characteristic tends to overcalculate distillation curve tails. Also, second equation can deal with negative temperatures from gas fractions.

The cut temperatures used as standard to configure simulation are shown in Table 4.11.

Table 4.11. Standard cut temperatures used for simulation

Fraction	T5%	T95%
LPG (LPG)	IBP	32
Naphtha (LN+HN)	32	193
Light Naphtha (LN)	32	88
Heavy Naphtha (HN)	88	193
Kerosene (KER)	193	277
Diesel (DSL)	277	343
Atmospheric Gas Oil (AGO)	343	427
Light Vacuum Gas Oil (LVGO)	427	566
Heavy Vacuum Gas Oil (HVGO)	566	677
Vacuum Residue (VCR)	677	FBP

4.4 Techno-Economical Analysis

To assess benefits from proposed renewables coprocessing in this work, three key parameters were estimated: sources of revenue, sources of costs and economical parameters.

For costs, both raw materials and utilities were estimated. Bio-oil market price was estimated through a separated techno-economic analysis, using as reference PNNL (2014) study, adapted to 3.5 ton/day biomass needed to supply approx. 20 kbbl/day of bio-oil (45% yield). Table 4.12 shows the parameters used, considering a pyrolysis plant annexed to a refinery (utilities share with the complex).

Discount rate was estimated through Capital Asset Pricing Model (CAPM) (Equation 4N),

considering free-of-risk rate (r_f) the Brazilian reference interest rate (SELIC) (12.25%) (Brazil Central Bank, 2024), the market-risk rate (r_m) as the Brazilian avg. 12-month accumulated inflation rate (4.71%) (IBGE, 2024) plus attractiveness profitability of 8%, average volatility risk for chemical sector $\beta = 1.36$, and country-inherent risk rate (α_{BR}) of 0.58% (difference between Brazil and USA 25-year treasury notes) (Brazil Central Bank and US Federal Reserve. 2024). Lastly, income taxes rate of 34% (Brazil Federal Reserve, 2017) and Opex/Capex ratio of 43%.

$$CAPM = r_f + \beta[(r_m - r_f) + \alpha_{BR}] \quad (4N)$$

Besides economical parameters, technical and yield considerations were made (Table 4.13). The process considered was composed of three main sections: pre-treatment (drying and milling of eucalyptus chips), pyrolysis and utilities sections.

Table 4.12. Economic parameters considered for bio-oil unit

Parameter	Value	References
Lifetime (years)	25	PNNL (2014)
Maximum Payback Time (years)	10	Assumption
CAPM (%)	13.04 (elevated risk)	Calculated
Income Taxes (IRPJ + CSLL) (%)	34	Brazil Federal Reserve (2025)
Construction time (years)	2	PNNL (2014)
CAPEX: 1st year (%)	25	Assumption
CAPEX: 2nd year (%)	75	Assumption
CAPEX: Indirect Costs (% Cost Equip.)	62	PNNL (2014)
CAPEX: Linear Depreciation (years)	10	Assumption
CEPCI 2011	585.7	-
CEPCI 2024 (estimated)	800	Assumption
Location Factor	1.35	-
FX (BRL/USD) (5-year average)	5.235	Brazil Central Bank, 2025
Working Capital (% CAPEX)	10	PNNL (2014)
Land (% CAPEX)	6	PNNL (2014)
Salvage Value (% CAPEX)	5	Assumption
Indirect Opex (% OPEX)	30	Assumption
Annual Maintenance (% CAPEX)	3	PNNL (2014)

To determine the minimum selling price (MSP), Capex was estimated using literature data (PNNL, 2014), with proper corrections of scale-up factor (SUF) (0.7 considered), location factor (LF) (1.35 considered), CEPCI index and currency inflation (Equation 4O). As for Opex, mass and energy balances were used to provide estimates.

$$CapEx_{construction} = CapEx_{reference}{}^{SUF}(LF)\left(\frac{CEPCI_{construction}}{CEPCI_{reference}}\right)\left(\frac{USD_{reference}}{USD_{construction}}\right) \quad (4O)$$

Usual methods of investment profitability were also calculated for the unit: payback time, return on investment (ROI) and net present value (NPV), each using discounted cash flow with CAPM rate. The remaining costs and sources of revenue were estimated as shown in Table 4.14.

To account carbon credits used in Brazil (CBIO) in RenovaBio, emissions levels were estimated to each petroleum fraction produced and its substituents (i.e.: fraction produced by coprocessing FPBO, presenting a percentage of renewable carbon), as well as LHV (Lower Heating Values). The value was estimated based on the assumption that complete renewable substituent is substantially less energetic and emits less CO_2 (Table 4.15). These values are sensitive to fraction of renewables present: the higher the renewable fraction in fossil, more the value of emissions and LHV distances from fossil product.

In this case, both emission levels and LHV were estimated with arbitrary factors (shown in Table 4.15 notes), to simplify this work. Future work can potentially improve these estimations, for example using literature references such as Pinho et al. 2022.

Table 4.13. Technical parameters considered for bio-oil unit

Parameter	Value	Reference
Pre-Treatment		
Yield (%wt)	98.5	Assumption
Initial Biomass Moisture (%wt)	50	PNNL (2014)
Final Biomass Moisture (%wt)	8	PNNL (2014)
Electricity (kWh/tonne)	60.60	PNNL (2014)
Pyrolysis		
Production (ton/year)	2,363,287	10% of 400 kbbl.day^{-1} refinery input
Bio-oil Density (kg/m^3)	1126.1	This work
Bio-oil yield (%wt)	60	Assumption
Syngas yield (%wt)	15	Assumption
Biochar yield (%wt)	25	Assumption
Inicial Moisture (%wt)	8	PNNL (2014)
Electricity (kWh/tonne)	18.74	PNNL (2014)
Cooling Water (m^3/tonne)[a]	3.012	PNNL (2014)
Wastewater (ton/tonne bio-oil)	0.10	Assumption
Costs		
Electricity (USD/kWh)	0.061	CCEE, 2022
Make-up Water (USD/m^3)[b]	0.07	SP Government – Brazil (2011-2025)
Wastewater Treatment (USD/m^3)[b]	1.00	SP Government – Brazil (2011-2025)
Biomass (USD/tonne)$_{(average)}$	33.15	RODRIGUES (2009); SILVA, (2012)

[a]Adapted using bio-oil density
[b]Assumption using technical weighting factor of 5 and 60% additional cost, to include wastewater treatment chemicals and electricity.

To evaluate profitability of the investment, the earnings before interest (EBITDA) variation was used, as shown in Equation 4P, assuming no change in fixed costs (contract labor, equipment rentals, maintenance, etc.) or SG&A (selling, general and administrative) expenses (R&D, administrative, IT etc.)

$$\Delta EBITDA = \frac{[\Delta Revenue - \Delta(COGS + Operating\ Expenses)]}{\Delta Revenue} \quad (4P)$$

$$\Delta Revenue = (Revenue_{Blend} + Revenue_{CBIOs}) - Revenue_{Oil}$$

Table 4.14. Economic parameters estimated to coprocessing analysis

Parameter	Value	Reference
Revenue		
Fuel Gas (USD/L)[1]	0.001	Comgás (Cosan - Brazil) (2024)
LPG (USD/L)[2]	0.992	ANP, 2021-2024
Naphtha (USD/L)[3]	0.776	ANP, 2021-2024
Kerosene (USD/L)[4]	0.781	ANP, 2021-2024
Diesel (USD/L)[5]	0.752	ANP, 2021-2024
AGO (USD/L)[6]	0.707	ANP, 2021-2024
ATR (USD/L)[7]	0.717	ANP, 2021-2024
LVGO (USD/L)[8]	0.687	ANP, 2021-2024
HVGO (USD/L)[9]	0.772	ANP, 2021-2024
VCR (USD/L)[10]	0.638	ANP, 2021-2024
Coke (USD/L)	0.063	Assumption/Industry Data
CBIO (USD/unity)	18.00	B3, 2021-2024 (approx. weighted average)
Costs		
Electricity (USD/kWh)	0.191	CCEE,2024
Low Pressure Steam (LP) (USD/tonne)	23.00	Turton et al., 2012
Medium Pressure Steam (MP) (USD/tonne)	25.00	Turton et al., 2012
High Pressure Steam (HP) (USD/tonne)	27.00	Turton et al., 2012
Super High-Pressure Steam (SHP) (USD/tonne)	29.00	Turton et al., 2012
Natural Gas (39350 kJ/m^3) (USD/Nm^3)[a]	0.876	Comgás (Cosan - Brazil) (2024)
H_2 (99 %vol.) (USD/Nm3)	0.750	Assumption/Industry Data
Cold Water (5 °C) (USD/tonne)	0.185	Turton et al., 2012
Make-up Water (25 °C) (USD/m3)	0.07	SP Government – Brazil (2011-2024)
Wastewater Treatment (USD/m3)[b]	1.00	SP Government – Brazil (2011-2024)
Bio-oil (USD/bbl)	-	This work
Oil barrel (USD/bbl)[c]	64.91	EIA, 2025

[1]Estimated same as natural gas
[2]Estimated as LPG 2021-2024 weighted average price
[3]Estimated as 50% Naphtha + 50% Gasoline A 2021-2024 average price
[4]Estimated as Jet Fuel 2021-2024 weighted average price
[5]Estimated as Diesel S-500 2021-2024 weighted average price
[6]AGO Estimated as FCC output: 5% Fuel Gas, 15% LPG, 45% Gasoline A, 15% Marine Diesel, 10% Fuel Oil A1, 5% Coke.
[7]ATR Estimated as VDU outputs: 5% Gases, 40% LVGO, 35% HVGO, 20% VCR (see below).
[8]LVGO Estimated as FCC output: 5% Fuel Gas, 15% LPG, 45% Gasoline A, 15% Marine Diesel, 10% Fuel Oil A1, 5% Coke.
[9]HVGO Estimated as HC output: 5% Fuel Gas, 5% LPG, 15% Naphtha, 65% Marine Diesel, 10% Fuel Oil B1.
[10]VCR Estimated as Delayed Coker/Deasphalting (50/50%) output: 2.5% LPG, 10% Naphtha, 40% Fuel Oil B2, 15% Asphalt, 15% Cement, 15% Coke.
[a]Estimated consumption of 30 MNm^3.month^{-1}.
[b]Assumption using technical weighting factor of 5 and 60% additional cost, to include wastewater treatment chemicals and electricity.
[c]Weighted average 2017-2021 for Brent/WTI blend (50/50%)
[D]Densities used for price conversions: LPG ~ 0.58 kg/L, Naphtha ~ 0.75 kg/L, Fuel Oil A1 ~ 1.025 kg/L, Fuel Oil B1 ~ 1.017 kg/L, Fuel Oil B2 ~ 0.968 kg/L, Asphalt ~ 0.85 kg/L, Cement ~ 1.09 kg/L

Table 4.15. Emission levels and LHV equations defined for CBIO calculations (RenovaBio, 2018; Ghanta *et al*., 2014; Masnadi *et al*., 2018)

Parameter	Equation	Reference
Emission Level (gCO_2/MJ)		
LPG[1]	63.20	RenovaBio, 2018
Naphtha[2]	71.33	RenovaBio, 2018
Kerosene[3]	72.89	RenovaBio, 2018
Diesel[4]	74.43	RenovaBio, 2018
AGO[5]	76.29	Estimated[C]
ATR[6]	79.67	Estimated[C]
LVGO[7]	78.20	Estimated[C]
HVGO[8]	80.15	Estimated[C]
VCR[9]	82.16	Estimated[C]
LPG (Green)[a]	47.40	Estimated
Naphtha (Green)[a]	53.50	Estimated
Kerosene (Green)[a]	54.67	Estimated
Diesel (Green)[a]	55.82	Estimated
AGO (Green)[a]	57.22	Estimated
ATR (Green)[a]	59.76	Estimated
LVGO (Green)[a]	58.65	Estimated
HVGO (Green)[a]	60.11	Estimated
VCR (Green)[a]	61.62	Estimated
LHV (MJ/kg)		
LPG[1]	46.47	RenovaBio, 2018
Naphtha[2]	43.54	RenovaBio, 2018
Kerosene[3]	46.47	RenovaBio, 2018
Diesel[4]	42.29	RenovaBio, 2018
AGO[5]	43.35	Estimated[C]
ATR[6]	45.27	Estimated
LVGO[7]	44.43	Estimated[C]
HVGO[8]	45.54	Estimated[C]
VCR[9]	46.68	Estimated[C]
LPG (Green)[b]	41.82	Estimated
Naphtha (Green)[b]	39.19	Estimated
Kerosene (Green)[b]	41.82	Estimated
Diesel (Green)[b]	38.06	Estimated
AGO (Green)[b]	39.01	Estimated
ATR (Green)[b]	40.74	Estimated
LVGO (Green)[b]	39.99	Estimated
HVGO (Green)[b]	40.99	Estimated
VCR (Green)[b]	42.01	Estimated

[1]Estimated as LPG
[2]Estimated as 50% Petrochemical Naphtha + 50% Gasoline
[3]Estimated as Jet Fuel
[4]Estimated as Diesel
[5]ATR Estimated as VDU outputs: 45% LVGO, 35% HVGO, 20% VCR (see note C below).
[a]Estimated as 25% reduction on gCO_2/MJ
[b]Estimated 10% reduction in LHV vs fossil alternative
[c]Estimated as 2.5% increase for each cut

5. Results

5.1 Blend Modeling

5.1.1 Bio-oil Modeling

Datasets 1 and 2 were populated, according to methodology described in section 4.1, with data from Amutio *et al*. (2015), Gómez-Monedero *et al*. (2015), Lazzari *et al*. (2018), Rodrigues (2018), PNNL (2014), Chang *et al*. (2013), Merckel (2014), Wang *et al*. (2014) and Gholizadeh *et al*. (2019). Complete results can be seen in Appendix A2.

A total of 393 components with chemical formula and properties were listed (excluding crude oil light-ends, H_2S and mercaptans) and 145 populated Dataset 1. This deviation is due to the construction of the database had been initiated with listing of components from bio-oil of different sources, such as sugarcane bagasse bio-oil, which presents some components not usually found in wood bio-oil.

Composition results can be seen in Table 5.1 and 5.2. Methodology of this section can be found in section 4.1.

Table 5.1. Chemical groups fraction results from random selected scenario

Chemical Groups (i)	Chemical Group Average Mass Fraction (Y_i)	Corrected Average Mass Fraction ($Y_{c,i}$)	Selected components (j = 40)
Acids	12.88%	8.33%	Acetic Acid; Propanoic Acid; 4-hydroxy-3-methoxy-benzoic acid
Alcohols	1.78%	1.15%	2-furanmethanol; Methanol; 3-buten-2-ol
Aldehydes	1.71%	1.10%	Furfural; Formaldehyde; Glutaraldehyde
Furans	4.37%	2.83%	Furan; 2,3-dihydrobenzofuran; 1,2,3-trimethoxybenzene
Ethers	2.64%	1.71%	Eucalyptol
Esters	2.89%	1.87%	1,2-dimethyl-propyl acetate; octyl acetate
Heterocyclic (N, S)	0.82%	0.53%	2,4,5-trimethylpyridine; dibenzothiophene
Hydrocarbons	2.66%	1.72%	4-ethenyl-1,4-dimethylcyclohexene; 1-methyl-1-ethyl-cyclopentane
Ketones	7.12%	4.60%	2(3H)-dihydrofuranone; 3-hydroxy-2-methyl-4H-4-pyranone; 1-hydroxy-2-propanone; 1,3-cyclopentanedione
Phenolics	29.42%	19.02%	2-hydroxyphenol; 2-methoxy-4-(prop-1-en-1-yl)phenol; 4-hydroxyphenol; 2,6-dimethoxyphenol; phenol
Sugars	1.19%	10.22%	Levoglucosan; β-D-Arabinopyranose; Cellobiose
Water	32.51%	30.03%	Water
Lignin Derived	0.00%	16.88%	Pinoresinol; 2-phenyl-2,3-dihydro-1-benzofuran; 3,5-dimethoxy-stilbene; dehydroabietic acid; dibenzofuran; sinapyl alcohol, coumaryl alcohol, conipheryl alcohol, 2-phenyl-2,3-dihydro-1-Benzofuran, Phenyl Coumaran Compounds (pseudocomponent), β-O-4 Compounds
Total	**100,00**	**100,00**	**-**

Table 5.1 shows ~30% of total mixture being composed by water, ~35% of total mixture contribution from lignin degradation (phenolics + lignin derived compounds) and ~35% contribution from hemicellulose and cellulose degradation products (complex sugars, acids, aldehydes, ketones and others), concordant to literature data presented in section 3.2.

An important detail is the increase in sugars content, mainly due to the struggle in identifying complex sugars in the experimental samples. Most of literature data report only levoglucosan presence, while several anhydrous sugars, intermediates from cellulose/hemicellulose degradation that decompose rather than boil, are also present. This presence of complex sugars and furans correctly accounts for incomplete pyrolysis of cellulose and hemicellulose (Wang *et al*., 2020), while incomplete lignin degradation can be accounted by complex phenolic compounds, as explained in section 3.2 (Lazaridis *et al*., 2018). Table 5.2 shows the selected compounds, MW/BP, chemical group's avg. MW/BP, component contribution in chemical group and final mass fraction after ratios optimization (section 4.1).

Table 5.2 shows the scenario where EUC30 (30 wt.% water in bio-oil) was achieved. It is seen that phenolics and lignin derived coupled with sugars represent almost half (46.97 wt.%) of bio-oil. These groups have also the highest MW and BP, ranging from 140 to 650 $g.mol^{-1}$ and 245 to 560 °C on average, therefore contributing directly to middle distillates fractions. Apart from water, the rest of bio-oil (23.84%), have lighter components with MW between 60 and 140 g.mol-1 and BP between 115 and 225 °C on average, composing mostly upper distillate products, for example naphtha.

Model was integrated with Aspen Plus® through Visual Basic for Applications® Software Integration, described in Appendix A1. Aspen simulation was configured to provide stream analysis of several properties listed in Table 5.3. Also, a "dry" version of EUC30 was provided, arbitrarily removing all water from it, as a reference for analysis only.

Table 5.2. Mass fraction results from EUC30 scenario

Components (j)	Molecular Weight (MW_j) (g/mol)	Boiling Point (BP_j) (°C)	Chemical Group (i)	Average Chemical Group MW (MW_i) (g/mol)	Average Chemical Group BP (BP_i) (°C)	Mass fraction contribution in group ($c_{j,i}$) (%)	Mass Fraction ($w_i = Yc_i * c_{j,i}$) (%)
Acetic Acid	60.05	117.9	Acids	75.23	189.74	70.44	5.87
Benzoic acid, 4-hydroxy-3-methoxy-	168.15	353.4	Acids	75.23	189.74	11.72	0.98
Propanoic Acid	74.08	141.2	Acids	75.23	189.74	17.84	1.49
Furanmethanol, 2-	98.10	170.0	Alcohols	60.59	117.50	24.87	0.29
Methanol	32.04	64.7	Alcohols	60.59	117.50	44.87	0.52
Butenol, 3-2-	72.11	97.3	Alcohols	60.59	117.50	30.26	0.35
Furancarbaldehyde, 2-	96.08	161.7	Aldehydes	92.26	178.03	8.40	0.09
Formaldehyde	30.03	-19.0	Aldehydes	92.26	178.03	10.72	0.12
Glutaraldehyde	100.11	187.0	Aldehydes	92.26	178.03	80.87	0.89
Furan	68.07	31.3	Aromatic/Furans	110.95	209.83	17.69	0.50
Benzofuran, 2,3-dihydro-	120.15	188.5	Aromatic/Furans	110.95	209.83	37.86	1.07
Benzene, 1,2,4-trimethoxy-	120.19	247.0	Aromatic/Furans	110.95	209.83	44.45	1.26
Eucalyptol	154.25	172.0	Ethers	154.25	172.00	100.00	1.71
Acetate, 1,2-dimethyl-propyl	130.19	122.0	Esthers	155.41	182.93	40.06	0.75
Acetate, Octyl	172.26	208.0	Esthers	155.41	182.93	59.94	1.12
Pyridine, 2,4,6-trimethyl-	121.18	170.0	Heterocyclic	141.87	248.63	67.20	0.36
Dibenzothiophene	184.26	332.6	Heterocyclic	141.87	248.63	32.80	0.17
Cyclohexene, 4-ethenyl-1,4-dimethyl	136.23	160.0	Hydrocarbons	124.22	142.38	50.00	0.86
Cyclopentane, 1-methyl-1-ethyl-	112.21	118.8	Hydrocarbons	124.22	142.38	50.00	0.86
Furanone, 2(3H)-dihydro-	86.09	204.0	Ketones	105.07	226.63	11.85	0.55
Pyranone, 3-hydroxy-2-methyl-4H-4-	126.11	284.7	Ketones	105.07	226.63	35.33	1.63
Cyclopentanedione, 1,3-	98.10	157.4	Ketones	105.07	226.63	46.57	2.14
Propanone, 1-hydroxy-2-	74.08	145.6	Ketones	105.07	226.63	6.25	0.29
Phenol, 2-hydroxy-	168.15	245.0	Phenolics	140.49	245.40	30.50	5.80
Phenol, 2-methoxy-4-(prop-1-en-1-yl)-	164.20	266.0	Phenolics	140.49	245.40	16.65	3.17
Phenol, 4-hydroxy-	110.11	286.0	Phenolics	140.49	245.40	11.29	2.15
Phenol, 2,6-dimethoxy-	154.16	261.0	Phenolics	140.49	245.40	17.17	3.27
Phenol	94.11	181.7	Phenolics	140.49	245.40	24.38	4.64
Levoglucosan	162.14	384.0	Sugar	199.36	470.65	21.02	2.15
β-D-arabinopyranose	150.13	333.2	Sugar	199.36	470.65	54.67	5.59
Cellobiose	342.30	667.0	Sugar	199.36	470.65	24.31	2.49
Phenol, 2,6-dimethoxy-4-(3-hydroxyprop-1-enyl)-	210.23	384.7	Lignin Derived	308.57[a]	385.50[a]	10.50	1.77
Phenol, 2-methoxy-4-(3-hydroxy-1-propenyl)-	180.20	332.0	Lignin Derived	308.57[a]	385.50[a]	10.50	1.77
Phenol, 4-(3-hydroxy-1-propenyl)-	150.17	323.5	Lignin Derived	308.57[a]	385.50[a]	10.50	1.77
Stilbene, 3,5-dimethoxy-	240.30	323.0	Lignin Derived	308.57[a]	385.50[a]	10.50	1.77
Dehydroabietic Acid	300.40	394.0	Lignin Derived	308.57[a]	385.50[a]	10.50	1.77
Benzofuran, di-	168.19	285.0	Lignin Derived	308.57[a]	385.50[a]	10.50	1.77
Phenyl Coumaran Compounds	633.56	406.4	Lignin Derived	308.57[a]	385.50[a]	10.50	1.77
β-O-4 Compounds	648.00	394.4	Lignin Derived	308.57[a]	385.50[a]	10.50	1.77
Benzofuran, 2-phenyl-2,3-dihydro-1-	196.24	300.4	Lignin Derived	308.57[a]	385.50[a]	10.50	1.77
Pinoresinol	358.40	556.0	Lignin Derived	308.57[a]	385.50[a]	10.50	1.77
Water	18.02	100.0	Water	18.02	100.00	100.00	30.03
Total	-	-	-	-		-	**100,00**

[a]Not defined in literature, obtained by input used in this work

Table 5.3. Integrated simulation of properties obtained from EUC30

Property	EUC30	EUC30DRY
IBP (°C)	34.74	16.86
T5% (°C)	97.58	107.44
T10% (°C)	98.49	120.79
T30% (°C)	109.89	181.04
T50% (°C)	176.39	246.16
T70% (°C)	261.08	295.42
T90% (°C)	374.27	566.55
T95% (°C)	623.79	632.76
FBP (°C)	914.29	1024.44
Specific Density (20 °C)	1.036	1.055
Kinematic Viscosity (cSt) (40 °C)	102	69
Heat Capacity ($kJ.kg^{-1}.K^{-1}$) (20 °C)	2284.79	1475.81
Thermal Conductivity (20 °C)	0.1533	0.1533

Table 5.4 shows properties calculated for the bio-oil composition obtained compared with literature data from Mante *et al*. (2016) and Varma *et al*. (2019). These two references present pine and cedar bio-oils properties, respectively, since no eucalyptus bio-oil distillation curve is available in literature.

It is seen that several properties such as molar ratios, water content, density, lower cut temperatures and characterization factors are similar between EUC30 and Varma *et al*. (2019) cedar bio-oil, which proves that the algorithm, aimed towards Varma *et al*. (2019) properties as targets, works as intended. Figure 5.1 shows the mean square error (MSE) of each optimization cycle performed (270 in total) to approximate EUC30 to Varma *et al*. (2019), demonstrating that the algorithm works properly, cycling through an average error of approximately 1.339% total MSE for all properties. The oscillation of the MSE is probably due to the nature of Excel® Solver algorithm, trying to find other solutions (other possible minima). Tests were performed with the other 2 references, and the algorithm responds similarly.

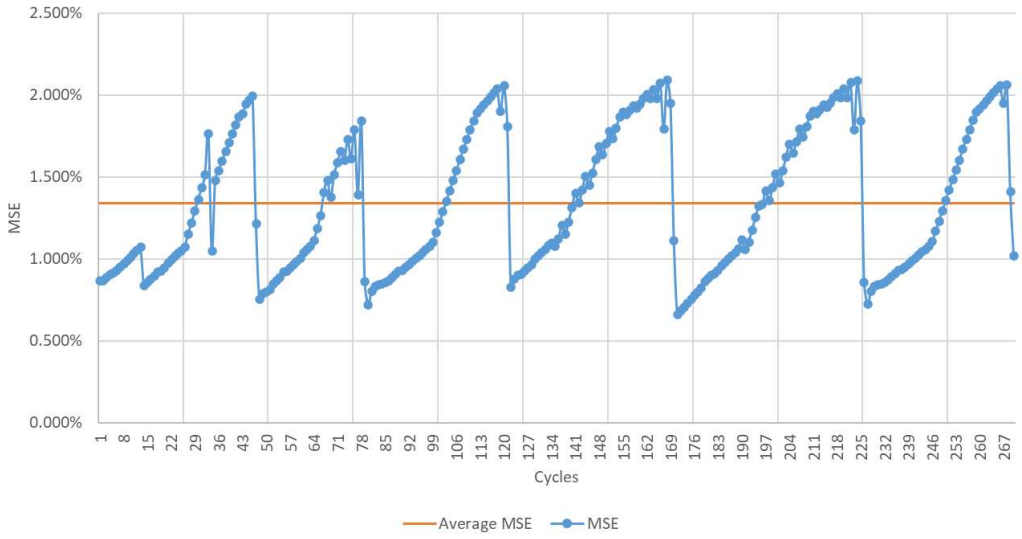

Figure 5.1. MSE for optimization cycles using Varma *et al*. (2019) biocrude as target

However, viscosity and higher cut temperatures present considerable deviations, that can be explained by three possible reasons.

First, the pyrolysis conditions and the water content. Since literature data to compose EUC30 used several different pyrolysis apparatuses, deviations from the final product are a challenge to be addressed in future work.

The second reason, is the difference between wood chemical structure. Due to hardwood lower activation energy in pyrolysis reactions, eucalyptus wood tends to have higher yields due to

higher volatiles production. These degraded components can be incorporated faster into bio-oil during pyrolysis, otherwise left to coking during softwood pyrolysis and separated. Therefore, it is possible that non-catalytic eucalyptus bio-oil composition can be heavier than other types of wood oils (Ding *et al*., 2017).

The third possible reason is the selection of components and the conditions of optimization. Since it is a challenge to map which heavy components are present in bio-oil, complex degradation products that increase density and viscosity, and boiling points could be present in references results. Identification of which components already present in modeling are suitable to impact final viscosity value towards reference data is left to be concluded in next steps of model tuning.

Table 5.4. EUC30 scenario properties calculated for bio-oil composition

Parameter	This work (EUC30)	This work (EUC30DRY)	Mante et al. (2016) (A)[a]	Mante et al. (2016) (B)[a]	Varma et al. (2019)
Biomass used	Eucalyptus	Eucalyptus	Pine	Pine	Cedar
	Hardwood	Hardwood	Softwood	Softwood	Softwood
MABP (°C)	224.80	194.76	-	-	-
VABP (°C)	203.02	281.99	281.96[c]	321.64[c]	202.13[c]
MW (g/mol)	131.60	126.19	-	-	-
H/C (molar)[b]	1.360	1.268	1.193	1.233	1.469
O/C (molar)[b]	0.424	0.378	0.357	0.239	0.437
IBP (°C)	34.74	16.86	93.92	109.44	66.84
T5% (°C)	97.58	107.44	108.66	109.48	82.26
T10% (°C)	98.49	120.79	109.52	139.74	96.13
T30% (°C)	109.89	181.04	222.40	294.26	145.60
T50% (°C)	176.39	246.16	294.42	349.96	194.16
T70% (°C)	261.08	295.42	350.90	386.05	248.29
T90% (°C)	374.27	566.55	432.55[c]	438.18[c]	326.46[c]
T95% (°C)	623.79	632.76	471.70[c]	463.18[c]	363.95[c]
FBP (°C)	914.29	1024.44	510.84[c]	488.17[c]	401.43[c]
Water (wt.%)	30.00	0.00%	20.20	8.66	22.0
Nitrogen (wt.%)	0.51	0.51	0.48	0.32	0.70
Sulphur (wt.%)	1.10	1.10	-	-	-
Specific Density (20 °C)	1.036	1.055	1.116	1.218	1.083
Kinematic Viscosity (cSt) (40 °C)	102	69	132	169	16.53
°API	5.1	2.6	-4.7	-15.3	-0.8
Classification °API	Extra Heavy	Extra Heavy	Extra Heavy	Extra Heavy	Extra Heavy
Watson/UOP K	8.6	8.7	8.2	7.7	8.2
Classification K	-	-	-	-	-

[a]Average boiling points from 6 different runs each
[b]Calculated from elemental analysis
[c]Obtained by extrapolated data in Aspen Plus®

Important to mention that sulfur content deviated from literature solely due to this work's assumption to include it. Some references, including PNNL (2013), state that sulfur can be encountered in bio-oil but in extremely low levels (< 0.1%), for that reason a sulfur component was

included in simulation. In this case, since there were no constraints in the optimizer to limit sulfur, it used the other atoms of these sulfur-present molecules as leverage to likely adjust inconsistencies in H/C and O/C ratios, driving sulfur content largely distant from literature references. Due to this result, it shall be removed from future optimizations, leaving only nitrogen compounds in the heteroatoms chemical group.

Mante *et al*. (2016) results, on other hand, differ considerably from this work's results, presenting more similar characteristics to the "dry" version of EUC30 (EUC30DRY). Once again, there is an obvious reason and a non-trivial one. The group results consisted in two scenarios of catalytic pyrolysis bio-oil, produced in a circulating bed reactor at different temperatures (425 °C and 465 °C). Although not mentioned in depth in this work's literature review, catalytic pyrolysis with regenerative catalysts (similar to a FCC's) stabilizes bio-oil produced in terms of reactive groups, such as carbonyls and ketones, and also removing water. In this sense, Mante *et al*. (2016) results are a more dry, viscous, dense and heavy fractions dominant bio-oil than Varma *et al.* (2019) bio-oil and, obviously, this work's results. This difference in pyrolysis process can also be identified as both references results are analyzed from softwood, with similar trees densities but different results.

Figure 5.2 shows the distillation curve for the fluids presented. Once again, the similarities between EUC30 and Varma *et al*. (2019) fluid can be seen, apart from higher water content reducing boiling points below 30% volume recovery and also final 10% range due to differences in heavy components modelled. Moreover, is inferred that, with the correct tuning, the model could be used to achieve the literature curves if needed (useful for highly detailed refinery production scheduling), as can be seen in Figure 5.3. However, these yields should be treated as a mathematical approximation, since the summed percentage is above or below 100% for all cases.

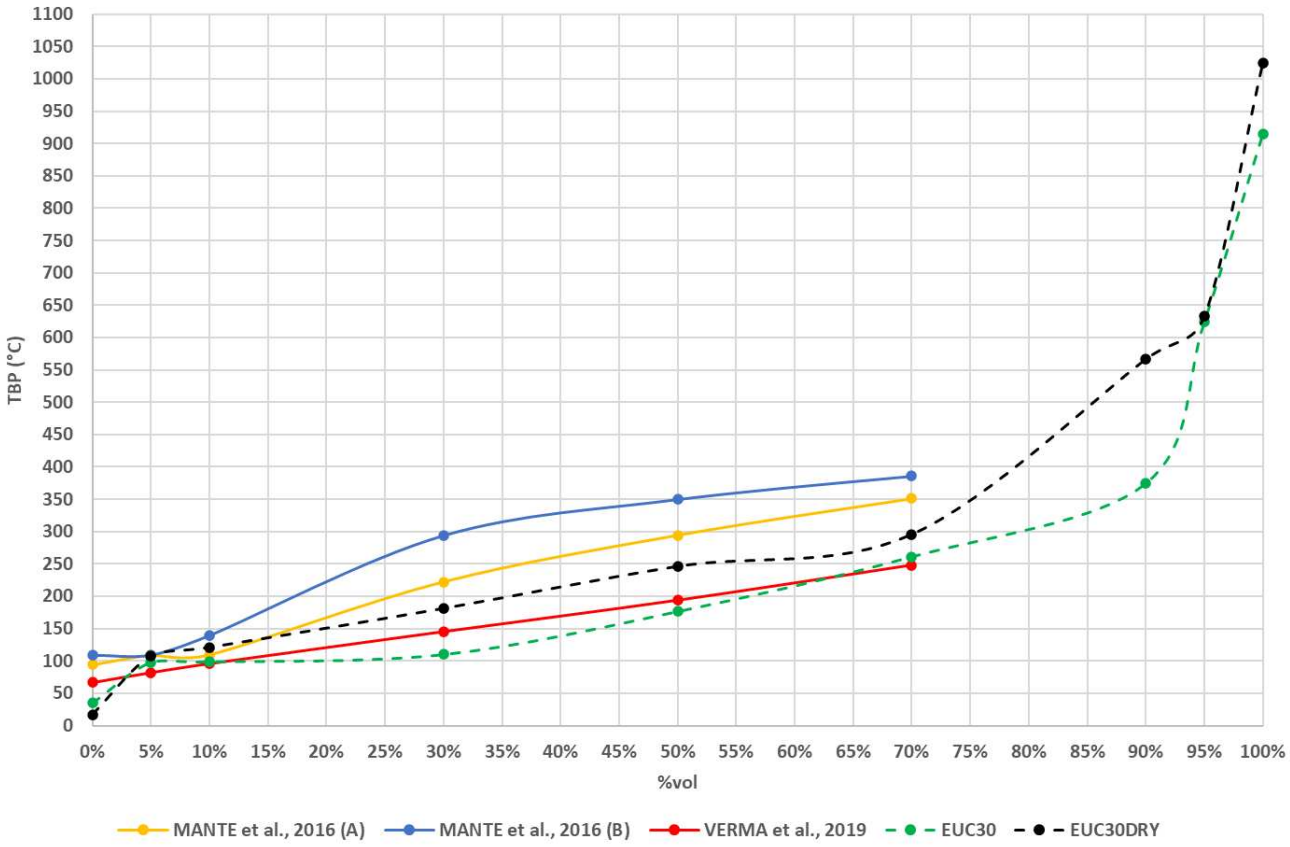

Figure 5.2. Distillation curves for EUC30 and literature data

Using the distillation curves, cut temperatures presented in section 3.1 and the logistic model presented in section 4.3, theoretical products distribution was calculated for each biocrude (Figure 5.3). The adjusted parameters are presented in Table 5.5. Due to the unnatural composition of EUC30 (which implies in nonlinearities), the precision of both equations adjusted is lower than for natural bio-oils, especially for curve tails (0-10% and 90-100%).

Table 5.5. Adjusted logistic equations parameters for biocrudes presented

Biocrude	A1	A2	A3	T0	R^2	B1	B2	T0	R^2
EUC30	-0.0331	0.9978	176.24	2.7262	0.9700	0.9526	0.0184	186.85	0.9579
EUC30DRY	-0.0066	0.9860	234.77	3.2741	0.9954	0.9504	0.0177	236.80	0.9913
Mante *et al*. (2016) A	0.0145	1.2883	3.0547	336.92	0.9943	1.0408	0.0139	297.74	0.9942
Mante *et al.* (2016) B	0.0483	1.2163	5.7091	373.11	0.9926	1.1913	0.0144	366.37	0.9935
Varma *et al*. (2019)	0.0128	1.5275	1.8789	677.21	0.9997	1.0230	0.0064	474.74	0.9948

Refer to Section 4.3 for the equations used.

As commented before, EUC30 is presented as a heavier oil similar to Varma *et al*. (2019), producing relevant portion quantity of middle distillates, but lower than Mante *et al.* (2016), which achieved higher yields for gasoils. Interpreting these results, it is clear that the higher quantity of

water negatively impacts the percentage of products with higher industrial value, however, comparing EUC30, EUC30DRY and Varma *et al*. (2019), with Mante *et al.* (2016)'s samples, it's clear that the stabilization of unstable chemical species, provided by the catalytic pyrolysis, has a more pronounced effect over the percentage of middle distillates, leaving explicit the advantages of an upgrading process to be carried out with FPBO's.

It is important to note that these yields are sensible to cut temperatures used, shown in the next section. Also, apart from improvements still needed in this evaluation, it is valid to mention that this approach is a break-through on the subject.

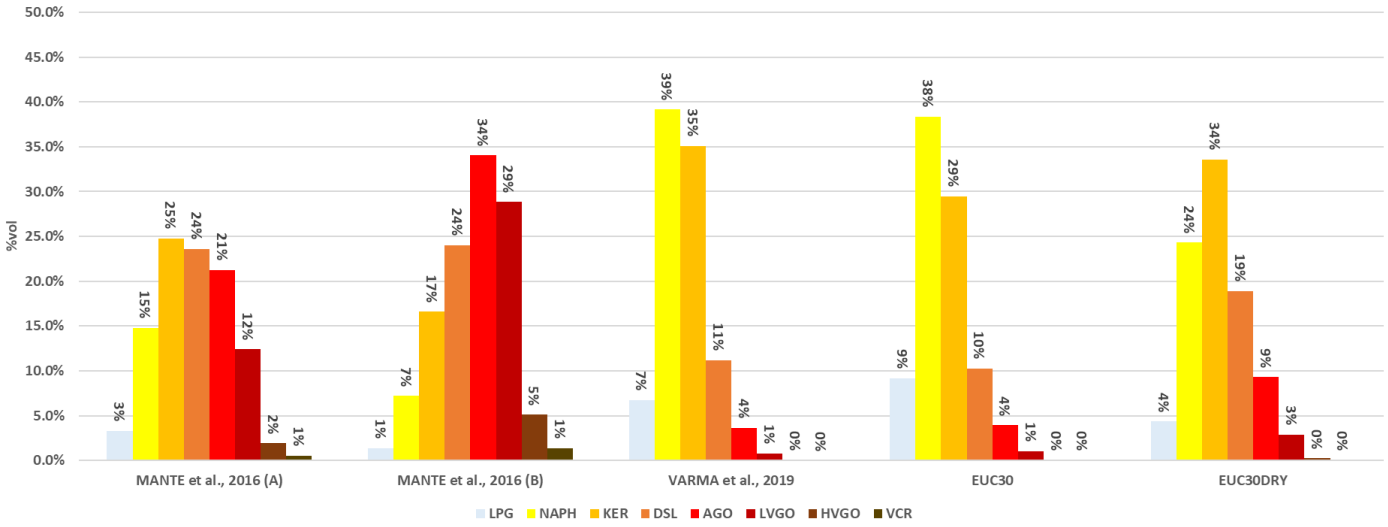

Figure 5.3. Theoretical approximate products distribution for bio-oils from literature and this work (equation 4M used – B1, B2, T0 parameters)

5.1.2 Crude oil Data

Brazilian crude oil was retrieved from several sources in literature, to obtain distillation curves and densities. Table 5.6 and 5.7 show the source and properties of each crude, as well as classification through °API and Watson K, divided by Santos and Campos basins, respectively.

Table 5.6. Santos basin selected information of crude oil assays

Field	Tupi (2011)	Sapinhoá (2015)	Iracema (2015)	Lapa (2018)	Mero (2019)	Sururu (2020)	Atapu (2021)	Sepia (2022)
Source	Aspen Hysys®	Aspen Hysys®	Aspen Hysys®	Total Energies	Total Energies	Total Energies	Total Energies	Total Energies
SG	0.8780	0.8198	0.8424	0.8386	0.8822	0.8843	0.8851	0.8911
°API	29.7	41.1	36.5	37.2	28.9	28.5	28.4	27.3
Classification API	Medium	Light	Light	Light	Medium	Medium	Medium	Medium
Watson K	10.8	11.0	11.2	11.8	11.1	10.8	10.9	10.8
Classification K	Naphthenic	Naphthenic	Naphthenic	Naphthenic	Naphthenic	Naphthenic	Naphthenic	Naphthenic
S (wt%)	0.283	0.379	0.281	0.570	0.320	0.350	0.400	0.400

N (wt%)	0.198	0.255	0.213	0.213	0.250	0.260	0.310	0.260
IBP	-161.48	-46.17	-37.37	-56.35	-0.54	-38.19	-23.13	-0.05
T5%	106.84	83.82	74.53	100.34	109.25	59.61	56.82	67.53
T10%	150.78	109.83	114.64	148.72	157.00	110.61	103.17	114.84
T30%	232.14	169.93	163.18	311.09	317.31	247.36	238.61	265.29
T50%	363.26	224.46	318.46	459.91	464.50	369.57	376.66	400.44
T70%	509.60	297.74	451.91	611.05	613.42	504.50	536.55	535.80
T90%	598.98	396.64	667.66	806.26	807.78	717.28	719.65	678.00
T95%	612.65	709.50	717.05	883.93	884.79	825.45	808.48	715.23
FBP	856.04	904.81	912.00	945.28	945.56	929.69	897.31	753.29
Light-Ends (wt%)								
Methane+Ethane	0.0180	0.0019	0.0025	0.0000	0.0000	0.0000	0.1000	0.0000
Propane	0.1484	0.0461	0.0635	0.1000	0.1000	0.5000	0.4000	0.4000
Iso-Butane	0.4093	0.3396	0.4842	0.1000	0.0000	0.3000	0.2000	0.2000
N-Butane	0.2878	0.3355	0.4862	0.2000	0.1000	0.7000	0.4000	0.5000
Iso-Pentane	0.3797	1.1023	1.1257	No data	No data	No data	No data	No data
N-Pentane	0.1752	0.3704	0.4506	No data	No data	No data	No data	No data
Cyclopentane	0.2489	0.3293	0.5491	No data	No data	No data	No data	No data

As can be seen, oils with different characteristics could be retrieved, including several from Pre-salt fields, all the examples present in Table 5.6. The pre-salt oil is considerably lighter than conventional crude found in Campos basin, with predominant naphthenic classification and lower sulfur and nitrogen contents than similar API crudes found outside pre-salt formation.

As stated in section 3.4, bio-oil coprocessing tend to increase complexity and spend regarding hydrotreating processes, in this sense, pre-salt oils lower aromatic and heteroatoms content exposes a possible window for insertion of a more costly raw material in the chain.

Table 5.7A. Campos basin selected information of crude oil assays

Field	Marlim (1997)	Albacora Leste (2009)	Polvo (2009)	Roncador Leve (2011)	Frade (2012)	Peregrino (2013)	Roncador Heavy (2014)	Tubarão Martelo (2014)[a]
Source	Aspen HYSYS®	Aspen HYSYS®	Aspen HYSYS®	Equinor Energy	Aspen Hysys®	Equinor Energy	Equinor Energy	PetroRio S.A.
SG	0.9296	0.9297	0.9293	0.8867	0.9019	0.9750	0.9347	0.9279
°API	20.7	20.7	20.8	28.1	25.4	13.5	19.9	21.0
Classification API	Heavy	Heavy	Heavy	Medium	Medium	Heavy	Heavy	Heavy
Watson K	10.6	10.6	10.3	10.7	10.7	10.3	10.5	10,0
Classification K	Naphthenic	Naphthenic	Aromatic	Naphthenic	Naphthenic	Aromatic	Aromatic	Aromatic
S (wt%)	0.462	0.406	0.402	0.536	0.265	1.790	0,673	1.060
N (wt%)	0.440	0.380	0.457	0.308	0.484	0.731	0,387	0.530
IBP	-59.87	-57.79	-161.48	-65.07	-161.48	16.93	-67.31	45.22
T5%	115.24	116.58	110.63	66.92	124.46	159.84	124.36	96.67
T10%	185.89	187.29	129.79	119.35	149.37	232.38	178.41	109.25
T30%	336.42	337.10	239.11	247.55	246.04	387.14	339.99	187.78
T50%	465.90	466.35	427.59	371.33	388.62	502.81	440.70	287.06
T70%	573.53	573.78	544.65	484.72	501.59	623.65	542.68	435.87
T90%	708.14	708.25	639.67	629.73	772.39	797.98	702.84	558.00
T95%	760.55	760.98	674.99	696.83	800.82	881.58	758.09	692.52
FBP	875.87	874.16	856.04	780.84	851.57	965.19	875.97	827.25
Light-Ends (wt%)								
Methane+Ethane	0.0595	0.0053	0.0207	0.0900	0.0222	0.0000	0.0700	No data
Propane	0.3500	0.1215	0.2066	0.5200	0.0877	0.0509	0.1900	No data
Iso-Butane	0.1858	0.0597	0.1446	0.3100	0.1734	0.0619	0.0800	No data
N-Butane	0.4153	0.1947	0.3926	0.5400	0.0980	0.1256	0.1200	No data
Iso-Pentane	0.2994	0.2626	0.2893	0.3800	0.1605	0.1364	0.1100	No data
N-Pentane	0.2290	0.1616	0.5457	0.4600	0.0570	0.1371	0.1200	No data
Cyclopentane	0.1196	0.0725	No data	0.1100	0.0051	0.0382	0.0400	No data

[a]Tubarão Martelo (2014) field assay only contained fractions analysis; 90 vol% distilled considered at 556 °C - similar to Polvo field (< 7 km distance).

Table 5.7B. Campos basin selected information of crude oil assays (cont.)

Field	Tubarão Marterlo (2021)	Frade (2022)	Albacora Leste (2023)	Peregrino (2024)
Source	PetroRio S.A.	PetroRio S.A.	PetroRio S.A.	Equinor Energy
SG	0.9317	0.9289	0.9263	0.9700
°API	20.4	20.8	21.3	14.4
Classification API	Heavy	Heavy	Heavy	Heavy
Watson K	10.6	10.6	10.3	10.7
Classification K	Naphthenic	Naphthenic	Naphthenic	Aromatic
S (wt%)	1.040	0.708	0.556	1.630
N (wt%)	0.424	0.361	0.361	0.602
IBP	-12.00	-2.92	17.10	-0.05
T5%	126.23	108.65	99.49	156.15
T10%	187.14	145.43	133.02	222.66
T30%	327.37	309.23	310.17	381.97
T50%	439.80	451.87	456.28	506.21
T70%	560.61	568.52	584.14	630.91
T90%	716.99	765.93	784.43	773.97
T95%	767.43	862.06	872.62	815.17
FBP	825.53	940.38	943.43	859.56
Light-Ends (wt%)				
Methane+Ethane	0.0100	0.0211	0.0102	0.0100
Propane	0.1100	0.1065	0.0553	0.0600
Iso-Butane	0.0800	0.0925	0.0603	0.0500
N-Butane	0.2000	0.1859	0.1620	0.0900
Iso-Pentane	0.1700	0.1667	0.1583	0.1400
N-Pentane	0.2400	0.2033	0.2561	0.1500
Cyclopentane	0.0600	0.0398	0.0487	0.0400

Campos basin crudes, however, increase refineries costs due to 'bottom barrel' processing, which could be attenuated by blends with lighter fractions, including bio-oil, especially if FCC's has idle capacity. The theoretical products distribution of each crude retrieved can be seen in Figures 5.4 and 5.5, and the parameters used in Equation 4L/4M in Table 5.8. Cut temperatures used for the generation of these distributions are shown in Table 5.8

It can be seen that pre-salt crudes are especially favorable for producing middle atmospheric distillates directly destinated to hydrotreatment processes such as naphtha, kerosene and diesel fractions, corresponding to about 40% of whole crude. Average SG reported was 0.8750 (min.: 0.8198; max.: 0.9169), and also lower levels of sulfur 0.373 wt.% (min: 0.281 wt.%; 0.570 wt.%) and nitrogen 0.245 wt.% (min: 0.198 wt.%; max: 0.310 wt.%).

Table 5.8. Adjusted parameters for selected crude oils

Field	A1	A2	A3	T0	R^2	B1	B2	T0	R^2
Marlim (1997)	0.0471	1.2406	3.0118	534.93	0.9968	1.0539	0.0075	476.15	0.9984
Albacora Leste (2009)	0.0463	1.2432	3.0094	536.00	0.9969	1.0541	0.0075	476.69	0.9984
Polvo (2009)	0.0186	1.4627	2.0069	548.50	0.9715	1.0772	0.0071	433.35	0.9849
Roncador Light (2011)	0.0367	1.3465	2.1793	477.84	0.9985	1.0280	0.0080	380.19	0.9964
Tupi (2011)	0.0076	1.2074	2.3779	406.00	0.9757	1.0296	0.0083	377.79	0.9839
Frade (2012)	-0.1952	1.7309	1.2391	589.44	0.9957	0.9780	0.0083	382.46	0.9889
Peregrino (2013)	0.0121	1.2107	2.9505	567.06	0.9994	1.0138	0.0076	511.18	0.9982
Roncador Pesado (2014)	0.0530	1.1276	3.4726	482.54	0.9991	1.0198	0.0083	447.52	0.9993
Tubarão Martelo (2014)	-0.0388	1.1932	1.8834	328.42	0.9951	0.9728	0.0099	302.96	0.9778

Iracema (2015)	-0.1082	1.4282	1.2907	413.27	0.9887	0.9796	0.0083	323.19	0.9798
Sapinhoa (2015)	0.0198	0.9969	3.3592	225.87	0.9960	0.9668	0.0161	227.43	0.9938
Lapa (2018)	0.0128	1.5275	1.8789	677.21	0.9997	1.0230	0.0064	474.74	0.9948
Mero (2019)	0.0088	1.5075	1.9234	667.93	0.9997	1.0190	0.0066	477.72	0.9940
Sururu (2020)	0.0383	1.1999	2.1319	444.07	0.9997	0.9840	0.0078	373.77	0.9944
Atapu (2021)	0.0210	1.4728	1.6672	572.07	0.9993	1.0020	0.0071	391.15	0.9907
Tubarão Martelo (2021)	0.0189	1.3526	551.24	2.5338	0.9993	0.9316	422.43	0.0085	0.9982
Sepia (2022)	0.0047	3.1851	1305.26	1.4305	1.0000	0.8782	359.74	0.0077	0.9963
Frade (2022)	0.0371	1.2498	535.35	2.4105	0.9980	1.0076	451.23	0.0072	0.9959
Albacora Leste (2023)	0.0102	1.4638	630.37	1.9233	0.9983	1.0122	459.91	0.0069	0.9950
Peregrino (2024)	0.0120	1.6120	707.50	2.4602	1.0000	0.8634	463.47	0.0082	0.9986

Note: some crude R^2 results are equal to 1, which could indicate bad equation fitting.

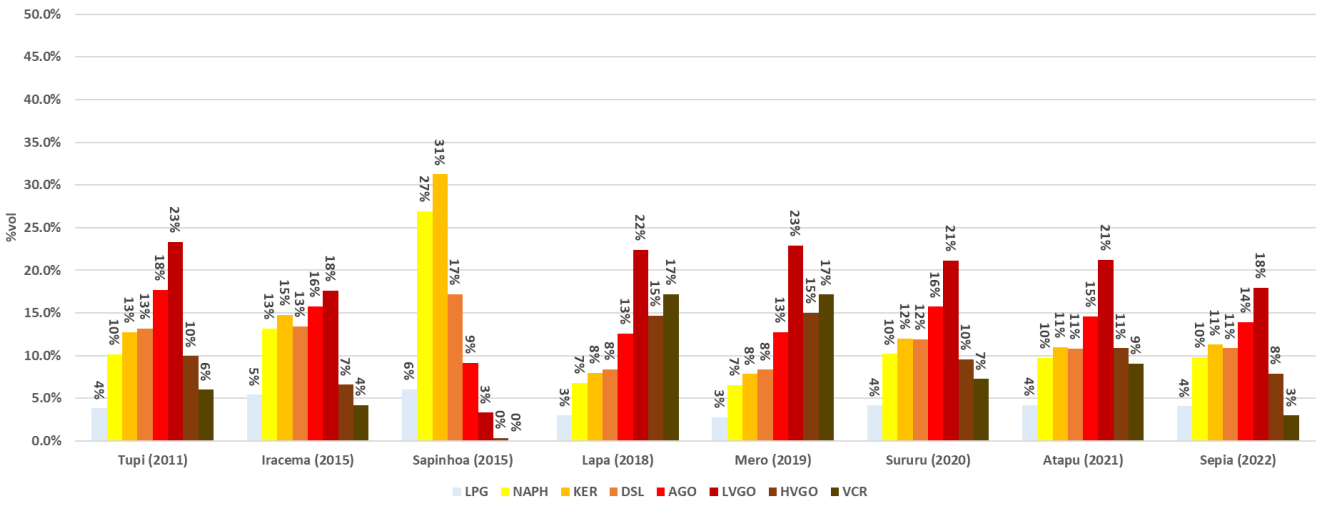

Figure 5.4. Santos basin theoretical products distribution (avg. total sum of fractions error ~ 5%)

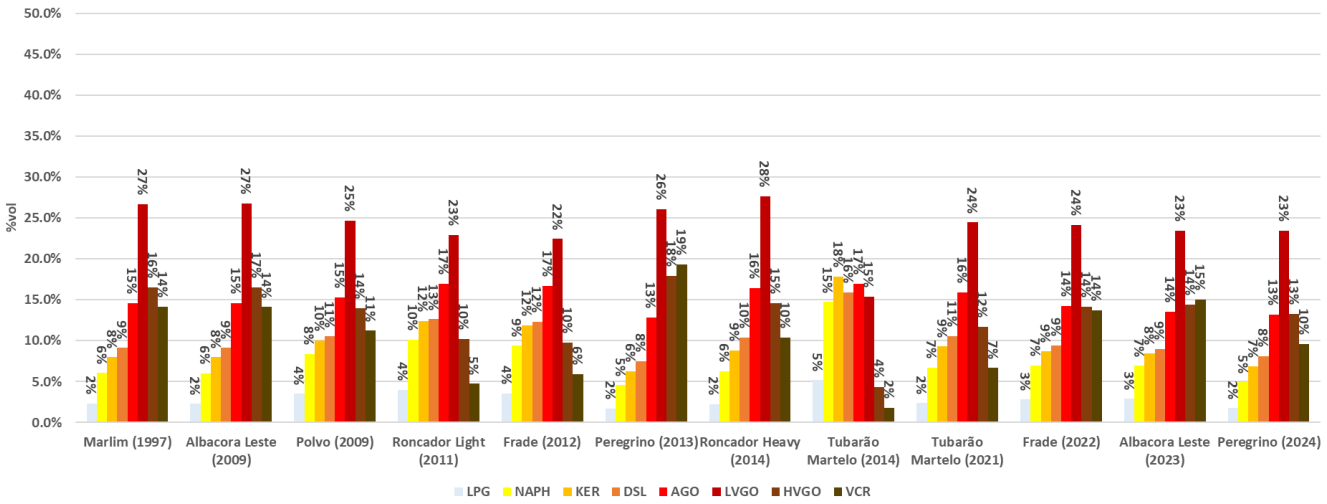

Figure 5.5. Campos basin theoretical products distribution (avg. total sum of fractions error ~ 5%)

Campos basin oils, oppositely, are more suitable for bottom distillates, such as atmospheric and vacuum gasoils destinated to the FCC, which correspond to 52% of crude volumes (excludes vacuum residue). Average SG of 0.9310 (min: 0.9019; max 0.9750), sulfur 0.794 wt.% (min: 0.265 wt.%; max: 1.790 wt.%) and nitrogen 0.455 wt.% (min: 0.361 wt.%; max: 0.731 wt.%).

5.2 Simulation

5.2.1 Desalting Unit and Heating Train

All crudes were evaluated to be blended with EUC30 and other developed bio-oils in this work. Since the number of possible combinations is too extensive, results focused on simulating a 10% blend (10% bio-oil/90% crude oil), with the latest data available, from Mero pre-salt field. Future work is suggested to evaluate the other combinations.

This percentage is an estimation following Pinho *et al.* (2017) experiments, where 10% bio-blends were the threshold to apparent quality issues in FCC coprocessing products. In the same way, Mero field was selected also due to lower lighter fractions (LPG and Naphtha) and lower sulfur/nitrogen contents than average, suitable to receive a higher load of light oxygenated compounds, as it is seen in Figures 5.6. and 5.7.

Initially, BIO1030 (code to more easily represent the 10% blend of EUC30 in crude) forms a two-phase flow as expected. In the desalting process (Figure 5.8), approximately 45 wt.% of total green content is lost in waste water stream, as the remaining 55 wt.%, approx. 2 wt.% is carried by gas stream (obtaining LPG-like fraction when stripped or mixed to full range naphtha stream) and 43% is maintained in organic phase. An optimization block was built in Aspen Plus® to vary both temperature and pressure inside desalting operation, focused on minimizing the loss of green content. A sensitivity analysis of this optimization can be seen in Figure 5.9.

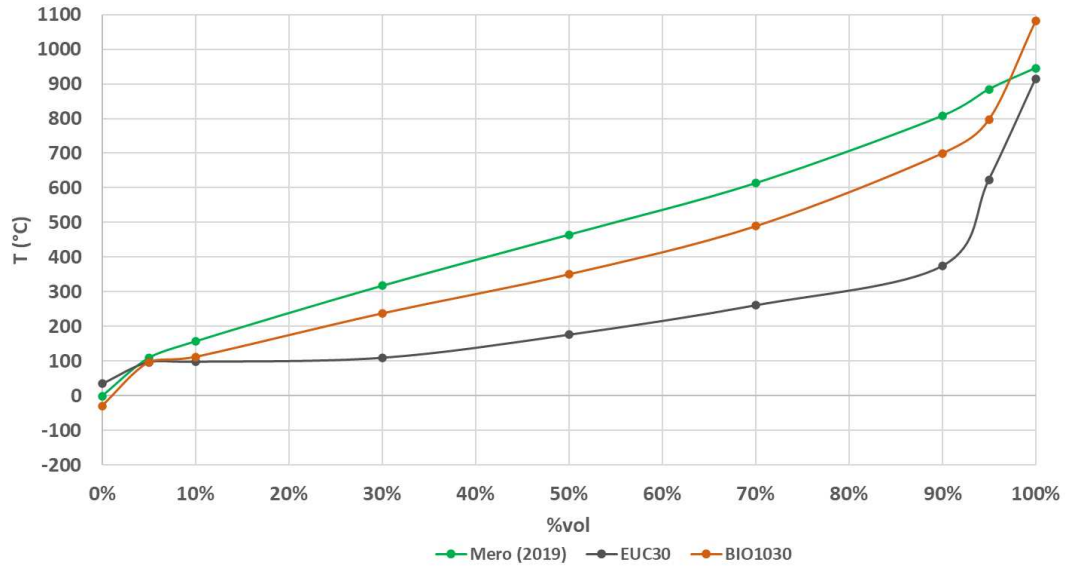

Figure 5.6. Distillation curves of Mero field, EUC30 and BIO1030

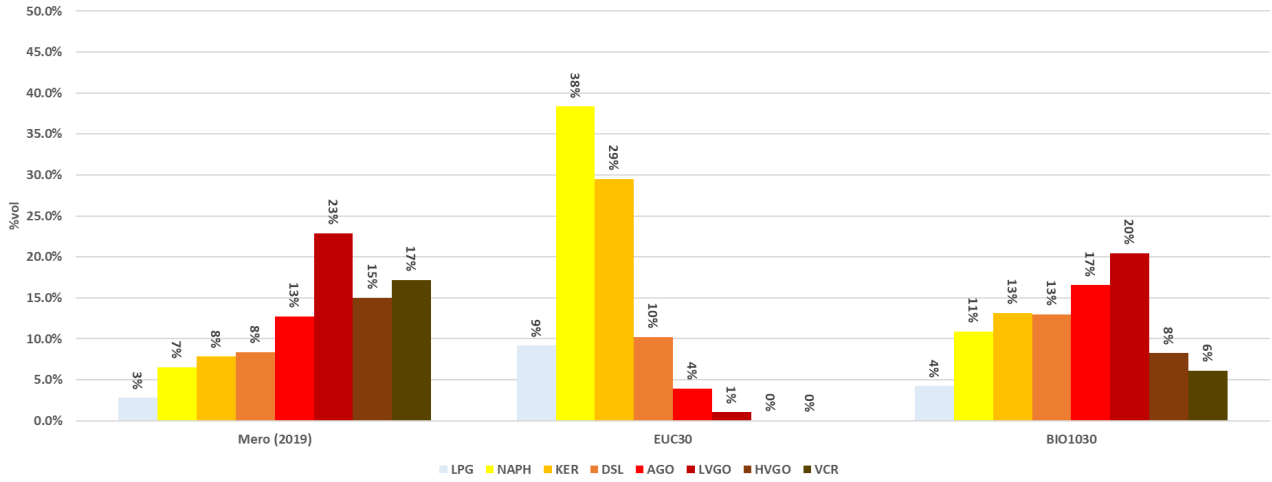

Figure 5.7. Theoretical products distribution for Mero field, EUC30 and BIO1030

Simulation was initially defined, for these preliminary results, without heat exchangers optimization, which included pumparounds and product streams redirecting. This dramatically simplified calculations, that will be addressed to the final version of this work. The cut temperatures used as standard are shown in section 4.3.

In boundary conditions of temperature and pressure, desalting unit separates 62 to 67 wt.% of total green content into waste water and gas streams combined, with most unfavorable condition presented at highest temperatures and lowest pressures, increasing solubility of green components.

The best condition was found at average temperatures range 100 to 140 °C and higher

pressures range 3 to 5 kgf.cm^{-2}, maintaining approximately 40 to 50 wt.% original green content in process oil stream. The optimizer was set to calculate this best condition, constrained to the values mentioned, according to feed specifications. Products from the desalting unit can be seen in detail in Table 5.9.

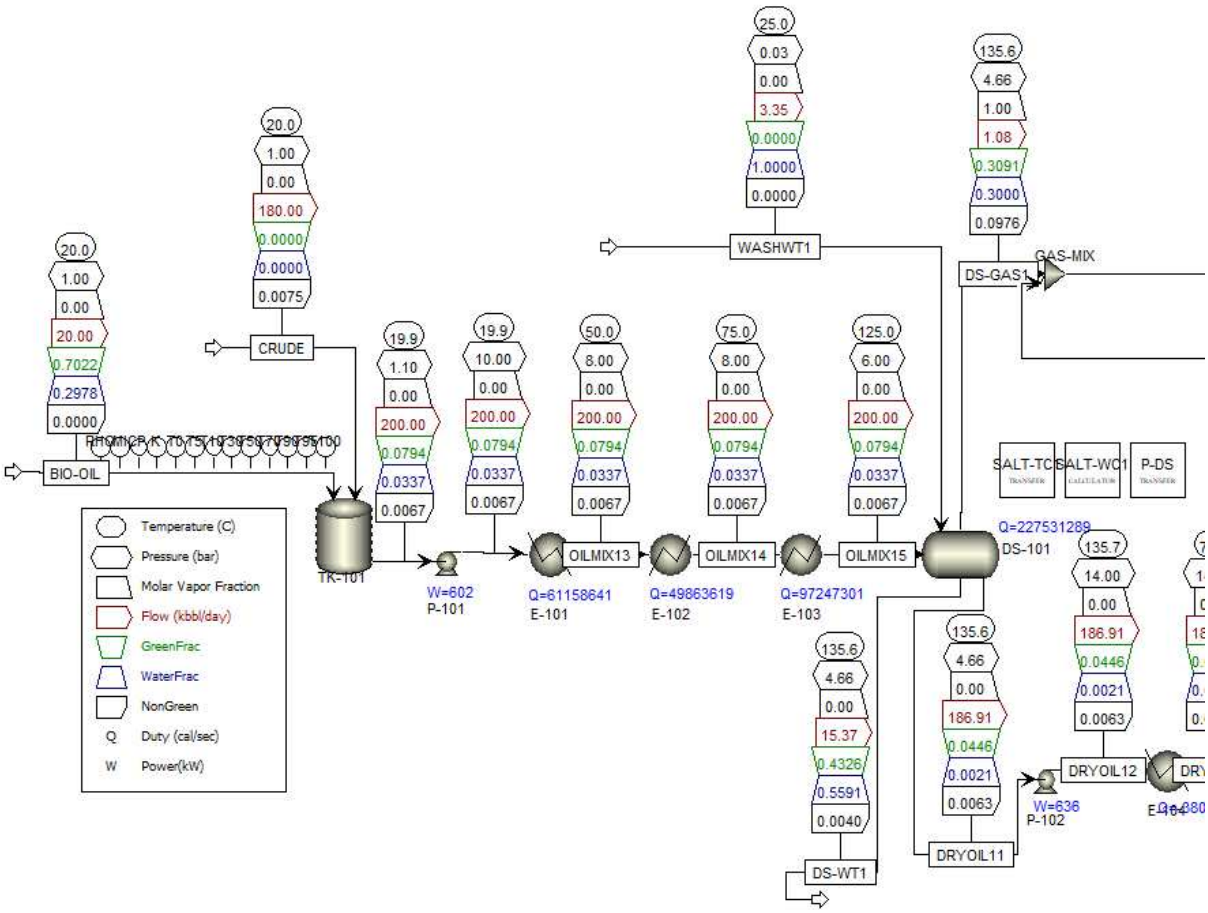

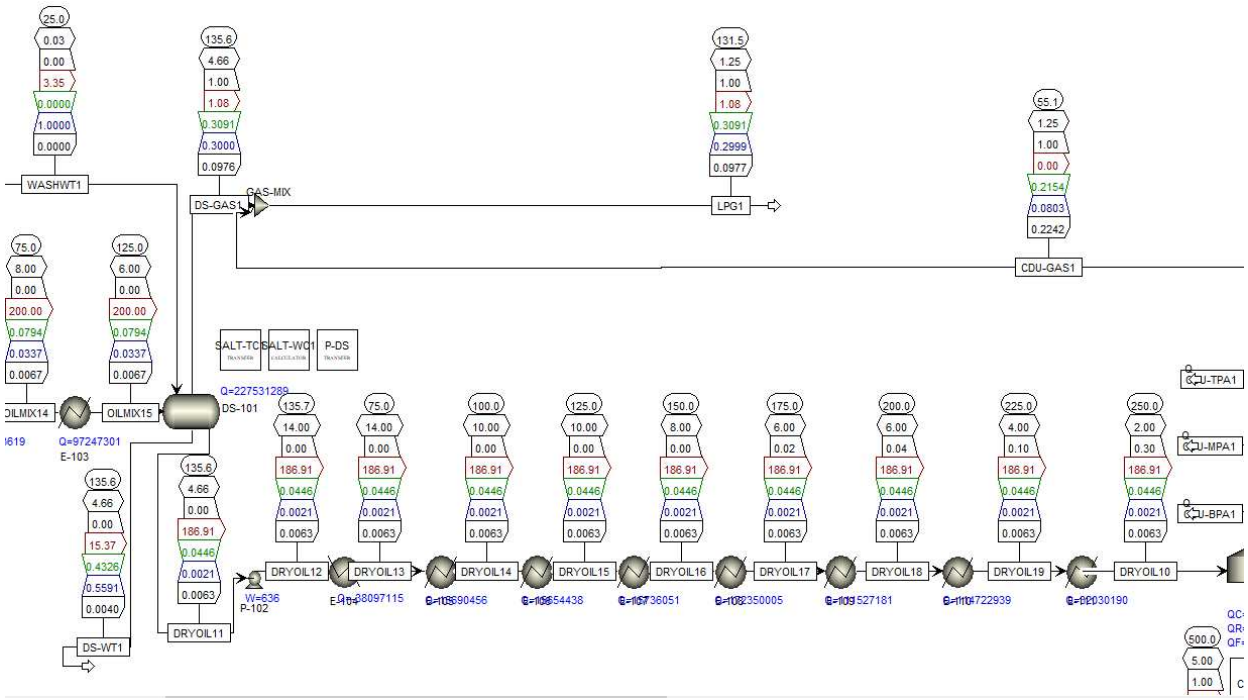

Figure 5.8. Desalting section in Aspen Plus® simulation

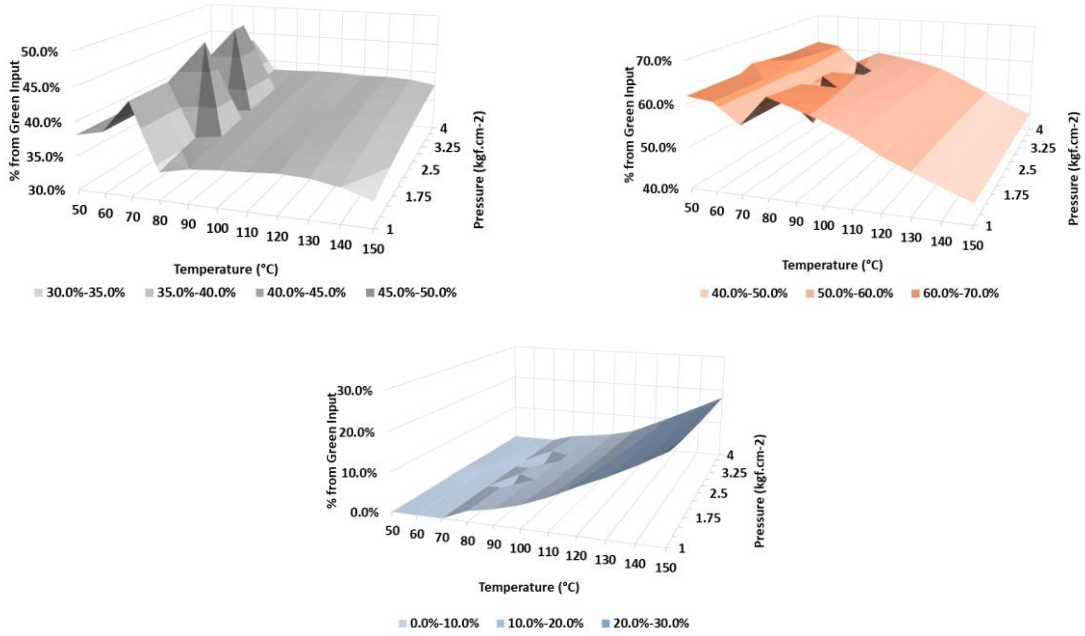

Figure 5.9. Desalter sensitivity analysis, showing green content of output oil (top left), waste water (top right) and gas (bottom) streams, subjected to temperature and pressure variation

The loss of green content could be a major concern in refinery operations, since waste water stream is aromatic-rich, costly to treatment. In the same way, gas stream which consist primarily by

light-ends and H_2S, is contaminated by oxygenated compounds impacting Merox conversion and amine removal units. Given these concerns, it's imperative that new approaches are investigated for this unit, as it may impact the outcomes of co-processing in the same magnitude or even more than the distillation itself.

In more detail, in the gas stream, where 30.91 wt.% are renewables, 23.69 wt.% of the 'green' ketones from feed are removed. While the liquid stream, with a renewable content of 4.46 wt.%, species extremely non-polar such as furans, ethers, esters and hydrocarbons, as well as, large lignin derived compounds are maintained and not washed away in the aqueous phase. With the exception of phenols and sugars, at least approx. 50 wt.% of the other groups are maintained.

The waste stream (water contaminated with organics, that shows 43.26 wt.% renewable content) 'washes' 99.99 wt.% of the sugars from feed, and more than 40 wt.% of acids, alcohols and phenols, all species with highly polar molecules, therefore, highly soluble in water. These results were expected, and an explicit indication that the desalting unit is a bottleneck for this kind of process. If no alternatives are found to mitigate this phase separation problem (e.g.: chemical additives in the desalting unit), the direct coprocessing of FPBO in the distillation area will likely not be a feasible option industrially. Physical properties of these streams are analyzed in the following section.

Table 5.9. Properties from products recovered in Desalter section

Stream	OILMIX15 (Feed)	DRYOIL11 (Organic Phase)	DS-GAS1 (Vapor)	DS-WT1 (Aqueous Phase)
H_2O (wt%)	3.37	0.21	30.00	55.91
Green (wt%)	7.94	4.46	30.91	43.26
H_2S (wt%)	0.24	0.20	4.03	0.38
Mercaptans (wt%)	0.04	0.05	0.05	0.01
Nitrogen Compounds (wt%)	0.22	0.22	2.86	0.00
IBP	-28.74	-11.00	-79.20	-50.36
T5%	97.01	96.68	-54.10	97.32
T10%	112.25	125.40	6.76	97.81
T30%	237.05	247.98	86.35	99.80
T50%	350.22	366.45	100.16	100.33
T70%	488.75	501.31	123.86	240.58
T90%	700.44	710.40	144.01	321.85
T95%	797.23	797.50	148.71	376.17
FBP	1086.91	1076.67	286.11	1771.86
Light-Ends (wt%)				
Methane+Ethane	0.00	0.00	0.00	0.00
Propane	0.08	0.08	1.61	0.01
Iso-Butane	0.08	0.08	1.21	0.01
N-Butane	0.00	0.00	0.00	0.00
N-Pentane[a]	0.97	1.00	7.18	0.07
N-Methyl Pentane[a]	0.53	0.56	2.85	0.02

N-Hexane[a]	0.71	0.75	2.99	0.03
N-Methyl Hexane[a]	0.95	1.00	2.99	0.04
N-Heptane[a]	1.37	1.46	3.11	0.04
N-Methyl Heptane[a]	1.68	1.79	2.81	0.06

[a]Estimated by pseudocomponents boiling point
PC34C, PC59C, PC73C, PC87C, PC101C, PC113C.

5.2.2 Crude Distillation Unit

As seen before, the 'dry' BIO1030 was pumped from the desalting unit containing 0.21 wt.% water and 4.46 wt.% green components. After heating up to 250 °C in heat train, it passed through the furnace of the atmospheric distillation unit, to then be separated between CDU Gas (mixed with Desalting gas and labeled as LPG), naphtha, kerosene, diesel and atmospheric gasoil fractions (Figure 5.10). Table 5.10 shows a summary of most important properties from the streams detailed.

Atmospheric distillation produced a top gaseous stream with 27.36 wt.% green compounds and 6.04 wt.% water vapor content. This stream is mixed with the desalting unit and labeled as LPG, which had 33.73 wt.% renewable content (0.32 wt.% of renewable total feed) (most of it coming from the desalting unit) and 11.11 wt.% water.

The LPG stream contained 13.2 wt.% of the ketones from the feed FPBO, which was expected considering the desalter gas stream. As for non-renewable content, it was mainly C5-C8 (~29.89 wt.%) not incorporated in naphtha, C10-C12 not condensed in kerosene fraction (~5.29 wt.%) and C3-C4 (~6.96 wt.%).

Distillation temperatures deviate from standard limits defined, which can be directly seen by temperature measurement, but also confirmed by two different perspectives. The first is the boiling point of some green groups, which are about 100 °C higher than average boiling point desired. The second indicator is the distribution of the hydrocarbons present in the stream, as gas stream should be propane and butane-rich, and light naphtha should contain high mass percentages of pentanes and hexanes, with low content of lighter or heavier compounds.

According to ANP, total pentanes should not exceed 2 %vol and total sulfur 0.014 wt.% in final LPG product, which by the explanations above, couldn't be met. In this case, gas stream must be optimized towards the removal of C5+ compounds through top stage/condenser temperature lowering, while naphtha has to be purified through a stripper column, that was removed priorly to simplify calculations.

Naphtha stream presented wider cut temperatures than expected. It presented light gases content of 3.01 wt.%, probably C3-C4 condensed or entrained in naphtha. The desired fraction, C5-

C8, presented ~59.99 wt.%, while higher BP fractions (C8-C12) ~22.32 wt.%, and renewable content of 11.74 wt.% (4.86 wt.% of total renewable feed). Green content was composed mainly by acids (5.14 wt.%, 43.69 wt.% of total feed), phenolics (2.39 wt.%, 8.91 wt.% of total feed) and ketones (2.06 wt.%, 31.63 wt.% of total feed). In the same way as non-green components, renewable percentages also have been affected by higher cut temperature, as phenolics should usually be in heavier fractions (average boiling ranges around 250 °C).

According to ANP, final gasoline produced from naphtha must have total sulfur not exceed 0.005 wt.%, SG equals to 0.715, T10% min of 65°C, T50% max of 80 °C, T90 equals to 190 °C, FBP below 215 °C, octane numbers of 82/93 (MON/RON), benzene and aromatics below 1 vol% and 35 vol%, respectively. The properties measured show that sulfur and higher-end cut temperatures are in line with the regulations, but lower-end cut temperatures and density are deeply affected by lighter hydrocarbons and green content, confirming that co-processing will need naphtha splitters and petrochemical units fed by petrochemical light naphtha will be both benefited and impacted by renewable content.

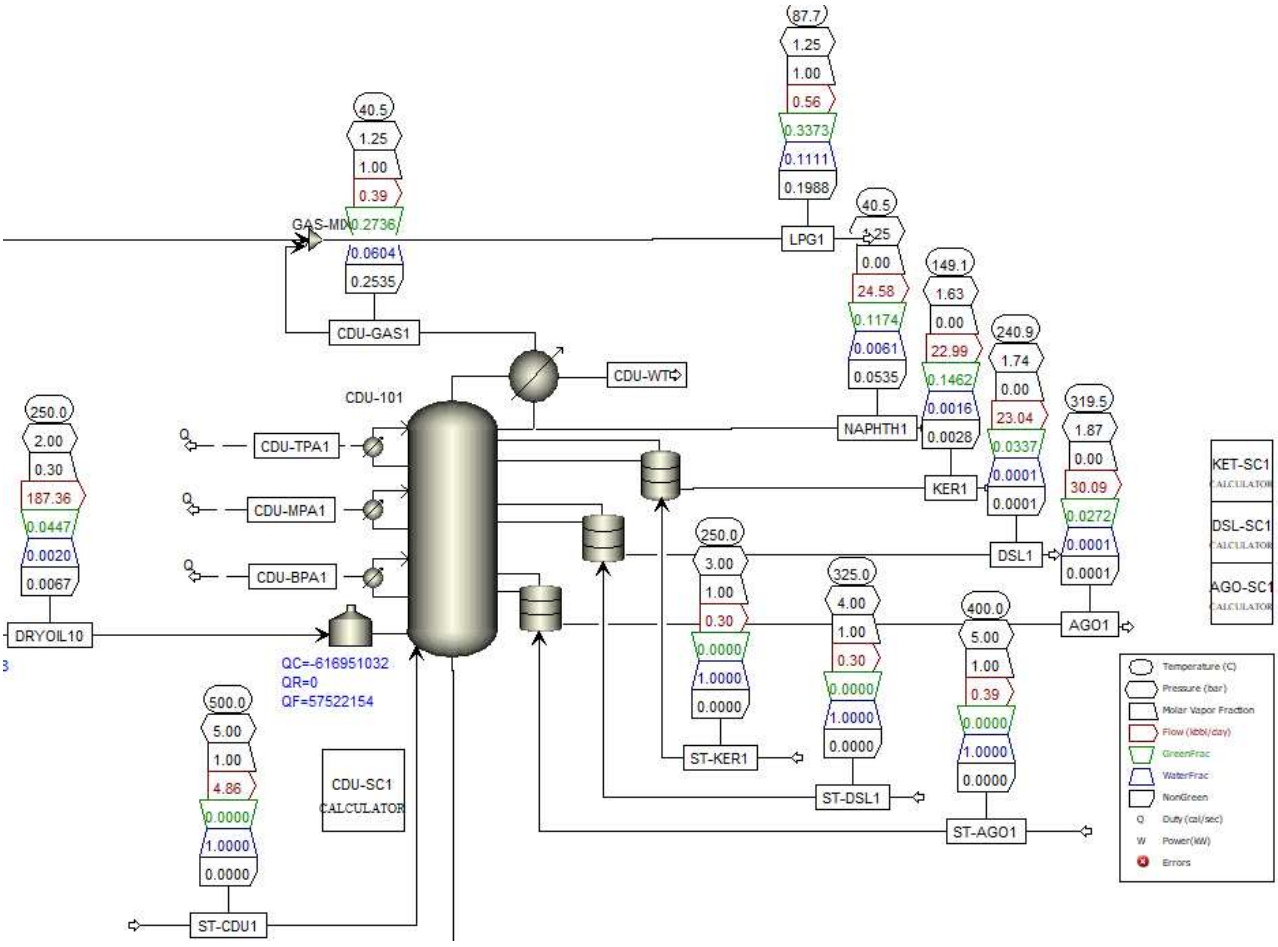

Figure 5.10. Atmospheric distillation section in Aspen Plus® simulation

In the same way, kerosene stream also presented tails cut temperatures out of the desired range. This stream was composed mainly by C10-C12 (~60.09 wt.%), but also presenting C5-C8 (~14.77 wt.%) and C14-C18 (10.06 wt.%) and renewable content of 14.62 wt.% (6.04 wt.% of total renewable feed), mainly composed by phenolics (8.19 wt.%, 30.50 wt.% of total feed) and furans (2.73 wt.%, 68.43 wt.% of total feed). These percentages explain the tails temperatures out of the desired range, as C5-C8 and furans represent components from naphtha boiling point range, and C14-C18 fractions and phenolics represent components on the diesel range.

For final jet fuel product, ANP defines max sulfur 0.3 wt.%, SG between 0.771-0.837, T10% max of 205 °C, FBP of 300 °C, aromatics max 25 vol%, flash point min 38 °C, freeze point max -47 °C and viscosity (20 °C) max of 8 mm^2/s. Most of these specifications weren't met, pushed by higher amounts of lighter components not stripped.

For the Diesel stream, the same cut temperature shift also can be seen, but with lower intensity. Non-renewable content presented was 84.84 wt.% for C14-C18 and 9.00 wt.% for C10-C12, while 3.37 wt.% for renewable content. The green fraction (3.37 wt.%, 1.45 wt.% of total renewable feed) was mainly composed of lignin derived components (2.32 wt.%, 9.28 wt.% of total feed). Analyzing these percentages, the cut temperatures were mainly impacted by C10-C12 (kerosene fractions).

Table 5.10. Properties from products recovered in CDU section

Stream	CDU GAS	LPG (mixed with desalting unit gas)	NAPH	KER	DSL	AGO	ATR
H_2O (wt%)	6.04	11.11	0.61	0.16	0.01	0.01	0.01
Green (wt%)	27.36	33.73	11.74	14.62	3.37	2.72	1.36
H_2S (wt%)	15.16	11.43	1.68	0.04	0.00	0.00	0.00
Mercaptans (wt%)	0.08	0.07	0.27	0.14	0.00	0.00	0.00
Nitrogen Compounds (wt%)	1.04	1.44	2.09	0.39	0.04	0.11	0.00
IBP (°C)	-48.32	-52.24	-11.08	106.51	180.51	235.22	328.25
T5% (°C)	-37.82	-40.92	37.73	143.48	212.68	279.00	372.56
T10% (°C)	-33.46	-36.19	62.07	159.92	226.50	298.18	391.66
T30% (°C)	-2.29	45.77	95.80	174.73	243.38	318.73	450.35
T50% (°C)	65.85	101.44	115.83	183.65	254.14	334.09	513.20
T70% (°C)	109.96	122.44	124.20	194.62	267.53	352.47	598.65
T90% (°C)	133.63	134.37	135.89	226.26	290.11	377.27	723.44
T95% (°C)	137.37	146.44	148.94	245.74	315.75	404.53	844.00
FBP (°C)	141.11	158.51	162.00	265.22	341.38	431.78	964.56
Spec. Density (20 °C)	0.003	0.002	0.813	0.766	0.734	0.738	0.616
Kin. Viscosity (20 °C) (cSt)	N/A*	N/A*	N/A*	N/A*	N/A*	N/A*	N/A*
Kin. Viscosity (40 °C) (cSt)	N/A*	N/A*	N/A*	N/A*	N/A*	N/A*	N/A*
Kin. Viscosity (80 °C) (cSt)	N/A*	N/A*	N/A*	N/A*	N/A*	N/A*	N/A*
Flash Point (°C)	-115.73	-118.58	-35.81	28.50	89.35	123.71	154.96
Pour Point (°C)	-204.22	-153.65	-80.60	-40.97	-15.14	-1.96	N/A

Cetane Number	23.83	28.19	21.06	21.91	24.70	20.79	13.03
Cloud Point (°C)	N/A*	N/A*	N/A*	N/A*	N/A*	N/A*	N/A*
Non-renewable (wt%)							
<C5	9.08	6.96	1.33	0.04	0.00	0.00	0.00
C5-C8	34.97	29.89	59.99	14.77	0.72	0.56	0.00
C10-C12	6.29	5.29	22.32	60.09	9.00	1.48	0.02
C14-C18	0.00	0.09	0.00	10.08	84.83	33.30	0.50
C20-C30	0.00	0.00	0.00	0.00	2.07	61.45	18.34
C32-C50	0.00	0.00	0.00	0.00	0.00	0.47	29.69
C52-C60	0.00	0.00	0.00	0.00	0.00	0.01	23.15
>C60	0.00	0.00	0.00	0.00	0.00	0.00	26.92

N/A*: properties couldn't be calculated in any run

For final diesel fuel product, ANP defines max sulfur 0.5 wt.%, SG between 0.815-0.850, T10% 180 °C, T50% between 245-295 °C, FBP 370 °C, flash point min 38 °C, viscosity (40 °C) between 2.0-4.5 mm^2/s, cetane number min 48 and water max 0.2 wt.%. In this case, cut temperatures are inside the desired ranges, as well as flash point and sulfur, but density is once again impacted by lower fractions present.

Lastly, atmospheric gasoil stream was composed of 61.45 wt.% C20-C30, 33.30 wt.% C14-C18, and 2.72 wt.% renewable content (1.62 wt.% of total renewable feed). Green components were majorly lignin derived compounds (4.64 wt.%, 18.52 wt.% of total feed). This composition also generated lower cut temperatures than desired, especially due to the diesel fractions present. No specific properties were analyzed for this stream, as it is generally fractionated is several other fractions, such as marine diesel and fuel oils.

To correct the deviation of lighter distillates, the design of the CDU unit must be improved. The modifications probably will affect stripper's draw stages and energy input (steam) to remove lighter components. For atmospheric kerosene, diesel and, mainly, atmospheric gasoil, the lighter tail of the distillation curve is also improved with higher energy input of stripping steam. This optimization is a topic for future work.

Another important aspect to review is the impact of different biocrudes that could be used. As could be seen, lighter petroleum fractions (LPG, Naphtha and Kerosene) are the ones that receive most renewable components from bio-oil, however, this can drastically change as these components become more stable and have their average boiling points increased, for example, after stabilization reactions caused both by natural processes (degradation of bio-oil) or industrial processes (reaction with alcohols, hydrotreating, etc.). Upgraded FPBO and HTL would probably generate more renewable content in heavier streams, especially diesel, fraction of most interest in most of Latin American countries. This investigation of the actual impact of upgrading is a topic for future projects.

5.2.3 Vacuum Distillation Unit

The CDU produced atmospheric residue that was pump to a vacuum distillation unit with only 1.36 wt.% renewable content (0.14 wt.% of total renewable feed) and almost no water (0.01 wt.%) (Figure 5.11). In the VDU (Figure 5.11), almost no renewable content is expected, and since most of these streams are first separated and then upgraded in hydrocrackers, coking units, etc., it is likely that green components are degraded.

However, heavier bio-oils do exist, especially after catalytic pyrolysis or hydrotreatment, as Mante *et al*. (2016) presented. In light of this fact, vacuum distillation unit was developed to better understand which kind of components are more inclined to be present in these streams, and how they behave in vacuum distillation together with heavy crude oil components.

Table 5.11. shows properties from products recovered. The top gaseous product, that usually is composed of sour water and some non-condensable gases, was in line with expectations with 22.63 wt.% water, 70.52 wt.% C20-C30 (gasoils), 4.62 wt.% C14-C18 (diesel), and only 0.71 wt.% renewable content mainly composed of lignin derived compounds (0.44 wt.%, 5.50 wt.% of total feed). In refineries, these gases are usually condensed as sour water and stripped to improve oil recovery.

Light vacuum gasoil fraction was produced with 67.55 wt.% C32-C50, 28.40 wt.% C20-C30 (gasoil), and virtually no other components, including renewable and water. This can be explained by the loss of the small fraction of green components to the top of the column, showing the need of improvements to be done in the simulation, especially on side products recycle, acting as internal scrubbers of these gases. In LVGO, cut temperatures observed were much more in line with expectations, compared to the cuts produced by the CDU. Still, the tails of the distillation curve (T0-10% and 90-100%) can be improved in the same way as mentioned before.

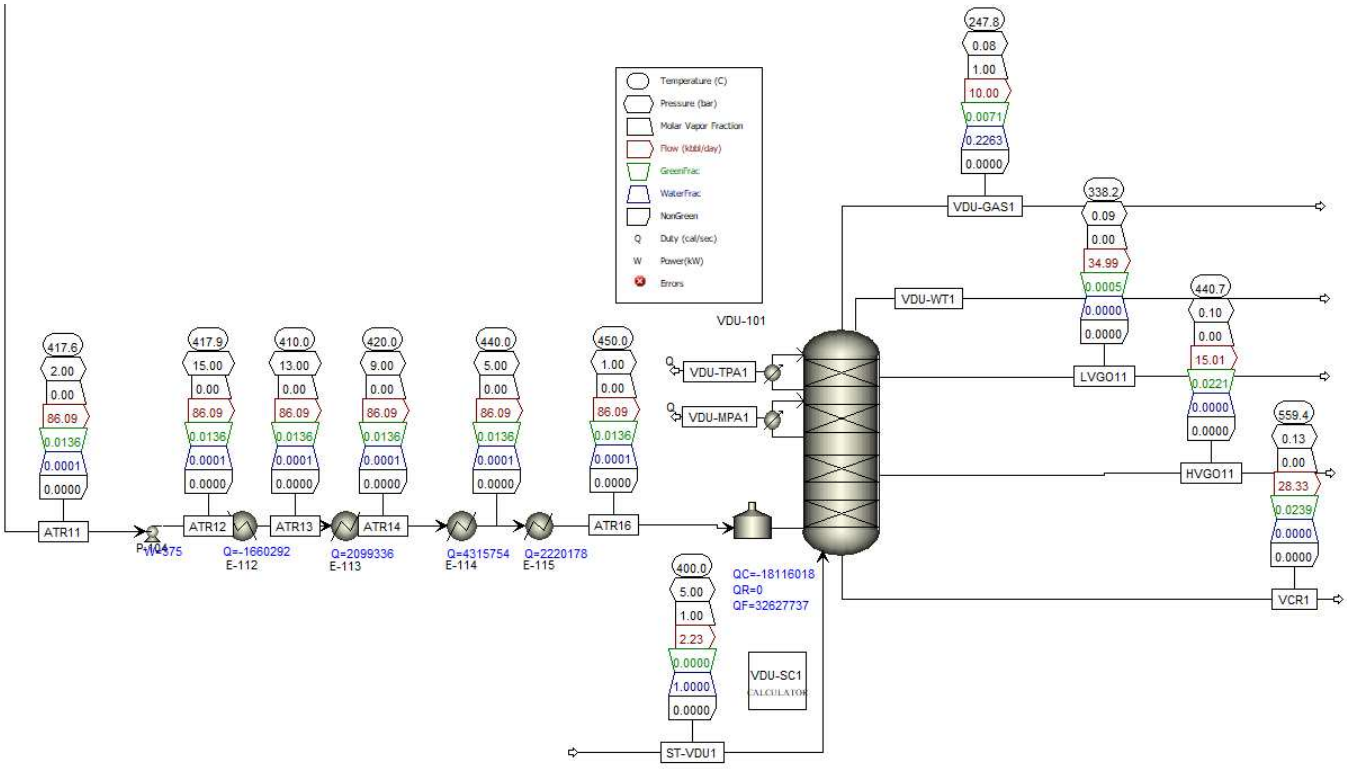

Figure 5.11. Vacuum distillation section in Aspen Plus® simulation

As for heavy vacuum gasoil, highest vacuum renewable content was observed 2.21 wt.% (0.68 wt.% of total renewable feed), with virtually no water present. Most of the HVGO is composed of C52-C60 (70.66 wt.%), C32-C50 (25.69 wt.%) and renewables, mainly lignin derived components (2.13 wt.%, 26.62 wt.% of total feed). This high content of the heavy components from FPBO indicate that pyrolysis efficiency in breaking down lignin as much as possible will impact bottom barrel conversion units in a co-processing scenario. Lastly, the cut temperatures of HVGO, differently from LVGO, are below the expectations, probably caused by a flow of stripping steam too low.

Table 5.11. Properties from products recovered in VDU section

Stream	VDU-GAS1	LVGO1	HVGO1	VCR1
H_2O (wt%)	22.63%	0.00%	0.00%	0.00%
Green (wt%)	0.71%	0.05%	2.21%	2.39%
H_2S (wt%)	0.00%	0.00%	0.00%	0.00%
Mercaptans (wt%)	0.00%	0.00%	0.00%	0.00%
Nitrogen Compounds (wt%)	0.01%	0.00%	0.00%	0.00%
IBP (°C)	163.28	390.86	436.25	524.39
T5% (°C)	166.44	410.85	487.13	560.21
T10% (°C)	167.68	418.97	509.01	575.06
T30% (°C)	340.14	437.31	526.80	621.41
T50% (°C)	366.26	455.36	539.00	674.58
T70% (°C)	376.74	476.34	556.86	707.95

T90% (°C)	397.39	507.28	578.82	863.84
T95% (°C)	417.10	529.34	610.99	929.05
FBP (°C)	436.80	551.39	643.15	994.26
Spec. Density (20 °C)	N/A*	0.775	0.747	1.067
Kin. Viscosity (20 °C) (cSt)	N/A*	N/A*	N/A*	N/A*
Kin. Viscosity (40 °C) (cSt)	N/A*	N/A*	N/A*	N/A*
Kin. Viscosity (80 °C) (cSt)	N/A*	N/A*	N/A*	N/A*
Flash Point (°C)	48.06	160.42	174.78	185.04
Pour Point (°C)	-35.27	4.96	-15.71	N/A
Cetane Number	18.76	25.36	22.58	14.65
Cloud Point (°C)	N/A*	N/A*	N/A*	N/A*
Non-renewable (wt%)				
<C5	0.00	0.00	0.00	0.00
C5-C8	0.03	0.00	0.00	0.00
C10-C12	0.22	0.00	0.00	0.00
C14-C18	4.62	0.01	0.00	0.00
C20-C30	70.52	28.40	0.75	0.00
C32-C50	1.27	67.55	25.69	0.23
C52-C60	0.00	3.98	70.66	26.61
>C60	0.00	0.00	0.68	70.77

N/A*: properties couldn't be calculated in any run

Finally, vacuum residue was produced with 2.39 wt.% renewable content (1.69 wt.% of total renewable feed) and virtually no water as well. Its composition is, as expected, formed by C60+ (70.77 wt.%), C52-C60 (26.61 wt.%) and the renewable lignin derived components (5.30 wt.%, 66.39 wt.% of total feed). The presence of HVGO fractions also impact lower-end cut temperatures, while renewables characterization shows the impact of which pyrolysis will have on refinery economics.

To improve the vacuum distillation unit, the same measures as CDU may be applied, increasing energy input to strip the lighter components. A cascade effect is seen in the VDU as well (LVGO presence in HVGO, HVGO in VCR). Although the VDU usually delivers its streams to conversion units, another importance of investigating and adjusting the simulation to correctly allocate the renewable contents in the correct streams is the fact that the whole intention of this work is leverage the production of renewable fuel and use of carbon credits. If the simulation does not reflect the correct components in each fraction, this could mislead the auditing of these credits.

5.3 Techno-Economical Analysis

5.3.1 Bio-oil Production Unit

Model pyrolysis plant was simulated separately in Microsoft Excel®, according to

specifications detailed in section 4.4. Input biomass was adapted to supply approx. 20 kbbl/day of bio-oil.

Not much public data is available on commercial-scale bio-oil production units. The company BTG Bioliquids mention a commercial unit of about 125 kbbl/year in Europe, while Ensyn reports 85 and 300 kbbl/year units (in Ontario and Quebec, Canada, respectively).

Given these references, to supply an average refinery of 200 kbpd capacity, the size of a FPBO would have to be twenty to thirty times the sizes of these units currently in operation. A unit of this size would need, at least, a 2 Mtonne/year supply of wood, which is approximately the same demand for a 700 ktonne/year kraft pulp plant (a small pulp unit, in general, as several pulp plants worldwide produce between 1.5 and 3.5 Mtonne/year pulp). With these considerations, it is not absurd, in terms of land and capacity, to evaluate a unit this size, however, in terms of risk and return of investment, as assessment between a pulp unit and a FPBO unit would have to be carried out.

In this study, it was assumed that bio-oil was produced and shipped directly from fast pyrolysis, without hydrotreating / hydrocracking, for this reason, unit either has to be integrated with refinery or the product must be transported hot, to prevent phase separation and polymerization.

Most of capital investment is directed to pyrolysis section (Table 5.12 and Figure 5.12.), while pre-treatment accounts for most of operational costs. The first result is mostly due to low pyrolysis technology knowledge, coupled with complexity of the system that, being exothermic, demands higher level of control. For the same reason, the exothermic process reduced operational costs, especially regarding utilities, in opposition to the pre-treatment section which deals with high humidity levels in biomass (50%).

Selling prices for bio-oil reach a minimum of 55.88 USD/bbl, approx. 86.1% of avg. crude oil price. However, in attractive prices condition, selling price of bio-oil is estimated as 63.79 USD/bbl, virtually equivalent to crude prices (as a reference, fuel oil for heating is worth about ~170 USD/bbl approximately, depending on crude prices). Literature reports several different minimum selling prices for biocrudes, depending on capacity, location of the plant, and many other parameters, so a comparison is almost irrelevant in this case, however, some examples are offered in this work (Zaini *et al*., 2021; Iglesias *et al*., 2021; Van Schalkwyk *et al*., 2020)

This result directs the efforts of coprocessing once again towards financial benefits of fossil substitution, for example tax subventions.

Table 5.12. Summarized results of bio-oil MSP simulation

Parameter	This Work (%)	This Work (Values)	Zaini et al. (2021)	Iglesias et al. (2021)	Van Schalkwyk *et al.* (2020)
Payback (years)[a]	-	14.42	-	-	-
Internal Rate of Return (IRR) (%)[a]	-	15.34	-	-	-
Net Present Value (MUS$)[a]	-	219.9	-	-	-
Bio-oil Minimum Selling Price (US$/bbl)	-	55.88	33.44 – 55.59[b]	70.9 – 117.80	-
Bio-oil Attractive Selling Price (US$/bbl)[a]	-	63.79	-	-	160.00
Crude oil Selling Price (US$/bbl)	-	64.91	-	-	-
CapEx (MUS$)	**100.0**	**1391.93**	-	-	-
Pre-treatment+Utilities	8.72	121.31	-	-	-
Pyrolysis	91.28	1270.63	-	-	-
OpEx (MUS$.year^{-1})	**100.0**	**79.78**	-	-	-
Pre-treatment+Utilities	56.67	45.22	-	-	-
Pyrolysis	43.33	34.57	-	-	-
Revenue (100% Bio-oil) (MUS$.year^{-1})[a]	-	421.03	-	-	-
EBITDA (MUS$.year^{-1})[a]	-	341.2	-	-	-
EBITDA Margin (%)[a]	-	81.05	-	-	-

[a]Set to return 5% of Capex invested, corrected by yearly inflation rate of 4.5%
[b]Approximated conversion

Although higher than desired, these results are in line with the study of Iglesias *et al.* (2021), that shows highest impacts on MSP allocated in plant capacity, bio-oil yield and operational expenses variations. Several authors reporting MSP higher than the obtained from the conditions of this work or Iglesias *et al*. (2021). This can be explained primarily by plant capacity impact as well as the absence of costly post-pyrolysis stabilization steps, such as hydrotreating, which were left for future work. (Vasalos *et al*., 2016).

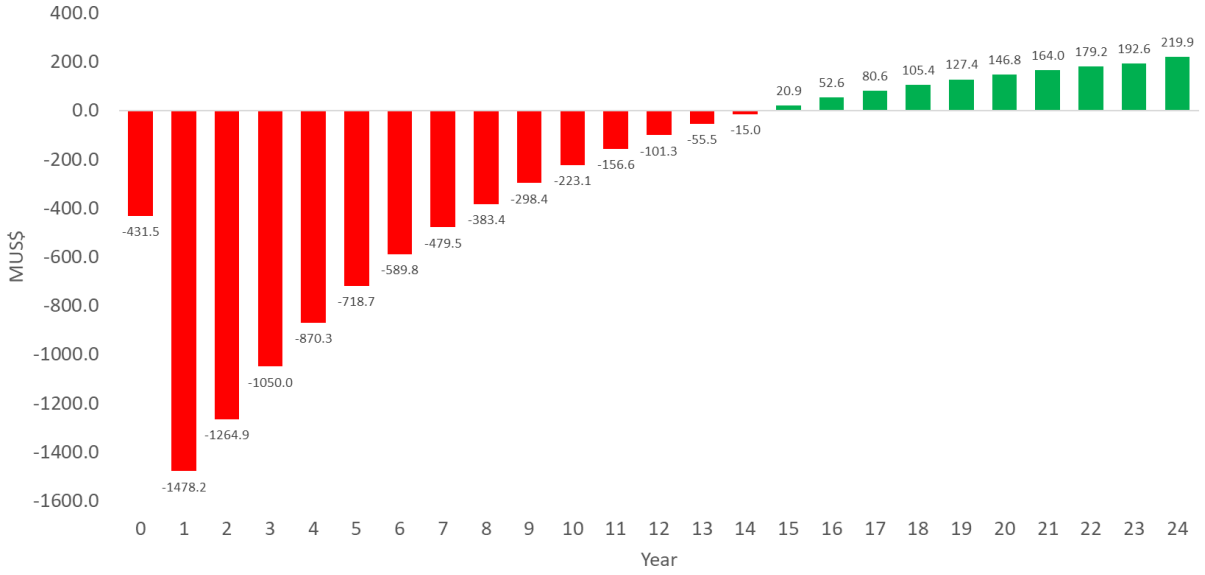

Figure 5.12. Discounted Cash Flow for pyrolysis unit at attractive selling price condition

5.3.2 Revenue and Costs

With simulation results for BIO1030, intermediary products prices were calculated, considering both the scenario with and without renewable percentages included (Table 5.13), which reduce LHV and consequently, price. In these preliminary results, only a direct calculation was made, leaving for the final version the complete simulation of a fossil distillation unit for comparison.

Table 5.13. Estimated price for renewable blends

Parameter	Fossil Price	Fossil LHV ($MJ.kg^{-1}$)	Renewable LHV ($MJ.kg^{-1}$)	Green (%)	Blend LHV ($MJ.kg^{-1}$)	Blend Price*	ΔPrice (%)	Revenue Reduction (MUSD/year)**
LPG (USD/L)	0.992	46.47	41.82	33.73	44.90	0.959	-3.37%	-1.09
Naphtha (USD/L)	0.776	43.54	39.19	11.74	43.03	0.767	-1.17%	-0.05
Kerosene (USD/L)	0.781	46.47	41.82	14.62	45.79	0.770	-1.46%	-0.06
Diesel (USD/L)	0.752	42.29	38.06	3.37	42.15	0.749	-0.34%	-0.02
AGO (USD/L)	0.707	43.35	39.01	2.72	43.23	0.705	-0.27%	-0.02
LVGO (USD/L)	0.687	44.43	39.99	0.05	44.43	0.687	-0.01%	0.00
HVGO (USD/L)	0.772	45.54	40.99	2.21	45.44	0.770	-0.22%	-0.01
VCR (USD/L)	0.638	46.68	42.01	2.39	46.57	0.636	-0.24%	-0.01
Total	-	-	-	-	-	-	-	-1.25

*Price estimated as proportional to LHV ratio between fossil and blend

It can be seen that, due to the lower heating values, prices estimated do not have linear correlation to the lower LHV proposed in section 4.4. Instead, due to non-linear parameters in production process altering renewable content in each stream (as well as LHV), technology-controllable parameters would change prices in the same as fossil products. This relation between

operational parameters and price impact is left to future works.

Table 5.14. CBIO revenue for produced renewables, considering emission levels difference

Parameter	Fossil EL ($g_{CO2}.MJ^{-1}$)	Green EL ($g_{CO2}.MJ^{-1}$)	Blend EL ($g_{CO2}.MJ^{-1}$)	NEEA ($g_{CO2}.MJ^{-1}$)	Blend LHV (MJ.kg-1)	Renewables (Mtonne/year)	Mitigation ($Mton_{CO2}.year^{-1}$)	CBIO (MUSD/year)
LPG	63.20	47.40	57.87	-5.33	44.90	0.02	-0.01	0.10
Naphtha	71.33	53.50	69.24	-2.09	43.03	1.07	-0.10	1.73
Kerosene	72.89	54.67	70.23	-2.66	45.79	1.06	-0.13	2.34
Diesel	74.43	55.82	73.80	-0.63	42.15	1.11	-0.03	0.53
AGO	76.29	57.22	75.77	-0.52	43.23	1.53	-0.03	0.62
LVGO	79.67	59.76	78.19	-0.01	44.43	1.80	0.00	0.02
HVGO	78.20	58.65	79.71	-0.44	45.44	0.79	-0.02	0.29
VCR	80.15	60.11	81.67	-0.49	46.57	1.82	-0.04	0.75
Total	-	-		-	-	9.20	-0.35	6.36

Table 5.14 shows the additional revenue obtained from RenovaBio program. It is seen that total CO_2 mitigated is low, since blend emission levels calculated from renewables fractions are almost equivalent to fossil use. This virtually leads to an also low additional revenue to the process. However, the key parameter that led to this result was the estimation of both emission levels and LHV for each fraction. A life cycle analysis of the production process of each raw material, crude oil and bio-oil, is needed to address the correct values that could promote financial gains allied to environmental gains.

As for costs, differences were accounted for raw material acquisition, utilities and the increase of heteroatoms in the process (increase in hydrogen consumption). Table 5.15 shows a review of main raw material prices. Important to notice that this direct cost difference did not take into account any target production goal, only the refinery input. That is, it does not consider yield impact of coprocessing bio-oil instead of crude oil solely, which also demands simulation of the unity with only fossil oil. This was left to the final version of this work and also may impact products selling prices.

As seen, EUC30 price are not expressively competitive, however, minimum selling price can provide a cost reduction of almost 60 MUS$ per year, a value that almost covers OPEX costs from the pyrolysis unit. If only raw material were the parameter considered in the evaluation, the investment would be considered potentially attractive, and an option to refinery and petrochemical investors to address sustainability goals.

Table 5.15. Raw material costs: crude oil, bio-oil and blend

Parameter	Price ($USD.bbl^{-1}$)	Total Oil Demand ($kbbl.day^{-1}$)	Blend Ratio (%)	Total Cost ($MUSD.year^{-1}$)
Mero Crude Oil	64.91	200	100	4,283.94
EUC30[a]	55.88	200	100	3,688.07
EUC30[b]	63.79	200	100	4,210.33
BIO1030[a]	64.01	200	10/90	4,224.35
BIO1030[b]	64.80	200	10/90	4,276.58
ΔTotal (Crude vs. BIO1030)[a]	-9.03	-	-	-59.59
ΔTotal (Crude vs. BIO1030)[b]	-1.12	-	-	-7.36

[a]Minimum selling price conditions

[b]Average-return selling price conditions

However, raw material is not the only parameter to be considered, as the co-processing implies in additional costs. Table 5.16 shows the difference of heteroatoms present in the refinery feed with only Mero crude oil vs. with BIO1030. The inclusion of renewables indeed caused the increase in hydrogen acquisition costs (+MUS$ 1,645.10).

Note that this analysis was made with total atoms input in all fractions (from NAPH to VCR), however part of the renewables is directed to cracking units, such as AGO, LVGO, HVGO and VCR, which do not need H_2 to perform catalytic reactions, decreasing the impact of additional H_2. Detailed calculations of this scenario are left for the final version of this work.

Another more detailed analysis needed is regarding the supply source. Since demand is increased twenty times, the use of natural gas during steam reforming for hydrogen production (method extensively used by refineries) could produce more CO_2 than what is being mitigated by coprocessing. Once again, a life cycle analysis is needed to address these challenges.

Table 5.16. H_2 costs: crude oil, bio-oil and blend

Parameter	O ($Mmol.year^{-1}$)	N ($Mmol.year^{-1}$)	S ($Mmol.year^{-1}$)	Total ($Mmol.year^{-1}$)	H_2 ($Mmol.year^{-1}$)	H_2 ($MNm^3.year^{-1}$)	Total Cost ($MUSD.year^{-1}$)
Mero Crude Oil	0	314	865	1179	7	0.16	43.00
BIO1025	34048	329	778	35155	68103	1626	1,688.11
ΔTotal	34048	15	-86	33977	68103	1626	1,645.10

As can be seen in the results above, the main operational challenge for coprocessing biocrudes is the hydrogen input for hydrodeoxygenation. Until today, there are not many options to avoid this problem if not by reacting it with other chemicals (usually called ‘stabilization’ of the biocrude), or producing it through other routes (hydrothermal liquefaction, for example), both options also presenting themselves as expensive and complex.

Finally, Table 5.17 shows a summary of costs vs. revenues for the entire comparison

scenario. It can be seen that hydrogen is the main offender of the profitability for this option. Details on the simulation can be seen in Appendix A3.

The consolidated financial results collaborate with previous specific analysis, indicating a severe impact by hydrogen consumption increase. Also, since the simulation is focused only on distillation section of the refinery, due to the lighter components from FPBO, increased costs in energy and water are also spotted. Overall, this scenario could be balanced if other units (bottom barrel processing units) were to be considered as well, usually high-energy consumers.

Table 5.17. Costs vs. Revenues for the entire scenario

Parâmetro	**USD.bbl-1**	**MUSD.year-1**
Total ΔCosts	**-31.22**	**-2060.23**
ΔSteam	+0.01	+0.70
ΔEletrictricity	-0.10	-6.71
ΔNatural Gas	-2.75	-181.60
ΔProcess Water	-2.85	-188.37
ΔH2	-26.23	-1731.11
ΔRaw Material	+0.71	+46.86
Total ΔRevenue	**+0.08**	**+5.11**
ΔCBios	+0.10	+6.36
ΔSales	-0.02	-1.25
Total	**-31.14**	**-2055.11**

Opposingly, it's confirmed that CBIOs can actually generate revenue to a refinery. New studies should be carried out to evaluate upgraded versions of biocrudes in co-processing, where more stable components and less heteroatoms are present, evaluating if the revenue increase continues positive, but with less impact on costs.

6. Conclusions

The first conclusion of this work is that this is an innovative work. There are no literature involving modeling of bio-oil with an optimizer, a full-scale simulation of distillation co-processing, and a full evaluation of carbon credits potentially involved in this operation.

The second conclusion of this work is that the main objective was achieved. Results have shown that bio-oil can be satisfactorily modelled by surrogate components, selected judiciously through experimental data. Moreover, although GC-MS data do not represent mass fractions of the components in a mixture directly, the results can be used as mathematical inputs to optimize bio-oil composition. The method, however, suffers from the absence of experimental data on complex structures, especially complex sugars and lignin derived components, which had to be estimated and/or left as input variables.

The model was successfully integrated with Aspen Plus® to produce distillation curves and any other property present in Aspen databases or PCES, optimizing the composition definition for the biocrude based on literature references.

Overall, modelled bio-oil is very similar to bio-oil reported in literature by Mante *et al*. (2016) and Varma *et al*. (2019), with molar ratios, distillation curve, density and heteroatoms content below 20% average difference in both cases. Viscosity, on the opposite, still needs improvements, since it highly depends on complex structures present in real bio-oil. Sulphur content should be removed from FPBO surrogate as it was assumed initially, but not commonly reported in literature.

This automated method of simulations can be implemented with all 40 (or more) surrogate components defined, however increased computational power is required, i.e. big data cloud computing. The goal of this section of the work was to build a method with robust estimation of bio-oil components using solely easily acquired properties, such as molar ratios and density.

Also, this modeling algorithm can be a starting path to what could be called a soft sensor for biogenic carbon in refineries' products. This can be useful in several ways: 1) To refiners, which would know how bio-crude would behave inside their units and speed-up crude analysis processes; 2) Regulation agencies, facilitating audits; 3) Traders, facilitating pricing based on surrogate composition through key components that translate the real composition, matching key properties. A recommendation for future work would be the improvement of the optimization algorithm in terms of error validation criteria.

The third conclusion of this work is that the additional objectives were achieved, as it was

seen that Aspen Plus® simulation of bio-oil is complex, but possible in the same proportion of complexity. The components selected from literature need to be carefully configured, as well as equations to be used to estimate each property correctly. UNIFAC has proven to be an adequate method to simulate bio-oil, achieving values close to experimental distillation curves, although complete validation is only possible after complete experimental analysis of a bio-oil sample. Also, given the scarcity of FPBO data, UNIFAC had to be used and several chemical structures had to be drawn, showing that databases are still incomplete and a challenge to represent FPBO mixtures (even surrogate mixtures).

The distillation process was simulated also satisfactorily, but with areas for improvements. In the desalting section (simulation section which was an innovative step rarely seen in literature), the severe problem regarding aqueous phase separation exposed a crucial limitation of this coprocessing insertion point. As mentioned in the results section, aromatic content in aqueous stream and oxygenated compounds in gas stream can be major concerns for the refinery.

Future studies can evaluate if alternatives exist to mitigate these problems (e.g.: chemicals addition to desalting unit), otherwise the applicability of this coprocessing route may not be feasible industrially. Another investigation may be carried out to verify if separating the phases of FPBO prior to blending could make the strategy viable (i.e.: blending only the organic phase with crude oil, routing the aqueous fraction to other ends, like chemicals production).

In the crude distillation unit, overall energy input will have to be increased, since several products presented undesired lighter fractions incorporated, especially gasoil fraction. The same applies for vacuum distillation unit. Heat integration also needs to be included in the simulation, to accounts differences in utilities spending between conventional processing and coprocessing.

Bio-oil price estimation addresses the commonly found problem of parity to crude oil prices, challenging the applicability of coprocessing. However, it was seen that if minimum selling prices are practiced, savings associated with crude oil acquisition are present. Additional costs regarding energy input still to be better evaluated.

The method for the estimation of CBIO, although effective for an initial evaluation, still needs improvements, since the lower estimations for emission levels and LHV for blends break-even with CO_2 mitigation proposed in the process and, therefore, potentially generating virtually no additional income.

References

ABDEL-RAOULF MES. *Crude Oil Emulsions – Composition Stability and Characterization.* InTech Croatia. 2012.

AL-ASSADY QMAA. *Characterization of petroleum fractions*. Iraqi Journal of Mechanical and Material Engineering, 9(2):223-238. 2009.

Ali AAM, Mustafa MA, Yassin KE. A techno-economic evaluation of bio-oil co-processing within a petroleum refinery. Biofuels. 2018.

AL-KAISI MM, YIN X. *Tillage and Crop Residue Effects on Soil Carbon and Carbon Dioxide Emission in Corn–Soybean Rotations*. Atmospheric Pollutant and Trace Gas, 34(2):437-445. 2005.

ALOMAIR O, JUMAA M, ALKORIEM A, HAMED M. *Heavy oil viscosity and density prediction at normal and elevated temperatures*. Journal of Petroleum Exploration and Production Technology, 6:253-263. 2016.

AMUTIO M, LOPEZ G, ALVAREZ J, OLAZAR M, BILBAO J. *Fast pyrolysis of eucalyptus waste in a conical spouted bed reactor*. Bioresource Technology, 194:225-232. 2015.

ANDRADE LA, BATISTA FRX, LIRA TS, BARROZO MAS, VIEIRA LGM. *Characterization and product formation during the catalytic and non-catalytic pyrolysis of the green microalgae Chlamydomonas reinhardtii*. Renewable Energy, 119:731-740. 2018.

ANDRADE, ENC. *LVIII. A theory of the viscosity of liquids. —Part II*. The London, Edinburgh, and Dublin Philosophical Magazine and Journal of Science Series 7, 17(113):698-732. 1934.

ANDRADE, ENC. *XLI. A theory of the viscosity of liquids. —Part I*. The London, Edinburgh, and Dublin Philosophical Magazine and Journal of Science Series 7, 17(112):497-511. 1934.

ARAÚJO DJC, MACHADO AV, VILARINHO MCLG. *Availability and Suitability of Agroindustrial Residues as Feedstock for Cellulose-Based Materials: Brazil Case Study*. Waste and Biomass Valorization, 10:2863-2878. 2019.

ARAÚJO RCS, PASA VMD, MARRIOTT PJ, CARDEAL ZL. *Analysis of volatile organic compounds in polyurethane coatings based on Eucalyptus sp. bio-oil pitch using comprehensive two-dimensional gas chromatography (GC × GC)*. Journal of Analytical and Applied Pyrolysis, 88(1):91-97. 2010.

ASTM International. *Standard Specification for Pyrolysis Liquid Biofuel – ASTM D7544-12.*

2017

ASTM International. *Standard Test Method for Determination of Carbonyls in Pyrolysis Bio-Oils by Potentiometric Titration – ASTM E3146-20.* 2020.

AUERSVALD M, KEJLA L, ESCHENBACHER A, THI HD, GEEM KMV, ŠIMÁČEK P. *Detailed characterization of sulfur compounds in fast pyrolysis bio-oils using GC × GC-SCD and GC–MS*. Journal of Analytical and Applied Pyrolysis, 159:105288. 2021.

B3 S.A. Bolsa, Brasil, Balcão – Historical CBIO Prices. 2022.

BALDASSIN R. *Fast pyrolysis of whole sugarcane in a pilot fluidized bed reactor*. Thesis (Doctorate). Faculty of Agricultural Engineering – FEAGRI, State University of Campinas. 2015.

BARCELÓ AR, ROS LVG, GABALDÓN C, LÓPEZ-SERRANO M, POMAR F, CARRIÓN JS, PEDREÑO MA. *Basic peroxidases: The gateway for lignin evolution?* Phytochemistry Reviews, 3:61-78. 2004.

BATHOLOMEW CH, FARRAUTO RJ. *Fundamentals of Industrial Catalytic Processes.* John Wiley & Sons. 2011.

BECOOL – Brazil-EU. *Cooperation for Development of Advanced Lignocellulosic Biofuels.* 2020. Available at: https://www.becoolproject.eu/page/4/

BENÉS M, BILBAO R, SANTOS JM, MELO JA, WISNIEWSKI JR. A, FONTS I. *Hydrodeoxygenation of Lignocellulosic Fast Pyrolysis Bio-Oil: Characterization of the Products and Effect of the Catalyst Loading Ratio*. Energy&Fuels, 33(5):4272-4286.2019.

BENNACEUR F, BENDOB A. *Crude Oil Prices and Banks Performance in The Arab Maghreb Countries (Algeria – Libya – Tunisia – Morocco): Cross Section Analysis*. Inter Joun of Finan Manag. 6(6):1-10. 2017.

BLACK S, FERRELL III JR. *Accelerated aging of fast pyrolysis bio-oil: a new method based on carbonyl titration*. RSC Advances, 10 (10046). 2020.

Bloomberg Business Wire. *Biofuels Market Analysis with Impact of COVID-19 2020-2024 | Increased Adoption of Renewable Sources of Energy to boost the Market Growth | Technavio*. 2020.

Bloomberg Business Wire. *Global Green Chemicals Market Will Grow at a CAGR of 10% During 2019-2023 | Technavio*. 2019.

BNP Paribas. *Primary research into the practical implications of ESG integration*. 2019.

BONDI A. *van der Waals Volumes and Radii*. The Journal of Physical Chemistry, 68(3):441-451. 1964.

BOUCHER ME, CHAALA A, ROY C. *Bio-oils obtained by vacuum pyrolysis of softwood bark as a liquid fuel for gas turbines. Part I: Properties of bio-oil and its blends with methanol and a pyrolytic aqueous phase*. Biomass and Bioenergy, 19(5):337-350. 2000.

Brazil Central Bank. *Selic Rate*. 2022. Available at: https://www.bcb.gov.br/controleinflacao/taxaselic

Brazil's Chamber of Deputies. *PL 1873/2021 - Establishes the National Program for Advanced Renewable Fuels with the objective of encouraging research and promoting the production and consumption of advanced biofuels.* 2021.

Brazilian Federal Reserve. Normative Instruction RFB No 1700, March 14 2017.

Brazilian National Logistics Association (ABRALOG). *Pre-salt layer should have greater impact on logistics than agribusiness*. 2019. Available at: https://www.abralog.com.br/noticias/pre-sal-deve-ter-impacto-maior-na-logistica-do-que-teve-o-agronegocio/

Brazilian Trees Institute (IBÁ). *Yearly Report 2024*. 2024.

BRIDGWATER, AV. *Review of fast pyrolysis of biomass and product upgrading*. Biomass and Bioenergy, 38:68-94. 2012.

BRUHN CHL, PINTO ACC, JOHANN PRS, BRANCO CCM, SALOMÃO MC, FREIRE EB. *Campos and Santos Basins: 40 Years of Reservoir Characterization and Management of Shallow- to Ultra-Deep Water, Post- and Pre-Salt Reservoirs - Historical Overview and Future Challenges*. Offshore Technology Conference, Rio de Janeiro, Brazil, 2017.

BTG Biofuels. Production Capacity. 2024. Available at: btg-bioliquids.com

CASTELLO D, PEDERSEN TH, ROSENDAHL LA. *Continuous Hydrothermal Liquefaction of Biomass: A Critical Review.* Energies 11:3165. 2018.

CASTRO NM. Brazilian carbon credit first trade at near $10/CBIO. S&P Global Platts. 2020. Available at: https://www.spglobal.com/platts/pt/market-insights/latest-news/oil/061220-brazilian-carbon-credit-first-trade-at-near-10cbio

CCEE – Electric Energy Commercialization Chamber. *Energy Prices Dashboard*. 2022. Available at: https://www.ccee.org.br/web/guest/precos/painel-precos

CHANG S, ZHAO Z, ZHENG A, LI X, WANG X, HUANG Z, HE F, LI H. *Effect of hydrothermal pretreatment on properties of bio-oil produced from fast pyrolysis of eucalyptus wood in a fluidized bed reactor*. Bioresource Technology, 138:321-328. 2013.

ChemSpider – Royal Society of Chemistry – UK. 2022. Available at: http://www.chemspider.com

CHEN T, LI L, ZHAO R, WU J. *Pyrolysis kinetic analysis of the three pseudocomponents of biomass–cellulose, hemicellulose and lignin*. Journal of Thermal Analysis and Calorimetry, 128:1825-1832. 2017.

CHEN X, ZHANG H, SONG Y, XIAO R. *Prediction of product distribution and bio-oil heating value of biomass fast pyrolysis*. Chemical Engineering and Processing – Process Intensification, 130:36-42. 2018.

Climate Action Tracker. *Warming Projections Global Update*. 2021 Available at: CAT - Warming Projections Global Update - September 2019 UNSG Summit NYC | Climate Action Tracker.

COKER, AK. *Petroleum Refining Design and Applications Handbook.* John Wiley & Sons. 2018.

COSAN – Comgás. Piped Natural Gas Fees – Industrial Segment. 2022. Available at: https://www.comgas.com.br/tarifas/industrial/

COUTINHO DM, FRANÇA D, VANINI G, GOMES AO, AZEVEDO DA. *Understanding the molecular composition of petroleum and its distillation cuts*. Fuel, 311:122594. 2022.

CRUZ PL, IRIBARREN D, DUFOUR J. *Life Cycle Costing and Eco-Efficiency Assessment of Fuel Production by Coprocessing Biomass in Crude Oil Refineries.* Energies, 12(24):4664. 2019.

CRUZ PL, MONTERO E, DUFOUR J. *Modeling of co-processing of HDO-oil with VGO in a FCC unit*. Fuel, 196:362-370. 2017.

DANIELIS R, SCORRANO M, GIANSOLDATI M. *Decarbonising transport in Europe: Trends, goals, policies and passenger cars scenarios.* Research in Transportation Economics. 2021.

DANILOV VA, GARTMAN TN, SOVETIN FS, SARTAKOV MV, SHATALOV KI. *Comparison of Results of Oil Fractions Separation Process Modeling Using real and Pseudocomponents*. Chemistry and Technology of Fuels and Oils, 57:224-229. 2021.

DHULESIA H. *Equation Fits ASTM Distillations*. Hydrocarbon Processing Magazine, 62(9):179-180. 1984.

DING Y, EZEKOYE OA, LU S, WANG C, ZHOU R. *Comparative pyrolysis behaviors and reaction mechanisms of hardwood and softwood*. Energy Conversion and Management, 132:102-109. 2017.

DORTMUND DATA BANK Software & Separation Technology GmbH (DDBST). *The UNIFAC Consortium*. 2021. Available at: UNIFAC - TUC (ddbst.de)

DOS SANTOS RE, DOS SANTOS IFS, BARROS RM, BERNAL AP, FILHO GLT, DA SILVA FGB. *Generating electrical energy through urban solid waste in Brazil: An economic and energy comparative analysis*. Journal of Environmental Management, 231:198-206. 2019

DREXLER S, CORREIA EL, JERDY AC, CAVADAS LA, COUTO P. *Effect of CO2 on the dynamic and equilibrium interfacial tension between crude oil and formation brine for a deepwater Pre-salt field*. Journal of Petroleum Science and Engineering, 190:107095. 2020.

DUFOUR A. *Thermochemical Conversion of Biomass for the Production of Energy and Chemicals*. Focus Energy Series. Wiley-ISTE. 2016.

DUSSAN K, DOOLEY S, MONAGHAN R. *Integrating compositional features in model compounds for a kinetic mechanism of hemicellulose pyrolysis*. Chemical Engineering Journal, 328:943-961, 2017.

ELIAS A, TREVISAN OV. *An Experimental Investigation on Phase Behavior of a Light Oil and CO2*. Journal of Petroleum Science and Engineering, 145:22-23. 2016.

ENDERS MSP. *Analytical methods for identification and quantification of saline and sediment species in oil*. Doctorate Thesis, Federal University of Santa Maria, Brazil. 2019.

ENERGETIC RESEARCH COMPANY (EPE). *Conjuncture Analysis of Biofuels 2020. 2020.*

ENERGETIC RESEARCH COMPANY (EPE). *Information System for Energy – SIEnergia.* 2022.

ENERGETIC RESEARCH COMPANY (EPE). *National Energy Balance 2021*. 2021.

ENERGETIC RESEARCH COMPANY (EPE). *Ten-Year Energy Expansion Plan 2030*. 2020.

ENERGY RESEARCH COMPANY (EPE). *Carbon Pricing: Risks and Opportunities for Brazil – Technical Note EPE/DEA/GAB/014/2020*. 2020.

ENSYN TECHNOLOGIES. 2022. http://www.ensyn.com/

EURAXESS, Horizon 2020 work program. *2018-2020 – What's in it for Brazil*. 2017. Available at: https://euraxess.ec.europa.eu/worldwide/brazil/horizon-2020-work-programme-2018-2020-%E2%80%93-what%E2%80%99s-it-brazil

FACCINI CS, VECCHIA ID, RIBEIRO D, ZINI CA, CARAMÃO EB. *Comprehensive Two-Dimensional GC with TOF-MS Detection: Study of Pyrolytic Bio-Oil of Kraft Mill Residues*. Journal of the Brazilian Chemical Society, 24(7):1085-1098. 2013.

FARRAPEIRA RO, ANDRADE YB, KRAUSE LC, BJERK TR, CARAMÃO EB, SCHNEIDER JK. *GC×GC in the Characterization of the Bio-Oil from Brazilian Biomass: A Review*. Brazilian Journal of Analytical Chemistry, 8(33):19-41. 2021.

FERNANDES HA, ZANELATO LN, DECOTE PAP, SANTOS HN, SENGER CM, DIAS FC, MULLER EI, FLORES EMM, MENDES LAN, VICENTE MA, SANTOS MFP. *Effects of calcium, magnesium, and strontium chlorides in determining the total acid number using potentiometric titration*. Fuel, 311:122522. 2022.

FONSECA FG, FUNKE A, DAHMEN N. *Aspen Plus™ Modeling of Fractional Condensation Schemes for Production of Fast Pyrolysis Bio-oil*. 27th European Biomass Conference and Exhibition, Portugal, 3BV.7.9:1227-1233

FONTS I, ATIENZA-MARTINEZ M, CARSTENSEN HH, BENÉS M, PIRES APP, GARCIA-PEREZ M, BILBAO R. *Thermodynamic and Physical Property Estimation of Compounds Derived from the Fast Pyrolysis of Lignocellulosic Materials*. Energy Fuels, 35(21):17114-17137. 2021.

FRANÇA D, COUNTINHO DM, BARRA TA, XAVIER RS, AZEVEDO DA. *Molecular-level characterization of Brazilian pre-salt crude oils by advanced analytical techniques*. Fuel, 293:120474.

FRANK M, WOLFE P. *An algorithm for quadratic programming*. Naval Research Logistics Quarterly, 3(1-2):95-110. 1956.

FREGOLENTE PBL, FREGOLENTE LV, MACIEL MRW. *Water Content in Biodiesel, Diesel, and Biodiesel–Diesel Blends*. Journal of Chemical Engineering Data, 57(6):1817-1821

FRENCH RJ, STUNKEL J, BALDWIN RM. *Mild Hydrotreating of Bio-Oil: Effect of Reaction Severity and Fate of Oxygenated Species*. Energy&Fuels, 25(7):3266-3274. 2011.

FU G, CASTILLO PA, MAHALEC V. *Impact of crude distillation unit model accuracy on refinery production planning*. Frontiers of Engineering Management, 5(2):195-201. 2018.

GATIBONI TL. *Use of ultrasound for the demulsification of oil from the pre-salt*. Masters Dissertation, Federal University of Santa Maria, Brazil. 2020.

Getúlio Vargas Foundation (FGV). *Auctions for Exploration and Production of Oil and Natural Gas in Brazil. FGV Energia notebooks*, Year 1, No 1. 2014.

GHANTA M, FAHEY D, SUBRAMANIAM B. *Environmental impacts of ethylene production from diverse feedstocks and energy sources*. Appl Petrochem Res, 3:167-179. 2014.

GHOLIZADEH M, HU X, LIU Q. *A mini review of the specialties of the bio-oils produced from pyrolysis of 20 different biomasses*. Renewable and Sustainable Energy Reviews, 114(109313). 2019.

GÓMEZ-MONEDERO B, BIMBELA F, ARAUZO J, FARIA J, RUIZ MP. *Pyrolysis of Red Eucalyptus, Camelina Straw, and Wheat Straw in an Ablative Reactor*. Energy Fuels, 29:1766-1775. 2015.

GONÇALVES HL, FREGOLENTE PBL, MACIEL MRW, FREGOLENTE LV. *Formulation of hydrogels for water removal from diesel and biodiesel*. Separation Science and Technology, 56(2):374-388. 2019.

GUEDES CLB, ADÃO DC, QUESSADA TP, BORSATO D, GALÃO OF, DI MAURO E, PÉREZ JMM, ROCHA JD. *Avaliação de biocombustível derivado do bio-óleo obtido por pirólise rápida de biomassa lignocelulósica como aditivo para gasolina*. Química Nova, Vol. 33, No. 4, Pp. 781-786, 2010.

GUIMARÃES, GCP. *Climate change and carbon pricing: challenges and opportunities for Brazil's carbon markets*. São Paulo's Public Policies Debate Center, Brazil. 2021.

HAMILTON LC, BELL E, HARTTER J, SALERNO JD. *A change in the wind? US public views on renewable energy and climate compared.* Energy, Sustainability and Society, 8:11. 2018.

HAMILTON T. *The Case for Burying Charcoal*. MIT Technology Review. 2007.

HAYDARY J. *Chemical Process Design and Simulation: Aspen Plus and Aspen HYSYS Applications, Chapter 13 Design and Simulation Using Pseudocomponent.* John Wiley & Sons. 2018.

HEIDARI A, KHARI E, YOUNESI H, LU HR. *Optimization and statistical analysis of performance parameters for bio-oil production from eucalyptus leaves using fast pyrolysis*. Journal of Cleaner Production, 241:118394. 2019.

HERTZOG J, MASE C, HUBERT-ROUX M, AFONSO C, GIUSTI P, BARRÈRE-MANGOTE C. *Characterization of Heavy Products from Lignocellulosic Biomass Pyrolysis by Chromatography and Fourier Transform Mass Spectrometry: A Review*. Energy Fuels, 35(22):17979-18007. 2021.

HORST DJ. *Evaluation of energy production from lignins contained in biomass.* Thesis (Master's degree). Postgraduate in Production Engineering – Federal Technological University of Paraná (UFTPR). 2013.

HOSSEINIFAR P, SHAHVERDI H. *Development of a generalized model for predicting the composition of homologous groups derived from molecular type analyses to characterize petroleum fractions*. Journal of Petroleum Science and Engineering, 204:108744. 2021.

HSU CS, ROBINSON PR. *Springer Handbook of Petroleum Technology*. Springer International Publishing. 2017.

http://ipeadata.gov.br/ExibeSerie.aspx?serid=40940&module=M

HUSAIN Z, ANSARI KB, CHATAKE VS, URUNKAR Y, PANDIT AB, JOSHI JB. *Valorization of biomass pellets to renewable fuel and chemicals using pyrolysis: characterization of pyrolysis products and its application*. Indian Chemical Engineer, 62(1):78-91. 2020.

HWANG J, BOUVET N, SOHN K, YOON Y. *Stability characteristics of non-premixed turbulent jet flames of hydrogen and syngas blends with coaxial air*. International Journal of Hydrogen Energy. 38(12):5139-5149. 2013.

IBGE - Brazilian Institute of Geography and Statistics. *Broad National Consumer Price Index (IPCA)*. 2022. https://ibge.gov.br/estatisticas/economicas/precos-e-custos/9256-indice-nacional-de-precos-ao-consumidor-amplo.html?=&t=o-que-e

IEA Bioenergy (International Energy Agency). *Task 34 – Advancing bioenergy through Pyrolysis, Hydrothermal Liquefaction and Solvent Liquefaction of Biomass.* 2020. Available at: https://task34.ieabioenergy.com/bio-crude/

IGLESIAS SP, MIYAZAKI MR, MARIANO AP, FRANCO TT, *Techno-economic assessment of bio-oil produced from Eucalyptus forestry residues*. Industrial Crops and Products, 171. 2021.

INEA (Innovation and Networks – European Commission), Horizon 2020. *Residue2Heat*. 2016. Available at: https://ec.europa.eu/inea/en/horizon-2020/projects/h2020-energy/biomass-

biofuels-alternative-fuels/residue2heat

INEA (Innovation and Networks – European Commission), Horizon 2020. *Residue2Heat – Renewable Residential heating with fast pyrolysis bio-oil*. 2016. Available at: https://ec.europa.eu/research/participants/documents/downloadPublic?documentIds=080166e5b7627236&appId=PPGMS

INTERNATIONAL ENERGY AGENCY (IEA). *World Energy Outlook 2024*. 2024.

IOWA STATE UNIVERSITY. *Bio-oil production and characterization*. 2020. Available at: https://www.cbe.iastate.edu/rcbrown/bio-oil-production-and-characterization/

IPEA - Institute of Applied Economic Research. *EMBI+ (Emerging Markets Bond Index Plus)*. 2022.

JONG S, HOEFNAGELS R, FAAIJ A, SLADE R, MAWHOOD R, JUNGINGER, M. *The feasibility of short-term production strategies for renewable jet fuels – a comprehensive techno-economic comparison*. Biofuels, Bioproducts and Biorefining, 9(6). 2015.

JOUBERT JE, CARRIER M, STAHL R, KNOETZE JH. 2011. *Fast Pyrolysis of Eucalyptus grandis*. Article presented at: Annual Student Symposium 2011, Matieland, South Africa. 2011.

KAWAMOTO H. *Lignin pyrolysis reactions*. Journal of Wood Science, 63:117-132. 2017.

KHAN MA, ADEWUYI YG. *Techno-economic modeling and optimization of catalytic reactive distillation for the esterification reactions in bio-oil upgradation*. Chemical Engineering Research and Design, 148:86-101. 2019.

KOSA M, BEN H, THELIANDER H, RAGAUSKAS AJ. *Pyrolysis oils from CO2 precipitated Kraft lignin.* Green Chemistry, 11:2977-3316. 2011.

KRUTOF A, HAWBOLDT KA. *Thermodynamic model of fast pyrolysis bio-oil advanced distillation curves*. Fuel, 261:116446. 2020.

KRUTOF A, HAWBOLDT KA. *Thermodynamic model of fast pyrolysis bio-oil advanced distillation curves*. Fuel, 261:116446. 2020.

KURODA K, ASHITANI T, FUJITA K, HATTORI T. *Thermal Behavior of β-1 Subunits in Lignin: Pyrolysis of 1,2-Diarylpropane-1,3-diol-type Lignin Model Compounds*. Journal of Agricultural and Food Chemistry, 55(8):2770-2778. 2007.

LAZARIDIS PA, FOTOPOULOS AP, KARAKOULIA AS, TRIANTAFYLLIDIS KS. 2018. *Catalytic Fast Pyrolysis of Kraft Lignin with Conventional, Mesoporous and Nanosized ZSM-5*

Zeolite for the Production of Alkyl-Phenols and Aromatics. Nano-(bio) catalysis in lignocellulosic biomass valorization, 6(295). 2018.

LAZZARI E, SCHENA T, MARCELO MCA, PRIMAZ CT, SILVA AN, FERRÃO MF, BJERK T, CARAMÃO EB. *Classification of biomass through their pyrolytic bio-oil composition using FTIR and PCA analysis*. Industrial Crops & Products, 111:856-864. 2018.

LEE H, KIM H, YU MJ, KO CH, JEON JK, JAE J, PARK SH, JUNG SC, PARK YK. 2016. *Catalytic Hydrodeoxygenation of Bio-oil Model Compounds over Pt/HY Catalyst*. Scientific Reports, 6(28765). 2016

LEHTO J, OASMAA A, SOLANTAUSTA Y, KYLÖ M, CHIARAMONTI D. *Review of fuel oil quality and combustion of fast pyrolysis bio-oils from lignocellulosic biomass*. Applied Energy. 116:178-190. 2014.

LENG E, HE B, CHEN J, LIAO G, MA Y, ZHANG F, LIU S, E J. *Prediction of three-phase product distribution and bio-oil heating value of biomass fast pyrolysis based on machine learning*. Energy, 236:121401. 2021.

LENG L, LI H, YUAN X, ZHOU W, HUANG H. *Bio-oil upgrading by emulsification / microemulsification: A Review*. Energy, 161:214-232. 2018.

LINDFORS C, PAASIKALLIO V, KUOPPALA E, REINIKAINEN M, OASMAA A, SOLANTAUSTA Y. *Co-processing of dry bio-oil, catalytic pyrolysis oil, and hydrotreated bio-oil in a micro activity test unit*. Energy & Fuels, 29:3707-3714. 2015.

MANGILI PV, AHÓN VRR. *Comparison of PVT correlations for predicting crude oil properties: the Brazilian Campos basin case study*. Brazilian Journal of Petroleum and Gas, 13(3): 129-157. 2019.

MANTE OD, DAYTON DC, SOUKRI M. *Production and distillative recovery of valuable lignin-derived products from biocrude*. RSC Advances, 6(96):94247-94255. 2016.

MASNADI MS, EL-HOUJEIRI HM, SCHUNACK D, LI Y, ENGLANDER JG, BADAHDAH A, MONFORT JC, ANDERSON JE, ALLINGTON TJ, BERGERSON JA, GORDON D, KOOMEY J, PRZESMITZKI S, AZEVEDO IL, BI XT, DUFFY JE, HEATH GA, KEOLEIAN GA, MCGLADE C, MEEHAN DN, YEH S, YOU F, WANG M, BRANDT AR. *Global carbon intensity of crude oil production*. Science, 361(6495):851-853. 2018.

MERCKEL RD. *Fast Pyrolysis of Tropical Biomass Species and Influence of Water Pretreatment on Product Distributions*. Master's Degree Thesis. University of Pretoria. 2014.

MICHAILOS S, BRIDGWATER A. *A comparative techno-economic assessment of three bio-oil upgrading routes for aviation biofuel production*. Int J of Energy Res, 1-23. 2019.

Ministry of Mines and Energy – MME. *Results of oil fields exploration right biding processes*. 2022. Available at: Resultados — Português (Brasil) (www.gov.br).

Ministry of Mines and Energy (MME) – Brazil. *RenovaBio Program.* 2022.

MJALLI FS, SHAHBAZ K, ALNASHEF IM. *Modified Rackett equation for modeling the molar volume of deep eutectic solvents*. Thermochimica Acta, 614:185-190. 2015.

MORGAN TJ, TURN SQ, SUN N, GEORGE A, GUPTA V. *Fast Pyrolysis of Tropical Biomass Species and Influence of Water Pretreatment on Product Distributions*. PLoS One, 11(3):01511368. 2016.

MUSSATTO SI. *Biomass Fractionation Technologies for a Lignocellulosic Feedstock Based Biorefinery*. Elsevier, 2016.

NAKAMURA T, KAWAMOTO H. *Thermal Behavior of β-1 Subunits in Lignin: Pyrolysis of 1,2-Diarylpropane-1,3-diol-type Lignin Model Compounds*. Journal of Wood Chemistry and Technology, 27(2):121-133. 2007.

NATIONAL AGENCY OF PETROLEUM, Natural Gas and Biofuels (ANP). *Biodiesel Producers Dashboard*. 2022.

NATIONAL AGENCY OF PETROLEUM, Natural Gas and Biofuels (ANP). *Ethanol Producers Dashboard*. 2022.

NATIONAL AGENCY OF PETROLEUM, Natural Gas and Biofuels (ANP). *Oil & Gas Production Dashboard*. 2022.

NATIONAL AGENCY OF PETROLEUM, Natural Gas and Biofuels (ANP). *RenovaBio – National Biofuels Policy – Law no. 13.576/2017*. 2017.

NATIONAL AGENCY OF PETROLEUM, Natural Gas and Biofuels (ANP). *RenovaBio – National Biofuels Policy – RenovaCalcMD: Method and tool to accounting of biofuels carbon intensity in the RenovaBio program.* 2018;

NATIONAL AGENCY OF PETROLEUM, Natural Gas and Biofuels (ANP). *Resolution No. 807*. 2020.

NATIONAL AGENCY OF PETROLEUM, Natural Gas and Biofuels (ANP). *Statistical Yearbook*. 2024.

NATIONAL CENTER FOR BIOTECHNOLOGY INFORMATION, U.S. National Library of Medicine. *PubChem.* 2022. Available at: https://pubchem.ncbi.nlm.nih.gov/

NATIONAL INSTITUTE OF STANDARDS AND TECHNOLOGY (NIST), U.S. Department of Commerce. 2022. Available at: https://www.nist.gov/

NREL – National Renewable Energy Laboratory. *Bio-Oil Analysis Laboratory Procedures*. Disponível em: https://www.nrel.gov/bioenergy/bio-oil-analysis.html

OASMAA A, KÄLLI A, LINDFORS C, ELLIOTT DC, SPRINGER D, PEACOCKE C, CHIARAMONTI D. *Guidelines for Transportation, Handling, and Use of Fast Pyrolysis Bio-Oil. 1. Flammability and Toxicity*. Energy & Fuels, 26(6):3864-3873. 2012.

OASMAA A, PEACOCKE C. *Properties and fuel use of biomass-derived fast pyrolysis liquids – A guide*. VTT Publications 731, 2010.

OASMAA A, PEACOCKE, C. 2001. *Fast Pyrolysis of Tropical Biomass Species and Influence of Water Pretreatment on Product Distributions*. VTT Publications, 450. 2001.

OASMAA A, VAN DE BELD B, SAARI P, ELLIOTT DC, SOLANTAUSTA Y. *Norms, Standards, and Legislation for Fast Pyrolysis Bio-oils from Lignocellulosic Biomass*. Energy & Fuels, 29(4):2471-2484. 2015.

OLIVÉRIO JL, BOSCARIOL F, FERREIRA RE. *Peer-reviewed paper Brazilian monetary carbon credits (CBio) optimized using sustainable mill technologies*. XXX ISSCT Congress, Argentina. 2019.

ONARHEIM K, SOLANTAUSTA Y, LEHTO J. *Process Simulation Development of Fast Pyrolysis of Wood Using Aspen Plus*. Energy Fuels, 29(1):205-217. 2015.

OPEC – Organization of the Petroleum Exporting Countries. *Oil Prices May 4th 2020*. Disponível em https://www.opec.org/opec_web/en/press_room/5818.htm

PACIFIC NORTHWEST NATIONAL LABORATORY (PNNL). *Biomass Direct Liquefaction Options: Technoeconomic and Life Cycle Assessment*. PNNL-23579. 2014.

PACIFIC NORTHWEST NATIONAL LABORATORY (PNNL). *Process Design and Economics for the Conversion of Lignocellulosic Biomass to Hydrocarbon Fuels – Fast Pyrolysis and Hydrotreating Bio-oil Pathway*. PNNL-23053. 2013.

PACIFIC NORTHWEST NATIONAL LABORATORY (PNNL). *Refinery Integration of Renewable Feedstocks*. 2014.

PATEL A, AGRAWAL B, RAWAL BR. *Optimization and statistical analysis of performance*

parameters for bio-oil production from eucalyptus leaves using fast pyrolysis. International Journal of Nanotechnology, 18:11-12. 2021.

PATIL ML, LALI AM, DALAI AK. *Catalytic hydrodeoxygenation of bio-oil model compound for production of fuel grade oil*. Asia-Pacific Journal of Chemical Engineering, 2317. 2019.

PATWARDHAN PR, BROWN RC, SHANKS BH. *Product Distribution from the Fast Pyrolysis of Hemicellulose*. Chemistry & Sustainability Energy & Materials, 4(5). 2011.

PEDERSEN KS, FREDENSLUNG AA, THOMASSEN P. *Properties of Petroleum and Natural Gases Volume 5*. Gulf Publishing Company - Book Division. 1989.

PELUCCHI M, CAVALLOTTI C, CUOCI A, FARAVELLI T, FRASSOLDATI A, RANZI E. *Detailed kinetics of substituted phenolic species in pyrolysis bio-oils*. Reaction Chemistry & Engineering, 4(3):490-506. 2019.

PENÍN L, LÓPEZ M, SANTOS V, ALONSO JL, PARAJÓ JC. Technologies for Eucalyptus wood processing in the scope of biorefineries: A comprehensive review". Bioresource Technology, 311, 123528. 2020.

PEREIRA GCQ, BRAZ DS, HAMAGUCHI M, EZEJI TC, FILHO RM, MARIANO AP. *Process design and economics of a flexible ethanol-butanol plant annexed to a eucalyptus kraft pulp mill*. Bioresource Technology, 250:345-354. 2018.

PETROBRAS S.A. *Pre-salt Regulatory Framework*. 2014.

PETROBRAS. *Pre-salt*. 2020. Available at: https://petrobras.com.br/pt/nossas-atividades/areas-de-atuacao/exploracao-e-producao-de-petroleo-e-gas/pre-sal/

PIGHINELLI ALMT, BOATENG AA, MULLEN CA, ELKASABI Y. *Evaluation of Brazilian biomasses as feedstocks for fuel production via fast pyrolysis*. Energy for Sustainable Development, 21:42-50. 2014.

PIMENTA AS, MONTEIRO TVC, FASCIOTTI M, BRAGA RM, DE SOUZA EC, DE LIMA KMG. *Fast pyrolysis of trunk wood and stump wood from a Brazilian eucalyptus clone*. Industrial Crops and Products, 125:630-638. 2018.

PINHO AR, ALMEIDA MBB, MENDES FL, CASAVECHIA LC, TALMADGE MS, KINCHIN CM, CHUM HL. *Fast pyrolysis oil from pinewood chips co-processing with vacuum gas oil in an FCC unit for second generation fuel production*. Fuel, 188:462-473. 2017.

PINHO AR, ALMEIDA MBB, MENDES FL, XIMENES VL, CASAVECHIA LC. 2015. *Co-processing raw bio-oil and gasoil in an FCC Unit*. Fuel Proc. Tech. 131:159-166. 2015.

PINHO AR, ALMEIDA MBB, ROCHEDO PRR. *Renewable-Carbon Recovery in the Co-Processing of Vacuum Gas Oil and Bio-Oil in the FCC Process – Where Does the Renewable Carbon Go?*. Fuel Processing Technology, 01759. 2022.

PIRES APP, ARAUZO J, FONTS I, DOMINE ME, ARROYO AF, GARCIA-PEREZ ME, MONTOYA J, CHEJNE F, PFROMM P, GARCIA-PEREZ

POKE FS, RAYMOND CA. *Predicting Extractives, Lignin, and Cellulose Contents Using Near Infrared Spectroscopy on Solid Wood in Eucalyptus globulus*. Journal of Wood Chemistry and Technology, 26(2):187-199. 2006.

POLING BE, PAUSNITZ JM, O'CONNELL JP. *The Properties of Gases and Liquids 5th Edition*. McGraw-Hill. 2001.

POURZOLFAGHAR H, ABNISA F, DAUD WMAW, AROUA MK. *Atmospheric hydrodeoxygenation of bio-oil oxygenated model compounds: A review*. Journal of Analytical and Applied Pyrolysis, 133:117-127. 2018.

PROTÁSIO TP, LIMA MDR, TEIXEIRA RLC, ROSÁRIO FS, ARAÚJO ACC, ASSIS MR, HEIN PRG, TRUGILHO PF. *Influence of Extractives Content and Lignin Quality of Eucalyptus Wood in the Mass Balance of Pyrolysis Process*. BioEnergy Research. 2020.

PUBCHEM – National Library of Medicine – National Center for Biotechnology Information – USA, 2022. Available at: https://pubchem.ncbi.nlm.nih.gov/

RANGAIAH GP, BONILLA-PETRICIOCLET A. *Multi-Objective Optimization in Chemical Engineering – Developments and Applications*. John Wiley & Sons. 2013.

RIAZI MR. *Characterization and Properties of Petroleum Fractions*. ASTM International. 2005.

RIAZI MR. *Distribution model for properties of hydrocarbon-plus fractions.* Industrial & Engineering Chemical Research, 28(11):1731-1735. 1989.

RINALDI R, SCHÜTH F. *Design of solid catalysts for the conversion of biomass.*

ROCHA JHT, GONÇALVES JLM, FERRAZ AV, POIATI DA, JUNIOR JCA, HUBNER A. *Growth dynamics and productivity of a Eucalyptus grandis plantation under omission of N, P, K Ca and Mg over two crop rotation*. Forest Ecology and Management, 447:158-168. 2019.

RODRIGUES LD. *Contributions to the study of eucalyptus bark pyrolysis.* Thesis (Master's degree). Federal University of Espirito Santo. 2018

RODRIGUES MLM. *Technical-economic study of the implementation of small-scale biomass cogeneration in an industry.* Thesis (Master's degree). Pontifical Catholic University of Minas Gerais (PUCMG). 2009.

ROYAL SOCIETY OF CHEMISTRY. *ChemSpider*. 2022. Available at: https://www.chemspider.com/

SADER KM, HURTADO SIM, DELGADO ADG. *Computer-aided environmental and exergy analysis as decision-making tools for selecting bio-oil feedstocks*. Renewable and Sustainable Energy Reviews, 112:42-57. 2019.

SALINA FH, ALMEIDA IA, BITTENCOURT FR. 2019. *RenovaBio Opportunities and Biofuels Outlook in Brazil*. Renewable Energy and Sustainable Buildings: 391-399. 2019.

SANTOS MPS, MANOVIC V, HANAK DP. *Unlocking the potential of pulp and paper industry to achieve carbon-negative emissions via calcium looping retrofit*. Journal of Cleaner Production, 280(1):123431. 2021.

SÃO PAULO STATE GOVERNMENT, Secretary of State for the Environment, State Council for Water Resources. 2011. CRH No. 111, December 10th 2009. Available at: https://cetesb.sp.gov.br/posgraduacao/wp-content/uploads/sites/33/2016/09/Aula-4-Cobran%C3%A7a-pelo-Uso-da-%C3%81gua-Ana-L%C3%BAcia-Aur%C3%A9lio.pdf

SÃO PAULO STATE GOVERNMENT, Secretary of State for the Environment, State Council for Water Resources. 2011.CRH No. 123, March 21th 2011. Available at: https://cetesb.sp.gov.br/posgraduacao/wp-content/uploads/sites/33/2016/09/Aula-4-Cobran%C3%A7a-pelo-Uso-da-%C3%81gua-Ana-L%C3%BAcia-Aur%C3%A9lio.pdf

SCOWN CD, BARAL NR, YANG M, VORA N, HUNTINGTON T. *Technoeconomic analysis for biofuels and bioproducts*. Current Opinion in Biotechnology, 67:58-64. 2021.

SHEN D, JIN W, HU J, XIAO R, LUO K. *An overview on fast pyrolysis of the main constituents in lignocellulosic biomass to valued-added chemicals: Structures, pathways and interactions*. Renewable and Sustainable Energy Reviews, 51:761-774. 2015.

SHEN DK, GU S. *The mechanism for thermal decomposition of cellulose and its main products*. Bioresource Technology, 100(24):6496-6504, 2009.

SILVA ALP. *Cost of production, harvesting and transport of eucalyptus wood from the forest producer program in the south of Espírito Santo*. Thesis (Master's degree). Federal University of Espírito Santo (UFES). 2012

SINGH RK, SHRIVASTAVA DK, SARKAR A, CHAKRABORTY JP. *Co-pyrolysis of eucalyptus and sodium polyacrylate: optimization and synergistic effect*. Fuel, 277:118115. 2020.

SOLARTE-TORO JC, GONZÁLEZ-AGUIRRE JA, GIRALDO JAP, ALZATE CAC. *Thermochemical processing of woody biomass: A review focused on energy-driven applications and catalytic upgrading*. Renewable and Sustainable Energy Reviews, 136:110376. 2021.

SPEIGHT JG. *Handbook of Petroleum Analysis 2nd Edition.* John Wiley & Sons. 2015.

SPEIGHT JG. *Petroleum Chemistry and Refining 1st Edition*. Taylor & Francis. 1998.

SPEIGHT JG. *The Chemistry and Technology of Petroleum 5th Edition*. CRC Press. 2014.

STAŠ M, AUERSVALD M, VOZKA P. *Two-Dimensional Gas Chromatography Characterization of Pyrolysis Bio-oils: A Review*. Energy Fuels, 35(10):8541-8557. 2021.

STATOIL EQUINOR. *Crude oil assays*. 2020. Available at: https://www.equinor.com/en/what-we-do/crude-oil-and-condensate-assays.html

STEFANIDIS SD, KALOGIANNIS KG, LAPPAS, AA. *Co-processing bio-oil in the refinery for drop-in biofuels via fluid catalytic cracking*. WIREs En and Env 7(3):281. 2017.

SUCIU LG, MASIELLO CA, GRIFFIN RJ. *Anhydrosugars as tracers in the Earth system.* Biogeochemistry, 146:209-256. 2019

TALMADGE M, SINGH A, JIANG Y, ASKANDER J. *Strategies for Co-processing in Refineries – Techno-economic & Refinery Impact Analysis*. Paper presented at: SCR Project Meeting – National Renewable Energy Laboratory (NREL), Richland Washington, USA. 2021.

TANG Q, CHEN Y, YANG H, LIU M, XIAO H, WU Z, CHEN H, NAQVI SR. *Prediction of Bio-oil Yield and Hydrogen Contents Based on Machine Learning Method: Effect of Biomass Compositions and Pyrolysis Conditions*. Energy&Fuels, 34(9):11050-11060. 2020.

THE WORLD BANK. *Carbon Pricing Dashboard*. 2022.

TORRI IDV. *Caracterização de bio-óleos obtidos por pirólise da serragem de Eucalyptus sp. (hardwood) e picea abies (softwood) utilizando as técnicas de cromatografia gasosa acoplada à espectrometria de massas*. Masters Dissertation, Federal University of Rio Grande do Sul, Brazil. 2013.

TORROBA, A. *Liquid Biofuels Atlas 2020-2021*. Inter-American Institute for Cooperation on Agriculture (IICA). 2021.

TRAPP S, CROTEAU R. *Defensive Resin Biosynthesis in Conifers*. Annual Review of Plant Physiology and Plant Molecular Biology, 52:689-724. 2001.

TREESE SA, PUJADÓ PR, JONES DSJ. *Handbook of Petroleum Processing 2nd Edition*. Springer Reference. 2015.

TURTON R, BAILIE RC, WHITING WB. *Analysis, Synthesis and Design of Chemical Processes*. Prentice Hall. 2012.

U.S. ENERGY INFORMATION ADMINISTRATION (EIA). *Crude oil distillation and the definition of refinery capacity.* 2012.

UDDIN MN, TECHATO K, TAWEEKUN J, RAHMAN MM, RASUL MG, MAHILA TMI, ASHRAFUR SM. 2018. *An Overview of Recent Developments in Biomass Pyrolysis Technologies*. Biomass Processing for Biofuels, Bioenergy and Chemicals. 2018.

ULLAH Z, KHAN M, NAQVI SR, FAROOQ W, YANG H, WANG S, VO DVN. *A comparative study of machine learning methods for bio-oil yield prediction – A genetic algorithm-based features selection*. Bioresource Technology, 335:125292. 2021.

UNITED STATES ENVIRONMENTAL PROTECTION AGENCY (EPA). *Green House Gases*. 2021.

US DEPARTMENT OF AGRICULTURE (USDA) – Foreign Agricultural Service. *India: Biofuels Annual.* 2021-1.

US DEPARTMENT OF AGRICULTURE (USDA) – Foreign Agricultural Service. *China: Biofuels Annual.* 2021-2.

US DEPARTMENT OF AGRICULTURE (USDA) – Foreign Agricultural Service. *Brazil: Biofuels Annual.* 2021-3.

UZOEJINWA B, HE X, WANG S, ABOMOHRA AE, HU Y, WANG Q. *Co-pyrolysis of biomass and waste plastics as a thermochemical conversion technology for high-grade biofuel production: Recent progress and future directions elsewhere worldwide.* Energy Conversion and Management, 163:468-492. 2018.

VAN DYK S, SU J, MCMILLAN JD, SADDLER JJ. *Potential synergies of drop-in biofuel production with further co-processing at oil refineries*. Biofuels, Bioproducts and Biorefining, 13(3). 2019.

VANINI G, BARRA TA, SOUZA LM, MADEIRA NCL, GOMES AO, ROMÃO W, AZEVEDO DA. *Characterization of nonvolatile polar compounds from Brazilian oils by*

electrospray ionization with FT-ICR MS and Orbitrap-MS. Fuel, 282:118790. 2020.

VARMA AK, THAKUR LS, SHANKAR R, MONDAL P. *Production and distillative recovery of valuable lignin-derived products from biocrude*. Waste Management, 89:224-235. 2019.

VASALOS IA, LAPPAS AA, KOPALIDOU EP, KALOGIANNIS KG. *Biomass catalytic pyrolysis: process design and economic analysis*. WIREs Energy and Environment, 5. 2016.

WANG Q, TIAN D, HU J, SHEN F, YANG G, ZHANG Y, DENG S, ZHANG J, ZENG Y, HU Y. *Fates of hemicellulose, lignin and cellulose in concentrated phosphoric acid with hydrogen peroxide (PHP) pretreatment*. RSC Advances, 8:12714-12723. 2018.

WANG S, WANG Y, CAI Q, WANG X, JIN H, LUO Z. *Multi-step separation of monophenols and pyrolytic lignins from the water-insoluble phase of bio-oil.* Separation and Purification Technology, 122:248-255. 2014.

WANG Y, LENG F, CHEN J, ZHU L, LUO Z. *Separation and characterization of pyrolytic lignins from the heavy fraction of bio-oil by molecular distillation*. Separation and Purification Technology, 152:123-132. 2015.

WANG Y, WANG S, LENG F, CHEN J, ZHU L, LUO Z. *Separation and characterization of pyrolytic lignins from the heavy fraction of bio-oil by molecular distillation.* Separation and Purification Technology, 125:123-132. 2015.

WOLINETZ M. *Biofuels in Canada 2020: Tracking biofuel consumption, feedstocks, avoided greenhouse gas emissions and fuel cost impacts.* Navius Research. 2020.

WU L, WANG Y, ZHENG L, WANG P, HAN X. *Techno-economic analysis of bio-oil co-processing with vacuum gas oil to transportation fuels in an existing fluid catalytic cracker*. En Con And Man 197:111901. 2019.

WU L, YANG, Y, YAN T, WANG, Y, ZHENG L, QIAN K, HONG F. *Sustainable design and optimization of co-processing of bio-oil and vacuum gas oil in an existing refinery*. Renewable and Sustainable Energy Reviews, 130:109952. 2020.

YÁÑEZ É, MEERMAN H, RAMÍREZ A, CASTILLO É, FAAIJ A. *Assessing bio-oil co-processing routes as CO2 mitigation strategies in oil refineries.* Biofuels, Bioproducts & Biorefining, 15(1):305-333, 2020

YANG Z, KUMAR A, HUHNKE RL. *Review of recent developments to improve storage and transportation stability of bio-oil*. Renewable and Sustainable Energy Reviews, 50: 859-870. 2015.

YOUNG C. *Integration of Advanced Biofuels in Alberta*. Thesis (Master's degree). Graduate Program in Sustainable Energy – University of Calgary. 2019

YUAN X, SUN M, WANG C, ZHU X. *Full temperature range study of rice husk bio-oil distillation: Distillation characteristics and product distribution*. Separation and Purification Technology, 263:118382. 2021.

ZHANG P, YEE NW, FILIP SV, HETRICK CE, YANG B, GREEN WH. *Modeling study of the anti-knock tendency of substituted phenols as additives: an application of the reaction mechanism generator (RMG)*. Phys. Chem. Phys, 20:10637-10649. 2018.

Appendix A1 – Software Integration

A1.1. Algorithm for Bio-oil Components Simulation and Properties Optimization

The algorithm for software integration used in this work is presented below. The code presents the integration between Microsoft Excel and Aspen Plus, as well as optimization algorithm used to generate the best surrogate mixture possible for FPBO.

```
Public Sub Optimizer()

Dim i As Double
Dim j As Double
Dim ResultCompRange As Range
Dim FinalCompRange As Range
Dim cycle As Integer
Dim pasterror As Double
Dim currenterror As Double
Dim tolerance As Double
Dim variation As Double

tolerance = 0.0001 '10^-4 error
i = 1 'Cycles
j = 3 'Result Lines Identifier


'Multi-stage Optimization Cycles
For cycle = 1 To 60

   'Call Solver #1
   SolverComposition2 'Solver for Composition, constrained by H/C and O/C

   'Paste Results
   Set FinalCompRange = Sheets("Optimizer_Results").Range(Sheets("Optimizer_Results").Cells(j, 3), Sheets("Optimizer_Results").Cells(j, 40))
   Set ResultCompRange = Sheets("Bio-oil Eucalyptus Results").Range(Sheets("Bio-oil Eucalyptus Results").Cells(111, 7), Sheets("Bio-oil Eucalyptus Results").Cells(152, 7))
      ResultCompRange.Copy
      FinalCompRange.PasteSpecial Paste:=xlPasteValues, Operation:=xlNone, SkipBlanks:=False, Transpose:=True
   Sheets("Optimizer_Results").Cells(j, 1) = i 'Counting i
   Sheets("Optimizer_Results").Cells(j, 2) = j 'Counting j
   Sheets("Optimizer_Results").Cells(j, 46) = Sheets("Bio-oil Eucalyptus Results").Cells(158, 9) 'Name
   Sheets("Optimizer_Results").Cells(j, 47) = Sheets("Bio-oil Eucalyptus Results").Cells(159, 10) 'H/C
   Sheets("Optimizer_Results").Cells(j, 48) = Sheets("Bio-oil Eucalyptus Results").Cells(160, 10) 'O/C
   Sheets("Optimizer_Results").Cells(j, 49) = Sheets("Bio-oil Eucalyptus Results").Cells(169, 10) 'MW
   Sheets("Optimizer_Results").Cells(j, 50) = Sheets("Bio-oil Eucalyptus Results").Cells(170, 10) 'MABP

   'Call Aspen
   RunAspen2

   'Call Solver #2
   SolverProperties2 'Solver for Composition, constrained by properties

      Sheets("Bio-oil Eucalyptus Results").Cells(171, 10) = Sheets("Optimizer_Results").Cells(j, 51) 'RHO
      Sheets("Bio-oil Eucalyptus Results").Cells(172, 10) = Sheets("Optimizer_Results").Cells(j, 52) 'MI
      Sheets("Bio-oil Eucalyptus Results").Cells(173, 10) = Sheets("Optimizer_Results").Cells(j, 53) 'CP
      Sheets("Bio-oil Eucalyptus Results").Cells(174, 10) = Sheets("Optimizer_Results").Cells(j, 54) 'K
      Sheets("Bio-oil Eucalyptus Results").Cells(175, 10) = Sheets("Optimizer_Results").Cells(j, 55) 'T0
      Sheets("Bio-oil Eucalyptus Results").Cells(176, 10) = Sheets("Optimizer_Results").Cells(j, 56) 'T5
      Sheets("Bio-oil Eucalyptus Results").Cells(177, 10) = Sheets("Optimizer_Results").Cells(j, 57) 'T10
      Sheets("Bio-oil Eucalyptus Results").Cells(178, 10) = Sheets("Optimizer_Results").Cells(j, 58) 'T30
```

```
        Sheets("Bio-oil Eucalyptus Results").Cells(179, 10) = Sheets("Optimizer_Results").Cells(j, 59) 'T50
        Sheets("Bio-oil Eucalyptus Results").Cells(180, 10) = Sheets("Optimizer_Results").Cells(j, 60) 'T70
        Sheets("Bio-oil Eucalyptus Results").Cells(181, 10) = Sheets("Optimizer_Results").Cells(j, 61) 'T90
        Sheets("Bio-oil Eucalyptus Results").Cells(182, 10) = Sheets("Optimizer_Results").Cells(j, 62) 'T95
        Sheets("Bio-oil Eucalyptus Results").Cells(183, 10) = Sheets("Optimizer_Results").Cells(j, 63) 'T100

    i = i + 1
    j = j + 1

variation = 0.005

'Global MSE Check
    If cycle = 1 Then
        Sheets("Bio-oil Eucalyptus Results").Cells(201, 10) = cycle
    Else
        If (currenterror < tolerance) Then
            Sheets("Bio-oil Eucalyptus Results").Cells(201, 10) = cycle
            Exit For
        Else
            Sheets("Bio-oil Eucalyptus Results").Cells(104, 2) = Sheets("Bio-oil Eucalyptus Results").Cells(104, 2) + variation
            Sheets("Bio-oil Eucalyptus Results").Cells(105, 2) = Sheets("Bio-oil Eucalyptus Results").Cells(105, 2) + variation
            Sheets("Bio-oil Eucalyptus Results").Cells(106, 2) = Sheets("Bio-oil Eucalyptus Results").Cells(106, 2) + variation

            Sheets("Bio-oil Eucalyptus Results").Cells(142, 5) = Sheets("Bio-oil Eucalyptus Results").Cells(142, 5) + variation
            Sheets("Bio-oil Eucalyptus Results").Cells(143, 5) = Sheets("Bio-oil Eucalyptus Results").Cells(143, 5) + variation
            Sheets("Bio-oil Eucalyptus Results").Cells(144, 5) = Sheets("Bio-oil Eucalyptus Results").Cells(144, 5) + variation
            Sheets("Bio-oil Eucalyptus Results").Cells(145, 5) = Sheets("Bio-oil Eucalyptus Results").Cells(145, 5) + variation
            Sheets("Bio-oil Eucalyptus Results").Cells(146, 5) = Sheets("Bio-oil Eucalyptus Results").Cells(146, 5) + variation
            Sheets("Bio-oil Eucalyptus Results").Cells(147, 5) = Sheets("Bio-oil Eucalyptus Results").Cells(147, 5) + variation
            Sheets("Bio-oil Eucalyptus Results").Cells(148, 5) = Sheets("Bio-oil Eucalyptus Results").Cells(148, 5) + variation
            Sheets("Bio-oil Eucalyptus Results").Cells(149, 5) = Sheets("Bio-oil Eucalyptus Results").Cells(149, 5) + variation
            Sheets("Bio-oil Eucalyptus Results").Cells(150, 5) = Sheets("Bio-oil Eucalyptus Results").Cells(150, 5) + variation
            Sheets("Bio-oil Eucalyptus Results").Cells(151, 5) = Sheets("Bio-oil Eucalyptus Results").Cells(151, 5) + variation
            Sheets("Bio-oil Eucalyptus Results").Cells(201, 10) = cycle
        End If
    End If

currenterror = Sheets("Bio-oil Eucalyptus Results").Cells(200, 10)
Sheets("Optimizer_Results").Cells(j - 1, 64) = currenterror
Sheets("Optimizer_Results").Cells(j - 1, 65) = pasterror
pasterror = currenterror

DoEvents
Next

MsgBox ("Run Complete!")
End Sub
Sub SolverComposition2()
    Sheets("Bio-oil Eucalyptus Results").Select
    SolverReset
    SolverOptions Assumenonneg:=True
    'Constraints
        SolverAdd CellRef:="$B$104", Relation:=1, FormulaText:="1" 'sugar less than 1
        SolverAdd CellRef:="$B$105", Relation:=1, FormulaText:="1" 'water less than 1
        SolverAdd CellRef:="$B$106", Relation:=1, FormulaText:="1" 'lignin derived less than 1

        SolverAdd CellRef:="$C$104", Relation:=1, FormulaText:="0.18" 'sugar less than 0.18
        SolverAdd CellRef:="$C$104", Relation:=3, FormulaText:="0.05" 'sugar greater than 0.05
        SolverAdd CellRef:="$C$105", Relation:=1, FormulaText:="0.30" 'final water less than 0.30
        SolverAdd CellRef:="$C$105", Relation:=3, FormulaText:="0.18" 'final water greater than 0.18
        SolverAdd CellRef:="$C$106", Relation:=1, FormulaText:="0.2"  'final lignin derived less than 0.2
        SolverAdd CellRef:="$C$106", Relation:=3, FormulaText:="0.05" 'final lignin derived greater than 0.05
```

```
        SolverAdd CellRef:="$E$142", Relation:=3, FormulaText:="0.05" 'final lignin derived compound greater than 0.05
        SolverAdd CellRef:="$E$143", Relation:=3, FormulaText:="0.05" 'final lignin derived compound greater than 0.05
        SolverAdd CellRef:="$E$144", Relation:=3, FormulaText:="0.05" 'final lignin derived compound greater than 0.05
        SolverAdd CellRef:="$E$145", Relation:=3, FormulaText:="0.05" 'final lignin derived compound greater than 0.05
        SolverAdd CellRef:="$E$146", Relation:=3, FormulaText:="0.05" 'final lignin derived compound greater than 0.05
        SolverAdd CellRef:="$E$147", Relation:=3, FormulaText:="0.05" 'final lignin derived compound greater than 0.05
        SolverAdd CellRef:="$E$149", Relation:=3, FormulaText:="0.05" 'final lignin derived compound greater than 0.05
        SolverAdd CellRef:="$E$150", Relation:=3, FormulaText:="0.05" 'final lignin derived compound greater than 0.05
        SolverAdd CellRef:="$E$151", Relation:=3, FormulaText:="0.05" 'final lignin derived compound greater than 0.05

        SolverAdd CellRef:="$E$142", Relation:=1, FormulaText:="0.25" 'final lignin derived compound lower than 0.25
        SolverAdd CellRef:="$E$143", Relation:=1, FormulaText:="0.25" 'final lignin derived compound lower than 0.25
        SolverAdd CellRef:="$E$144", Relation:=1, FormulaText:="0.25" 'final lignin derived compound lower than 0.25
        SolverAdd CellRef:="$E$145", Relation:=1, FormulaText:="0.25" 'final lignin derived compound lower than 0.25
        SolverAdd CellRef:="$E$146", Relation:=1, FormulaText:="0.25" 'final lignin derived compound lower than 0.25
        SolverAdd CellRef:="$E$147", Relation:=1, FormulaText:="0.25" 'final lignin derived compound lower than 0.25
        SolverAdd CellRef:="$E$148", Relation:=1, FormulaText:="0.25" 'final lignin derived compound lower than 0.25
        SolverAdd CellRef:="$E$149", Relation:=1, FormulaText:="0.25" 'final lignin derived compound lower than 0.25
        SolverAdd CellRef:="$E$150", Relation:=1, FormulaText:="0.25" 'final lignin derived compound lower than 0.25
        SolverAdd CellRef:="$E$151", Relation:=1, FormulaText:="0.25" 'final lignin derived compound lower than 0.25

        SolverAdd CellRef:="$G$154", Relation:=2, FormulaText:="1" 'final components equal to 1

        SolverAdd CellRef:="$J$159", Relation:=1, FormulaText:="1.5" 'final H/C less than 1.75
        SolverAdd CellRef:="$J$159", Relation:=3, FormulaText:="1.0" 'final H/C greater than 1.25
        SolverAdd CellRef:="$J$160", Relation:=1, FormulaText:="0.5" 'final O/C less than 0.50
        SolverAdd CellRef:="$J$160", Relation:=3, FormulaText:="0.25" 'final O/C greater than 0.30

    'Goal - Minimize (2) the error by changing parameters
        SolverOk MaxMinVal:=2, ByChange:="$B$104:$B$106,$E$142:$E$151" 'minimize all differences by changing the parameters listed
        SolverSolve True

End Sub

Public Sub RunAspen2()

Dim k As Integer
Dim m As Integer
Dim minitial As Integer
Dim mfinal As Integer
Dim n As Integer
Dim p As Integer
'Dim step As Integer

Dim components() As String
Dim analysis() As String
Dim path           As String
Dim aspensimulation As Happ.HappLS
Dim node       As IHNode
Dim nodes      As IHNodeCol

'Running Aspen
path = "C:\Users\Daniel\Desktop\Bio-Oil Estimator V2.bkp" 'only needs to run once (opened), then must be commented
Set aspensimulation = Nothing
Set aspensimulation = GetObject(path)
aspensimulation.Visible = True
aspensimulation.SuppressDialogs = True

'Redimension table based on total components
n = aspensimulation.Tree.FindNode("\Data\Components\Specifications\Input\OUTNAME").Elements.Count
ReDim components(0 To n, 1 To 2)
```

```
components(0, 1) = "Component ID"
components(0, 2) = "Mass Fraction"

For k = 1 To n
components(k, 1) = aspensimulation.Tree.FindNode("\Data\Components\Specifications\Input\OUTNAME").Elements.Item(k - 1).Value
DoEvents
Next

'Redimentsion analysis table based on analysis selected
p = Worksheets("Optimizer_Results").Cells(2, Columns.Count).End(xlToLeft).Column - (2 + n + 8)
ReDim analysis(0 To p, 1 To 2)
analysis(0, 1) = "Analysis ID"
analysis(0, 2) = "Value"

For k = 1 To p
analysis(k, 1) = Worksheets("Optimizer_Results").Cells(2, 2 + n + 6 + k)
DoEvents
Next

'Inicial line of analysis
m = Worksheets("Optimizer_Results").Cells(Rows.Count, 1).End(xlUp).Row

   'Copy Inputs
   For k = 1 To n
      components(k, 2) = Worksheets("Optimizer_Results").Cells(m, k + 2) 'Copy mass fractions to table
      aspensimulation.Tree.FindNode("\Data\Streams\BIO-OIL\Input\FLOW\MIXED\" & components(k, 1)).Value = components(k, 2) 'Copy mass fractions to aspen
      DoEvents
   Next

   'Run Aspen
   aspensimulation.Engine.Reinit (4)
   aspensimulation.Engine.Run2

   'Copy Outputs
   For k = 1 To p
      analysis(k, 2) = aspensimulation.Tree.FindNode("\Data\Flowsheeting Options\Measurement\" & analysis(k, 1) & "\Output\MODEL\1").Value
      Worksheets("Optimizer_Results").Cells(m, 2 + n + 6 + k) = aspensimulation.Tree.FindNode("\Data\Flowsheeting Options\Measurement\" & analysis(k, 1) &
"\Output\MODEL\1").Value 'retrieve properties selected
      DoEvents
   Next

End Sub
Sub SolverProperties2()
   Sheets("Bio-oil Eucalyptus Results").Select
   SolverReset
   SolverOptions Assumenonneg:=True
   'Constraints
      SolverAdd CellRef:="$B$104", Relation:=1, FormulaText:="1" 'sugar less than 1
      SolverAdd CellRef:="$B$105", Relation:=1, FormulaText:="1" 'water less than 1
      SolverAdd CellRef:="$B$106", Relation:=1, FormulaText:="1" 'lignin derived less than 1

      SolverAdd CellRef:="$C$104", Relation:=1, FormulaText:="0.18" 'sugar less than 0.18
      SolverAdd CellRef:="$C$104", Relation:=3, FormulaText:="0.05" 'sugar greater than 0.05
      SolverAdd CellRef:="$C$105", Relation:=1, FormulaText:="0.30" 'final water less than 0.30
      SolverAdd CellRef:="$C$105", Relation:=3, FormulaText:="0.18" 'final water greater than 0.18
      SolverAdd CellRef:="$C$106", Relation:=1, FormulaText:="0.2"  'final lignin derived less than 0.2
      SolverAdd CellRef:="$C$106", Relation:=3, FormulaText:="0.05" 'final lignin derived greater than 0.05

      SolverAdd CellRef:="$E$142", Relation:=3, FormulaText:="0.05" 'final lignin derived compound greater than 0.05
      SolverAdd CellRef:="$E$143", Relation:=3, FormulaText:="0.05" 'final lignin derived compound greater than 0.05
      SolverAdd CellRef:="$E$144", Relation:=3, FormulaText:="0.05" 'final lignin derived compound greater than 0.05
      SolverAdd CellRef:="$E$145", Relation:=3, FormulaText:="0.05" 'final lignin derived compound greater than 0.05
```

```
    SolverAdd CellRef:="$E$146", Relation:=3, FormulaText:="0.05" 'final lignin derived compound greater than 0.05
    SolverAdd CellRef:="$E$147", Relation:=3, FormulaText:="0.05" 'final lignin derived compound greater than 0.05
    SolverAdd CellRef:="$E$149", Relation:=3, FormulaText:="0.05" 'final lignin derived compound greater than 0.05
    SolverAdd CellRef:="$E$150", Relation:=3, FormulaText:="0.05" 'final lignin derived compound greater than 0.05
    SolverAdd CellRef:="$E$151", Relation:=3, FormulaText:="0.05" 'final lignin derived compound greater than 0.05

    SolverAdd CellRef:="$E$142", Relation:=1, FormulaText:="0.25" 'final lignin derived compound lower than 0.25
    SolverAdd CellRef:="$E$143", Relation:=1, FormulaText:="0.25" 'final lignin derived compound lower than 0.25
    SolverAdd CellRef:="$E$144", Relation:=1, FormulaText:="0.25" 'final lignin derived compound lower than 0.25
    SolverAdd CellRef:="$E$145", Relation:=1, FormulaText:="0.25" 'final lignin derived compound lower than 0.25
    SolverAdd CellRef:="$E$146", Relation:=1, FormulaText:="0.25" 'final lignin derived compound lower than 0.25
    SolverAdd CellRef:="$E$147", Relation:=1, FormulaText:="0.25" 'final lignin derived compound lower than 0.25
    SolverAdd CellRef:="$E$148", Relation:=1, FormulaText:="0.25" 'final lignin derived compound lower than 0.25
    SolverAdd CellRef:="$E$149", Relation:=1, FormulaText:="0.25" 'final lignin derived compound lower than 0.25
    SolverAdd CellRef:="$E$150", Relation:=1, FormulaText:="0.25" 'final lignin derived compound lower than 0.25
    SolverAdd CellRef:="$E$151", Relation:=1, FormulaText:="0.25" 'final lignin derived compound lower than 0.25

    SolverAdd CellRef:="$G$154", Relation:=2, FormulaText:="1" 'final components equal to 1

    SolverAdd CellRef:="$J$159", Relation:=1, FormulaText:="1.5" 'final H/C less than 1.75
    SolverAdd CellRef:="$J$159", Relation:=3, FormulaText:="1.0" 'final H/C greater than 1.25
    SolverAdd CellRef:="$J$160", Relation:=1, FormulaText:="0.5" 'final O/C less than 0.50
    SolverAdd CellRef:="$J$160", Relation:=3, FormulaText:="0.25" 'final O/C greater than 0.30

  'Goal - Minimize (2) the error by changing parameters
    SolverOk SetCell:=Sheets("Bio-oil Eucalyptus Results").Cells(200, 10), MaxMinVal:=2, ByChange:="$B$104:$B$106,$E$142:$E$151" 'minimize cell respecting all differences
by changing the parameters listed
    SolverSolve True

End Sub
```

Appendix A2 – Datasets

This appendix includes all the datasets used for FPBO surrogate mixture modeling.

A2.1. Dataset 1 – Components Mass Fractions (5 sources)

Chang et al. (2013)

Compound	MW (g.mol^{-1})	BP (°C)	Formula	Chemical Group	Mass Fraction Assumed (%)
Acetic acid	60.05	117.90	C2H4O2	Acids	4.65
Propanoic acid	74.08	141.20	C3H6O2	Acids	0.1
Butanoic acid	88.11	163.50	C4H8O2	Acids	0.06
Benzoic acid, 4-hydroxy-3-methoxy-	168.15	353.40	C8H8O4	Acids	0.55
Acetic acid, 4-hydroxy-3-methoxyphenyl-	198.17	368.70	C9H10O4	Acids	0.04
Levoglucosan	162.14	384.00	C6H10O5	Sugars	4.13
Furanmethanol, 2-	98.10	170.00	C5H6O2	Alcohols	0.09
Furancarbaldehyde, 2-	96.08	161.70	C5H4O2	Aldehydes	0.63
Furancarboxaldehyde, 5-Methyl-2-	110.11	187.00	C6H6O2	Aldehydes	0.06
Furancarbaldehyde, 5-hydroxymethyl-	126.11	115.00	C6H6O3	Aldehydes	0.15
Benzaldehyde, 4-hydroxy-3-methoxy-	153.14	285.00	C8H8O3	Aldehydes	0.44
Propenal, 3-(4-hydroxy-2-methoxyphenyl)-2-	178.18	360.30	C10H10O3	Aldehydes	0.07
Benzaldehyde, 4-hydroxy-3,5-dimethoxy-	182.17	192.00	C9H10O4	Aldehydes	0.25
Butanone, 2-	72.11	75.60	C4H8O	Ketones	0.15
Propanone, 1-hydroxy-2-	74.08	145.55	C3H6O2	Ketones	1.96
Cyclopentenone, 2-1-	82.10	136.00	C5H6O	Ketones	0.14
Furanone, 2(5H)-	84.07	86.50	C4H4O2	Ketones	0.12
Pentenone, (E)-3-2-	84.12	122.00	C5H8O	Ketones	0.05
Butanedione, 2,3-	86.09	88.00	C4H6O2	Ketones	0.16
Butanone, 1-hydroxy-2-	88.11	153.00	C4H8O2	Ketones	0.18
Cyclopentenone, 2-methyl-2-1-	96.13	159.50	C6H8O	Ketones	0.06
Cyclopentenone, 3-methyl-2-1-	96.13	157.50	C6H8O	Ketones	0.06
Furanone, 3-Methyl-2(5H)-	98.10	222.40	C5H6O2	Ketones	0.04
Furanone, 4-methyl-2(5H)-	98.10	222.40	C5H6O2	Ketones	0.05
Furanone, 5-methyl-2(5H)-	98.10	209.00	C5H6O2	Ketones	0.05
Cyclopentanedione, 1,2-	98.14	174.00	C5H6O2	Ketones	0.35
Cyclopentenedione, 4-1,3-	98.14	226.00	C5H4O2	Ketones	0.02
Cyclopentanedione, 3-methyl-1-2-	112.13	170.00	C6H8O2	Ketones	0.25
Cyclopentenone, 3-ethyl-2-hydroxy-2-1	126.15	275.48	C7H10O2	Ketones	0.03
Acetophenone, 4-hydroxy-3-methoxy-	150.17	295.00	C9H10O2	Ketones	0.06
Acetophenone, 2,6-dihydroxy-4-methoxy-	182.17	256.50	C9H10O4	Ketones	0.14
Ethanone, 1-(4-Hydroxy-3,5-dimethoxyphenyl)	196.17	208.00	C10H12O4	Ketones	0.14
Phenol	94.11	181.70	C6H6O	Phenols	0.08
Phenol, 2-methyl-	108.14	191.00	C7H8O	Phenols	0.05
Phenol, 3-methyl-	108.14	202.20	C7H8O	Phenols	0.06
Phenol, 4-methyl-	108.14	201.90	C7H8O	Phenols	0.03
Phenol, 4-ethyl-	122.16	218.00	C8H10O	Phenols	0.06
Phenol, 2-methoxy-	124.14	205.00	C7H8O2	Phenols	0.19
Phenol, 2-methoxy-4-methyl-	138.16	221.00	C8H10O2	Phenols	0.13
Phenol, 2-methoxy-4-vinyl-	150.17	245.00	C9H10O2	Phenols	0.15
Phenol, 2,6-dimethoxy-	154.16	261.00	C8H10O3	Phenols	0.48
Phenol, 2-methoxy-4-(prop-1-en-1-yl)-	164.20	266.00	C10H12O2	Phenols	0.04
Phenol, 4-allyl-2-methoxy-	164.20	254.00	C10H12O2	Phenols	0.07
Phenol, 2-methoxy-4-propyl-	166.22	125.00	C10H14O2	Phenols	0.04
Phenol, 2,6-dimethoxy-4-(2-propenyl)-	194.23	168.55	C11H14O3	Phenols	0.75
Water	18.02	100.00	H2O	Water	26.00

Merckel (2014)

Compound	MW (g.mol^{-1})	BP (°C)	Formula	Chemical Group	Mass Fraction Assumed (%)
Acetic acid	60.05	117.90	C2H4O2	Acids	3.30
Vanillin lactoside	476.43	787.30	C20C28O13	Sugars	0.70
Propynol, 2-1-	56.06	115.00	C3H4O	Alcohols	1.90
Butenol, 3-2-	72.11	97.30	C4H8O	Alcohols	0.70
Furanmethanol, 2-	98.10	170.00	C5H6O2	Alcohols	1.00
Formaldehyde	30.03	-19.00	CH2O	Aldehydes	2.70
Ethanal	44.05	21.00	C2H4O	Aldehydes	0.30
Propenal, 2-	56.06	49.85	C3H4O	Aldehydes	2.20
Furancarbaldehyde, 2-	96.08	161.70	C5H4O2	Aldehydes	3.40
Benzene, 1,2,4-trimethoxy-	120.19	247.00	C9H12O3	Aromatics	2.90
Propanone, 2-	58.08	82.40	C3H6O2	Ketones	1.80
Butenone, 2-1-	70.09	102.35	C4H6O	Ketones	1.00
Propanone, 1-hydroxy-2-	74.08	145.55	C3H6O2	Ketones	1.80
Cyclopentenone, 2-hydroxy-2-1-	98.10	244.80	C5H6O2	Ketones	3.50
Cyclopentanedione, 3-methyl-1-2-	112.13	170.00	C6H8O2	Ketones	1.60
Propanone, 1-(acetyloxy)-2-	166.12	173.85	C5H8O3	Ketones	0.50
Ethanone, 1-(3,4-dimethoxyphenyl)-	180.20	287.05	C10H12O3	Ketones	3.50
Phenol, 3-methyl-	108.14	202.20	C7H8O	Phenols	1.20
Phenol, 2-hydroxy-4-methyl-	124.14	251.05	C8H10O2	Phenols	0.70
Phenol, 4-methoxy-	124.14	243.00	C7H8O	Phenols	2.00
Phenol, 2-methoxy-4-methyl-	138.16	221.00	C8H10O2	Phenols	1.90
Phenol, 2-hydroxy-3-methoxy-	140.14	268.00	C7H8O3	Phenols	3.10
Phenol, 2-methoxy-4-vinyl-	150.17	245.00	C9H10O2	Phenols	3.10
Phenol, 2-methoxy-4-Ethyl-	152.19	236.50	C9H12O2	Phenols	0.90
Phenol, 2,6-dimethoxy-	154.16	261.00	C8H10O3	Phenols	4.90
Phenol, 4-allyl-2-methoxy-	164.20	254.00	C10H12O2	Phenols	2.40
Phenol, 2-methoxy-4-(1-propenyl)-	164.20	253.50	C10H12O2	Phenols	0.80
Phenol, 2-hydroxy-	168.15	245.00	C6H6O2	Phenols	1.90
Phenol, 2,6-dimethoxy-4-(2-propenyl)-	194.23	168.55	C11H14O3	Phenols	3.00
Furan	68.07	31.30	C4H4O	Furans	0.60
Water	18.02	100.00	H2O	Water	30.00*

*Estimated

Wang et al. (2014)

Compound	MW (g.mol^{-1})	BP (°C)	Formula	Chemical Group	Mass Fraction Assumed (%)
Acetic acid	60.05	117.90	C2H4O2	Acids	12.67
Levoglucosan	162.14	384.00	C6H10O5	Sugars	5.50
Furancarbaldehyde, 2-	96.08	161.70	C5H4O2	Aldehydes	4.21
Benzaldehyde, 4-hydroxy-3-methoxy-	153.14	285.00	C8H8O3	Aldehydes	1.04
Benzaldehyde, 4-hydroxy-3,5-dimethoxy-	182.17	192.00	C9H10O4	Aldehydes	0.84
Propanone, 1-hydroxy-2-	74.08	145.55	C3H6O2	Ketones	3.75
Pyranone, 3-hydroxy-2-methyl-4H-4-	126.11	284.70	C6H6O3	Ketones	0.42
Phenol	94.11	181.70	C6H6O	Phenols	4.11
Phenol, 3-methyl-	108.14	202.20	C7H8O	Phenols	1.22
Phenol, 3,4-dimethyl-	122.16	227.00	C8H10O	Phenols	2.31
Phenol, 3-ethyl-	122.16	218.40	C8H10O	Phenols	0.47
Phenol, 2-hydroxy-4-methyl-	124.14	251.05	C8H10O2	Phenols	1.99
Phenol, 2-methoxy-	124.14	205.00	C7H8O2	Phenols	3.44
Phenol, 2-hydroxy-4-ethyl-	138.16	273.00	C8H10O2	Phenols	0.61
Phenol, 2-methoxy-4-methyl-	138.16	221.00	C8H10O2	Phenols	3.76
Phenol, 2-methoxy-4-vinyl-	150.17	245.00	C9H10O2	Phenols	2.28
Phenol, 2-methoxy-4-Ethyl-	152.19	236.50	C9H12O2	Phenols	1.09
Phenol, 2,6-dimethoxy-	154.16	261.00	C8H10O3	Phenols	2.36
Phenol, 2-methoxy-4-(prop-1-en-1-yl)-	164.20	266.00	C10H12O2	Phenols	5.21
Phenol, 4-allyl-2-methoxy-	164.20	254.00	C10H12O2	Phenols	1.10
Phenol, 2-methoxy-4-propyl-	166.22	125.00	C10H14O2	Phenols	1.00
Phenol, 2,6-dimethoxy-4-(2-propenyl)-	194.23	168.55	C11H14O3	Phenols	3.21
Water	18.02	100.00	H2O	Water	29.20

Gholizadeh et al. (2019)

Compound	MW ($g.mol^{-1}$)	BP (°C)	Formula	Chemical Group	Mass Fraction Assumed (%)
Formic acid	46.03	100.80	CH2O2	Acids	0.10
Acetic acid	60.05	117.90	C2H4O2	Acids	3.18
Acrylic acid	72.06	141.00	C3H4O2	Acids	0.10
Propanoic acid	74.08	141.20	C3H6O2	Acids	0.64
Butanoic acid	88.11	163.50	C4H8O2	Acids	0.32
Butenoic acid, 2-methyl-2-	100.11	176.00	C5H8O2	Acids	0.14
Pentenoic acid, 4-	100.12	188.50	C5H8O2	Acids	0.13
Benzoic acid, 3,4-dimethyl-	150.17	271.51	C9H10O2	Acids	0.14
Butanoic acid, 3-hydroxy-	104.10	269.20	C4H8O3	Acids	0.09
Butanedioc acid	118.00	395.50	C4H6O4	Acids	0.16
1,4:3,6-dianhydro-α-D-glucopyranose	144.13	247.44	C6H8O4	Sugars	0.34
Levoglucosan	162.14	384.00	C6H10O5	Sugars	2.07
Methyl β-D-ribofuranoside	164.07	348.70	C6H12O5	Sugars	0.85
Methanol	32.04	64.70	CH4O	Alcohols	0.55
Furanmethanol, 2-	98.10	170.00	C5H6O2	Alcohols	0.21
Formaldehyde	30.03	-19.00	CH2O	Aldehydes	0.20
Ethanal	44.05	21.00	C2H4O	Aldehydes	0.21
Propenal, 2-	56.06	49.85	C3H4O	Aldehydes	0.08
Furancarbaldehyde, 2-	96.08	161.70	C5H4O2	Aldehydes	0.51
Glutaraldehyde	100.11	187.00	C5H8O2	Aldehydes	0.94
Furancarboxaldehyde, 5-Methyl-2-	110.11	187.00	C6H6O2	Aldehydes	0.17
Benzaldehyde, 3-hydroxy	122.12	191.00	C7H6O2	Aldehydes	0.32
Benzaldehyde, 4-hydroxy-2-methyl-	136.15	265.50	C8H8O2	Aldehydes	0.11
Propanal, 3-(acetyloxy)-	116.12	165.50	C5H8O3	Aldehydes	0.18
Propenal, 2-methyl-3-phenyl-2-	146.19	251.60	C10H10O	Aldehydes	0.04
Propanone, 2-	58.08	82.40	C3H6O2	Ketones	0.55
Butanone, 2-	72.11	75.60	C4H8O	Ketones	0.07
Propanone, 1-hydroxy-2-	74.08	145.55	C3H6O2	Ketones	0.82
Cyclopentenone, 2-1-	82.10	136.00	C5H6O	Ketones	0.52
Furanone, 2(5H)-	84.07	86.50	C4H4O2	Ketones	0.51
Cyclopentanone	84.12	131.00	C5H8O	Ketones	0.17
Furanone, 2(3H)-dihydro-	86.09	204.00	C4H6O2	Ketones	2.81
Butanone, 3-methyl-2-	86.13	78.30	C5H10O	Ketones	0.25
Butanone, 1-hydroxy-2-	88.11	153.00	C4H8O2	Ketones	0.61
Cyclopentenone, 3-methyl-2-1-	96.13	157.50	C6H8O	Ketones	1.92
Pyranone, 2H-2-	96.80	209.00	C5H4O2	Ketones	0.11
Pentanone, 1-hydroxy-2-	102.13	152.00	C5H10O2	Ketones	0.05
Ethanone, 1-(2-furanyl)-	110.11	168.50	C6H6O2	Ketones	0.19
Cyclohexenone, 2-methyl-2-1-	110.15	200.30	C7H10O	Ketones	0.10
Cyclopentenone, 2,3-dimethyl-2-1-	110.15	172.40	C7H10O	Ketones	0.19
Cyclopentenone, 2-hydroxy-3-methyl-2-1-	112.13	243.00	C6H8O2	Ketones	2.65
Heptanone, 4-	114.19	143.90	C7H14O	Ketones	0.05
Ethanone, 1-phenyl-	122.14	202.00	C8H8O	Ketones	0.30
Cyclopentenone, 2,3,4-trimethyl-2-1-	124.18	183.00	C8H12O	Ketones	0.14
Cyclopentenone, 3-ethyl-2-1	126.20	157.50	C6H8O	Ketones	0.09
Furan, 5-acetyldihydro-2(3H)-one	128.13	286.30	C6H8O3	Ketones	0.22
Benzofuranone, 2(3H)-	134.13	249.00	C8H6O2	Ketones	0.04
Pyranone, 3-methyl-2H-1-2-benzo	160.17	294.55	C10H8O2	Ketones	0.92
Cyclohexanone, 3-ethyl-	126.20	184.70	C8H14O	Ketones	0.04
Cyclohexanone,4-methylene	110.15	173.70	C7H10O	Ketones	0.05
Cyclopentenone, 2-hydroxy-3-ethyl-2-1-	126.15	275.48	C7H10O2	Ketones	0.35
Cyclopentenone, 2-hydroxy-3,4-dimethyl-2-1-	126.15	245.80	C7H10O2	Ketones	0.21
Furanone, 5-(hydroxymethyl)-dihydro-2(3H)-	116.11	308.90	C5H8O3	Ketones	0.38
1-Indanone	132.16	243.00	C9H8O	Ketones	0.14
Pyranone, 4-hydroxy-3,4-dihydro-2H-1-benzo-2-	164.16	295.90	C9H8O3	Ketones	0.14
Acetate, 1,2-dimethyl-propyl	130.19	122.00	C7H14O2	Esthers	0.11
Acetate, 7-methyl-4-octanol	186.29	204.00	C11H22O2	Esthers	0.20
Eucalyptol	154.25	172.00	C10H18O	Ethers	1.35
Phenol	94.11	181.70	C6H6O	Phenols	0.87
Phenol, 2-methyl-	108.14	191.00	C7H8O	Phenols	0.68
Phenol, 3-methyl-	108.14	202.20	C7H8O	Phenols	0.07
Phenol, 3-hydroxy-	110.10	280.00	C6H6O2	Phenols	0.74
Phenol, 4-hydroxy-	110.11	286.00	C6H6O2	Phenols	2.75
Benzene, ethenyloxy-	120.15	155.55	C8H8O	Phenols	0.20
Phenol, 3,4-dimethyl-	122.16	227.00	C8H10O	Phenols	0.04

Phenol, 3,5-dimethyl-	122.16	219.50	C8H10O	Phenols	0.44
Phenol, 3-ethyl-	122.16	218.40	C8H10O	Phenols	0.18
Phenol, 3-hydroxy-4,5-dimethyl-	122.16	270.80	C8H10O2	Phenols	0.18
Phenol, 4-ethyl-	122.16	218.00	C8H10O	Phenols	0.23
Phenol, 2,3-dimethyl-	122.16	216.00	C8H10O	Phenols	0.17
Phenol, 2,4-dimethyl-	122.16	211.50	C8H10O	Phenols	0.38
Phenol, 2,5-dimethyl-	122.16	211.50	C8H10O	Phenols	0.13
Phenol, 2,6-dimethyl-	122.16	203.00	C8H10O	Phenols	0.16
Phenol, 2-hydroxy-4-methyl-	124.14	251.05	C8H10O2	Phenols	2.12
Phenol, 4-hydroxy-2-methyl-	124.14	283.00	C7H8O2	Phenols	0.97
Phenol, 2-methoxy-	124.14	205.00	C7H8O2	Phenols	2.25
Phenol, 2,5-dihydroxy-	126.11	334.50	C6H6O3	Phenols	0.29
Phenol, 2-allyl	134.17	220.00	C9H10O	Phenols	0.65
Phenol, 2,3,5-trimethyl-	136.19	231.10	C9H12O	Phenols	0.02
Phenol, 2-hydroxy-3-methyl-	124.13	241.05	C7H8O2	Phenols	0.51
Phenol, 5-ethyl-2-methyl-	136.19	225.40	C9H12O	Phenols	0.30
Phenol, 2-methoxy-3-methyl-	138.16	217.80	C8H10O2	Phenols	0.28
Phenol, 3-hydroxy-2-methyl-	124.14	264.00	C7H8O2	Phenols	0.33
Phenol, 3-methoxy-5-methyl-	138.16	255.70	C8H10O2	Phenols	0.39
Phenol, 3-hydroxy-4-ethyl-	138.16	273.80	C8H10O2	Phenols	1.11
Phenol, 4-hydroxy-2,6-dimethyl-	138.16	284.60	C8H10O4	Phenols	0.07
Phenol, 2-allyl-4-methyl-	148.20	233.80	C10H12O	Phenols	0.28
Phenol, isopropyl-2-methyl-	150.22	237.20	C10H14O	Phenols	0.07
Phenol, 3-acetoxy-	152.15	283.00	C8H8O3	Phenols	0.54
Phenol, 2-methoxy-4-Ethyl-	152.19	236.50	C9H12O2	Phenols	0.46
Phenol, 4-allyl-2-methoxy-	164.20	254.00	C10H12O2	Phenols	0.10
Phenol, 2-hydroxy-	168.15	245.00	C6H6O2	Phenols	5.06
Phenol, 2-(1-methylethoxy)-	152.19	102.00	C9H12O2	Phenols	0.19
Phenol, 4-(1-methylethyl)-	151.21	208.60	C9H11O	Phenols	0.04
Phenol, 5-methyl-2-isopropyl-	150.22	238.00	C10H14O	Phenols	0.03
Furan, 2-hydroxytetrahydro-	88.11	163.60	C4H8O2	Furans	0.29
Furan, 3,4-dimethyl-2,5-dihydro	98.14	113.00	C6H10O	Furans	0.16
Furan, 2-(methoxymethyl) tetrahydro	116.16	140.05	C6H12O2	Furans	0.14
Benzofuran, 2,3-dihydro-	120.15	188.50	C8H8O	Furans	0.38
Benzofuran, 7-methyl-	132.16	190.50	C9H8O	Furans	0.16
Water	18.02	100.00	H2O	Water	35.74

PNNL (2013)

Compound	MW ($g.mol^{-1}$)	BP (°C)	Formula	Chemical Group	Mass Fraction Assumed (%)
crotonic acid	86.09	184.70	C4H6O2	Acids	5.57
1,4-benzenediol	110.11	286.00	C6H6O2	Phenols	6.97
hydroxyacetone	74.08	145.55	C3H6O2	Ketones	8.29
3-methoxy-4-hydroxybenzaldehyde	153.14	285.00	C8H8O3	Aldehydes	6.97
isoeugenol	164.20	266.00	C10H12O2	Phenols	4.98
levoglucosan	74.08	145.55	C3H6O2	Sugars	5.97
cellobiose	342.30	667.00	C12H22O11	Sugars	33.86
dimethoxy stilbene	240.30	365.70	C16H16O2	Heavy	10.95
dibenzofuran	168.19	285.00	C12H8O	Heavy	2.21
dihydroabietic acid	300.40	394.00	C20H28O2	Heavy	2.99
oligomeric compounds β-O-4 bond	-	-	-	Heavy	9.15
phenyl coumaran compounds	-	-	-	Heavy	1.99
2,4,6-trimethyl pyridine	121.18	170.00	C8H11N	Heterocyclic	0.07
dibenzothiophene	184.26	332.60	C12H8S	Heterocyclic	0.03

A2.2. Dataset 2 – Chemical Groups Mass Fractions and reported commonly found compounds (4 sources)

Source	AMUTIO et al. (2015)	AMUTIO et al. (2015) Standarized	GÓMEZ et al. (2015)	GÓMEZ et al. (2015) Standarized	RODRIGUES et al. (2018)	RODRIGUES et al. (2015) Standarized	LAZZARI et al. (2019)	LAZZARI et al. (2015) Standarized
Acids	4.84	4.84	25.50	15.73	0.18	0.18	44.00	30.76
Alcohols	1.00	1.00	9.95	6.14	0.00	0.00	0.00	0.00
Aldehydes	2.24	2.24	0.83	0.51	2.03	1.99	3.00	2.10
Aromatics/Furans	5.91	5.91	9.86	6.08	2.04	2.00	5.00	3.50
Ethers	1.35	1.35	0.12	0.07	1.48	1.45	11.00	7.69
Esters	2.92	2.92	13.76	8.49	0.14	0.14	0.00	0.00
Heterocyclics	2.92	2.92	0.00	0.00	0.38	0.37	0.00	0.00
Hydrocarbons	2.92	2.92	4.61	2.84	0.00	0.00	7.00	4.89
Ketones	10.66	10.66	17.61	10.86	4.95	4.85	3.00	2.10
Phenolics	26.25	26.25	15.28	9.43	62.35	61.04	30.00	20.97
Sugars	3.25	3.25	2.47	1.52	0.00	0.00	0.00	0.00
Water	35.74	35.74	62.09	38.31	28.60	28.00	40.05	28.00

Source	AMUTIO et al. (2015)
Acids	Acetic acid; Propanoic acid
Alcohols	Methanol; 7-methyl-4-octanol acetate
Aldehydes	Glutaraldehyde; Hydroxy benzaldehyde; Furfural
Aromatics/Furans	-
Ethers	Eucalyptol
Esters	-
Heterocyclics	-
Hydrocarbons	-
Ketones	2-hydroxy-3-methyl-cyclopentenone; 3-methyl-cyclopentenone; 1,2-butyrolactone; furanone;
Phenolics	benzenediol; hydroquinone; 4-methyl-1,2-benzenediol; 2-methoxy-phenol
Sugars	levoglucosan; beta-ribopyranose
Water	water

Source	GÓMEZ et al. (2015)
Acids	acetic acid; methyl ester 9-octadecenoic acid, 7
Alcohols	methyl alcohol
Aldehydes	furfural
Aromatics/Furans	1-hydroxy-2-propanone;2,4-dimethylfuran
Ethers	-
Esters	-
Heterocyclics	-
Hydrocarbons	-
Ketones	-
Phenolics	3,4-dimethylphenol;2,3,5-trimethylphenol
Sugars	-
Water	Water

Source	RODRIGUES et al. (2018)
Acids	Highly complex acids
Alcohols	-
Aldehydes	propenal, 3-(4-hydroxy-3-methoxyphenyl)-2-; furfural
Aromatics/Furans	1,2,4-trimethoxybenzene
Ethers	-
Esters	-
Heterocyclics	-
Hydrocarbons	-
Ketones	-
Phenolics	2,6-dimethoxy-4-(2-propenyl)-phenol; 2,6-dimethoxy-phenol

Sugars	-
Water	Water

Source	LAZZARI et al. (2019)
Acids	palmitic acid
Alcohols	-
Aldehydes	benzaldehyde, 4-hydroxy-3-methoxy-; propenal
Aromatics/Furans	benzofuran, 2,3-dihydro
Ethers	1,2-dimethoxy-4-methyl-benzene
Esters	benzoic acid, 4-hydroxy-3-methoxy-, methyl ester
Heterocyclics	imidazoline
Hydrocarbons	-
Ketones	ethanone, 1-(2-hydroxy-5-methylphenyl)-; ethanone, 1-(4-hydroxy-3-methoxyphenyl)-
Phenolics	4-methyl-phenol;phenol;2-methoxy-5-methyl-phenol
Sugars	-
Water	Water

Appendix A3 – Simulation Results

This appendix includes all results of BIO1030 simulation (units with 100 index), compared with Mero crude simulation (units with 200 index).

Figure A3.1 Model Summary Results – Equipment

Name	E-101	E-102	E-103	E-104	E-105	E-106	E-107	E-108	E-109	E-110	E-111	E-112	E-113	E-114	E-115	E-201	E-202	E-203	E-204	E-205	E-206	E-207	E-208	E-209	E-210	E-211	E-212	E-213	E-214	E-215
Property method	UNIFAC	UNIFAC	UNIFAC	UNIFAC	UNIFAC	UNIFAC	UNIFAC	UNIFAC	UNIFAC	UNIFAC	UNIFAC	UNIFAC	UNIFAC	UNIFAC	UNIFAC	UNIFAC	UNIFAC	UNIFAC	UNIFAC	UNIFAC	UNIFAC	UNIFAC	UNIFAC	UNIFAC	UNIFAC	UNIFAC	UNIFAC	UNIFAC	UNIFAC	UNIFAC
Henry's component list ID																														
Electrolyte chemistry ID																														
Use true species approach for electrolytes	YES	YES	YES	YES	YES	YES	YES	YES	YES	YES	YES	YES	YES	YES	YES	YES	YES	YES	YES	YES	YES	YES	YES	YES	YES	YES	YES	YES	YES	YES
Free-water phase properties method	STEAM-TA	STEAM-TA	STEAM-TA	STEAM-TA	STEAM-TA	STEAM-TA	STEAM-TA	STEAM-TA	STEAM-TA	STEAM-TA	STEAM-TA	STEAM-TA	STEAM-TA	STEAM-TA	STEAM-TA	STEAM-TA	STEAM-TA	STEAM-TA	STEAM-TA	STEAM-TA	STEAM-TA	STEAM-TA	STEAM-TA	STEAM-TA	STEAM-TA	STEAM-TA	STEAM-TA	STEAM-TA	STEAM-TA	STEAM-TA
Water solubility method	3	3	3	3	3	3	3	3	3	3	3	3	3	3	3	3	3	3	3	3	3	3	3	3	3	3	3	3	3	3
Specified pressure [bar]	8	8	6	12	10	10	8	6	6	4	2	13	9	5	1	8	8	6	12	10	10	8	6	6	4	2	13	9	5	1
Specified temperature [C]	50	75	125	75	100	125	150	175	200	225	250	410	420	440	450	50	75	125	75	100	125	150	175	200	225	250	410	420	440	450
Specified vapor fraction				0															0											
Specified heat duty [cal/sec]																														
EO Model components																														
Calculated pressure [bar]	8	8	6	14	10	10	8	6	6	4	2	13	9	5	1	8	8	6	14	10	10	8	6	6	4	2	13	9	5	1
Calculated temperature [C]	50	75	125	75	100	125	150	175	200	225	250	410	420	440	450	50	75	125	75	100	125	150	175	200	225	250	410	420	440	450
Calculated vapor fraction	0	0	0	0	0	0	0	0.022565569	0.038396293	0.097829822	0.301940592	0	0	0	0.001772243	0	0	0	0	0	0	0	0.006687494	0.015246982	0.050267608	0.241849643	0	0	0	0.002009013
Calculated heat duty [cal/sec]	61158664.7	49863690.4	97247202.8	-37571809.7	18790516.1	18661473.2	18665810.7	267251060	128305633	112114742	29779943.9	-617082.1	2103596.75	4324269.95	2222605.96	4136648.16	3779165.24	8213451.28	-8379610.47	4069894.79	4183384.11	4435892.09	4700998.5	4976050.72	5505937	7311244.16	883763.741	1321873.15	2691688.61	1374549.94
Temperature change [C]																														
Degrees of superheating [C]																														
Degrees of subcooling [C]																														
Pressure-drop correlation parameter																														
Net duty [cal/sec]	61158664.7	49863690.4	97247202.8	-37571809.7	18790516.1	18661473.2	18665810.7	267251060	128305633	112114742	29779943.9	-617082.1	2103596.75	4324269.95	2222605.96	4136648.16	3779165.24	8213451.28	-8379610.47	4069894.79	4183384.11	4435892.09	4700998.5	4976050.72	5505937	7311244.16	883763.741	1321873.15	2691688.61	1374549.94
First liquid / total liquid	0.757066614	0.757769324	0.76181583	0.994462444	0.997340067	1	1	1	1	1	1	1	1	1	1	1	1	1	0.994100605	0.996770047	0.999994285	1	1	1	1	1	1	1	1	1
Total feed stream CO2e flow [kg/hr]	0	0	0	0	0	0	0	0	0	0	0	0	0	0	0	0	0	0	0	0	0	0	0	0	0	0	0	0	0	0
Total product stream CO2e flow [kg/hr]	0	0	0	0	0	0	0	0	0	0	0	0	0	0	0	0	0	0	0	0	0	0	0	0	0	0	0	0	0	0
Net stream CO2e production [kg/hr]	0	0	0	0	0	0	0	0	0	0	0	0	0	0	0	0	0	0	0	0	0	0	0	0	0	0	0	0	0	0
Utility CO2e production [kg/hr]	0	0	0	0	0	0	0	0	0	0	0	0	0	0	0	0	0	0	0	0	0	0	0	0	0	0	0	0	0	0
Total CO2e production [kg/hr]	0	0	0	0	0	0	0	0	0	0	0	0	0	0	0	0	0	0	0	0	0	0	0	0	0	0	0	0	0	0
Utility usage																														
Utility cost																														
Utility ID																														

Flash3		
Name	**DS-101**	**DS-201**
Property method	**UNIFAC**	**UNIFAC**
Henry's component list ID		
Electrolyte chemistry ID		
Use true species approach for electrolytes	**YES**	**YES**
Free-water phase properties method	**STEAM-TA**	**STEAM-TA**
Water solubility method	**3**	**3**
Flash specification	**TP**	**TP**
Temperature [C]	**125**	**125**
Pressure [bar]	**4**	**4**
Specified vapor fraction		
Specified heat duty [cal/sec]		
EO Model components		
Outlet temperature [C]	125	125
Outlet pressure [bar]	3.91	4
Vapor fraction	0.002090856	0
Calculated heat duty [cal/sec]	53516751.6	1961038.38
Net duty [cal/sec]	53516751.6	1961038.38
First liquid / total liquid	0.612502775	0.639766235
Total feed stream CO2e flow [kg/hr]	0	0
Total product stream CO2e flow [kg/hr]	0	0
Net stream CO2e production [kg/hr]	0	0
Utility CO2e production [kg/hr]	0	0
Total CO2e production [kg/hr]	0	0
Utility usage		
Utility cost		
Utility ID		

Pump						
Name	**P-101**	**P-102**	**P-103**	**P-201**	**P-202**	**P-203**
Property method	UNIFAC	UNIFAC	UNIFAC	UNIFAC	UNIFAC	UNIFAC
Henry's component list ID						
Electrolyte chemistry ID						
Use true species approach for electrolytes	YES	YES	YES	YES	YES	YES
Free-water phase properties method	STEAM-TA	STEAM-TA	STEAM-TA	STEAM-TA	STEAM-TA	STEAM-TA
Water solubility method	3	3	3	3	3	3
Model Type						
Specified discharge pressure [bar]	10	14	15	10	14	15
Specified pressure increase [bar]						
Specified pressure ratio						
Specified power required [kW]						
Pump efficiencies	0.7	0.7	0.7	0.7	0.7	0.7
Driver efficiencies	0.95	0.95	0.95	0.95	0.95	0.95
Suction area [sqm]						
Hydraulic static head [m-kgf/kg]						
Number of curves						
Operating shaft speed [rpm]						
Impeller diameter [meter]						
EO Model components						
Fluid power [kW]	400.117265	454.855029	250.340332	400.172838	479.967784	285.450734
Calculated brake power [kW]	571.596093	649.792898	357.629046	571.675483	685.668263	407.786764
Electricity [kW]	601.680098	683.992524	376.451628	601.763667	721.756066	429.249225
Volumetric flow rate [l/min]	26974.1977	27047.8709	11554.1692	26977.9442	28798.067	13174.6493
Calculated discharge pressure [bar]	10	14	15	10	14	15
Calculated pressure change [bar]	8.9	10.09	13	8.9	10	13
Calculated pressure ratio						
NPSH available [m-kgf/kg]	12.0621998	0	0	12.4785567	9.94278112	0
NPSH required						
Head developed [m-kgf/kg]	112.539017	137.657506	150.539822	114.208889	136.852843	151.26744
Pump efficiency used	0.7	0.7	0.7	0.7	0.7	0.7
Net work required [kW]	601.680098	683.992524	376.451628	601.763667	721.756066	429.249225
Specific speed, operating						
Suction sp. speed, operating						
Head coefficient						
Flow coefficient						
Total feed stream CO2e flow [kg/hr]	0	0	0	0	0	0
Total product stream CO2e flow [kg/hr]	0	0	0	0	0	0
Net stream CO2e production [kg/hr]	0	0	0	0	0	0
Utility CO2e production [kg/hr]	208.724676	237.27911	130.592227	208.753666	250.379399	148.907876
Total CO2e production [kg/hr]	208.724676	237.27911	130.592227	208.753666	250.379399	148.907876
Utility usage [kW]	601.680098	683.992524	376.451628	601.763667	721.756066	429.249225
Utility cost [$/hr]	46.6302076	53.0094206	29.1750011	46.6366842	55.9360951	33.2668149
Utility ID	ENERGY	ENERGY	ENERGY	ENERGY	ENERGY	ENERGY

PetroFrac				
Name	**CDU-101**	**CDU-201**	**VDU-101**	**VDU-201**
Property method	**UNIFAC**	**UNIFAC**	**UNIFAC**	**UNIFAC**
Henry's component list ID				
Electrolyte chemistry ID				
Use true species approach for electrolytes	**YES**	**YES**	**YES**	**YES**
Free-water phase properties method	**STEAM-TA**	**STEAM-TA**	**STEAM-TA**	**STEAM-TA**
Water solubility method	**3**	**3**	**3**	**3**
Number of stage	**35**	**35**	**10**	**10**
Distillate rate [kbbl/day]	**25**	**25**	**10**	**5**
Bottoms rate [kmol/hr]				
Stage 1 / condenser pressure [bar]	**1.25**	**1.25**	**0.075**	**0.075**
Stage 2 pressure [bar]				
Bottom stage pressure [bar]	**2**	**2**	**0.125**	**0.125**
Furnace duty [cal/sec]				
Fractional overflash (Mass /Mole /StdVol)			**0.03**	**0.03**
Furnace temperature [C]	**425**	**425**		
Furnace pressure [bar]	**2**	**2**	**0.15**	**0.15**
EO Model components				
Condenser / top stage temperature [C]	40.15486	40.0001671	244.245309	185.788063
Condenser / top stage pressure [bar]	1.25	1.25	0.075	0.075
Condenser / top stage heat duty [cal/sec]	-562472933	-43341095.2	-17739839.5	-14924507.5
Condenser / top stage subcooled duty				
Condenser / top stage distillate rate [kmol/hr]	1639.80978	1582.39402	999.140639	1008.09891
Condenser / top stage reflux rate [kmol/hr]	190.106946	12036.2155	2327.97611	2017.02242
Condenser / top stage reflux ratio	0.115932316	7.60633281	2.3299784	2.00081797
Condenser / top stage free water distillate rate [kmol/hr]	2116.27721	2330.84199	0	0
Condenser / top stage free water reflux ratio	0	0	0	0
Total feed stream CO2e flow [kg/hr]	0	0	0	0
Total product stream CO2e flow [kg/hr]	0	0	0	0
Net stream CO2e production [kg/hr]	0	0	0	0
Utility CO2e production [kg/hr]	0	0	0	0
Total CO2e production [kg/hr]	0	0	0	0
Condenser utility usage [kg/hr]	135453853	10437334.8	4259276.47	3583324.61
Condenser utility cost [$/hr]	5648425.66	435236.862	56.6852757	47.6892601
Condenser utility ID	**CTWATER**	**CTWATER**	**CDWATER**	**CDWATER**
Reboiler utility usage				
Reboiler utility cost				
Reboiler utility ID				

Mixer				
Name	**GAS-MIX**	**GAS-MIX2**	**TK-101**	**TK-201**
Property method	**UNIFAC**	**UNIFAC**	**UNIFAC**	**UNIFAC**
Henry's component list ID				
Electrolyte chemistry ID				
Use true species approach for electrolytes	**YES**	**YES**	**YES**	**YES**
Free-water phase properties method	**STEAM-TA**	**STEAM-TA**	**STEAM-TA**	**STEAM-TA**
Water solubility method	**3**	**3**	**3**	**3**
Specified pressure [bar]	**0**	**0**	**1.1**	**1.1**
Temperature estimate [C]				
EO Model components				
Outlet temperature [C]	83.5212637	71.5474587	19.857981	20.0471032
Calculated outlet pressure [bar]	1.25	1.25	1.1	1.1
Vapor fraction	0.99999668	0.939331993	0	0
First liquid /Total liquid	1	1	0.737158783	1
Total feed stream CO2e flow [kg/hr]	0	0	0	0
Total product stream CO2e flow [kg/hr]	0	0	0	0
Net stream CO2e production [kg/hr]	0	0	0	0

Utilities								
Name	**CDWATER**	**CTWATER**	**ENERGY**	**FREON**	**HP-ST**	**LP-ST**	**MP-ST**	**V-MP-ST**
Utility type	**WATER**	**WATER**	**ELECTRICITY**	**REFRIGERATIO**	**STEAM**	**STEAM**	**STEAM**	**STEAM**
Specified price [$/kg]		**0.0417**		**0.185**				
Specified cooling value [cal/gm]				**-4**				
Specified inlet degrees subcooled [C]								
Specified outlet degrees subcooled [C]								
Specified inlet degrees superheated [C]								
Specified outlet degrees superheated [C]								
Specified electricity price [$/kWhr]			**0.0775**					
Specified energy price [$/kJ]	**0.000000212**	**0.000000212**		**0.00000274**	**0.0000025**	**0.0000019**	**0.0000022**	**0.0000022**
Specified inlet pressure [atm]	**1**	**1**		**1**				
Specified outlet pressure [atm]	**1**	**1**		**1**				
Specified inlet temperature [C]	**5**	**25**		**5**	**250**	**125**	**175**	**175**
Specified outlet temperature [C]	**20**	**40**		**15**	**249**	**124**	**174**	**174**
Specified inlet vapor fraction					**1**	**1**	**1**	**1**
Specified outlet vapor fraction					**0**	**0**	**0**	**0**
Specified CO2 emission factor [kg/cal]			0.000000234	0.000000234	0.000000234	0.000000234	0.000000234	0.000000234
Specified CO2 energy source efficiency factor	**1**	**1**	**0.58**	**1**	**0.85**	**0.85**	**0.85**	**0.85**
Calculated heating/cooling value [cal/gm]	-14.9939603	-14.9490215		-2.15123498	411.542431	523.521299	485.992082	485.992082
Calculated mass price [$/kg]		0.0417		0.185				
Calculated inlet enthalpy [cal/gm]	-3809.46011	-3789.48006		-1003.71601	-3145.05267	-3166.78509	-3152.79571	-3152.79571
Calculated outlet enthalpy [cal/gm]	-3794.46615	-3774.53104		-1001.56477	-3556.59511	-3690.30639	-3638.78779	-3638.78779
Calculated inlet pressure [bar]	1.01325	1.01325		1	39.1334349	2.32178779	8.92520875	8.92520875
Calculated outlet pressure [bar]	1.01325	1.01325		1	38.4966395	2.25120518	8.71680526	8.71680526
Calculated inlet temperature [C]	5	25		5	250	125	175	175
Calculated outlet temperature [C]	20	40		15	249	124	174	174
Calculated inlet vapor fraction	0	0		0	1	1	1	1
Calculated outlet vapor fraction	0	0		0	0	0	0	0
Calculated purchase price [$/cal]	8.87602E-10	0.0417	0.0775					
Calculated total cost [$/hr]	104.374536	6083662.53	264.654224	0	0	0	0	0
Calculated total usage rate [kg/hr]	7842601.07	145891188		0	0	0	0	0
Calculated total Electric usage [kW]			3414.89321					
Calculated CO2 emission factor [kg/cal]			0.000000234	0.000000234	0.000000234	0.000000234	0.000000234	0.000000234
Calculated CO2 emission rate [kg/hr]			1184.63695					

Figure A3.2 – Stream Summary

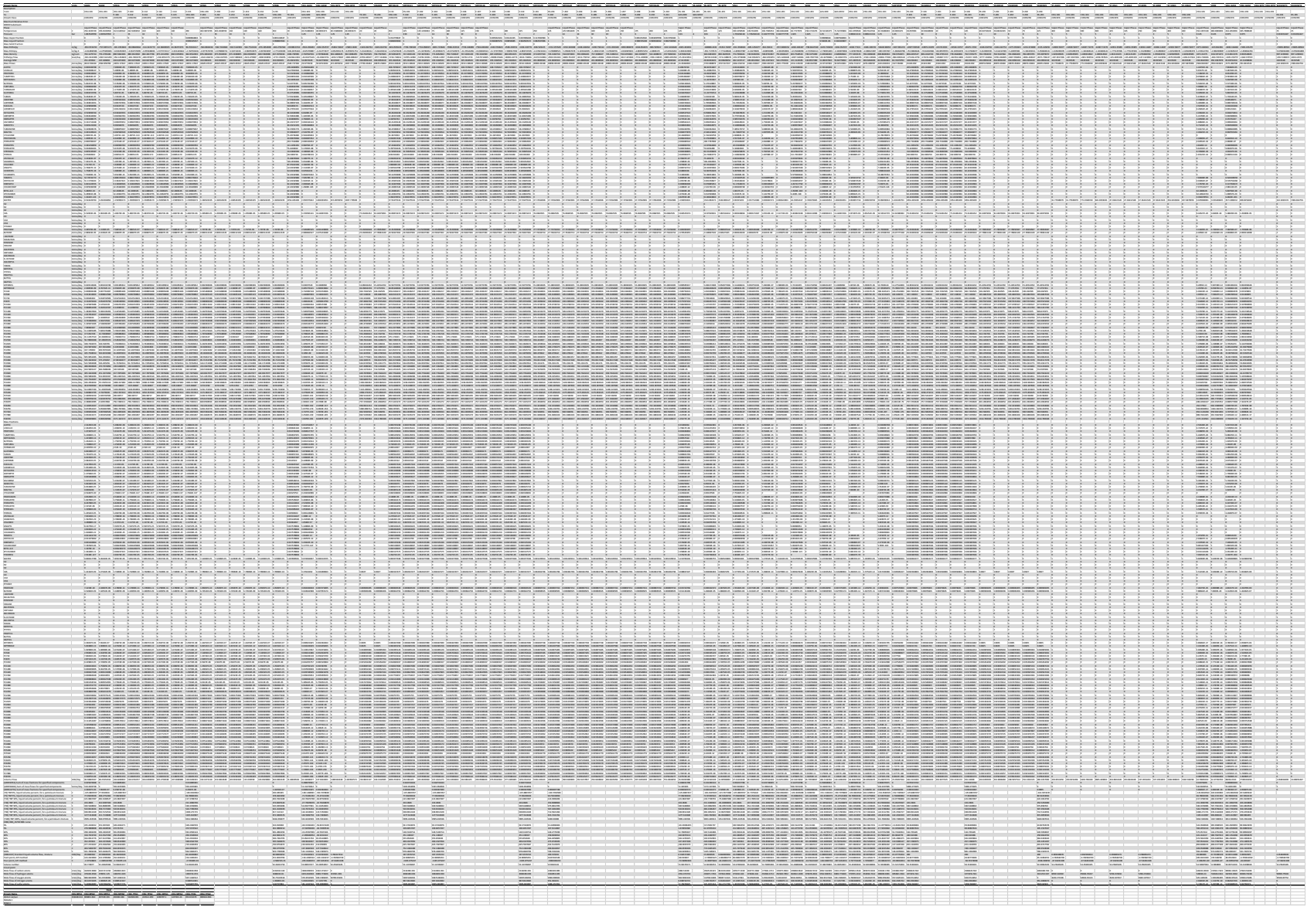

Publications

FERNANDES DS, FREGOLENTE LV, MACIEL MRW. *Simulation of eucalyptus bio-oil and Brazilian crude oils blends distillation: effects, challenges and opportunities*. 12th International Conference Distillation & Absorption, Toulouse. 2022.

Collaborative Publications

DEUBER RS, BRESSANIN JM, FERNANDES DS, GUIMARÃES HR, CHAGAS MF, BONOMI A, FREGOLENTE LV, WATANABE MDB. *Production of Sustainable Aviation Fuels from Lignocellulosic Residues in Brazil through Hydrothermal Liquefaction: Techno-Economic and Environmental Assessments*. Energies, 16(6), 2723. 2023.

DEUBER RS, FERNANDES DS, BRESSANIN JM, WATSON J, CHAGAS MF, BONOMI A, FREGOLENTE LV, WATANABE MDB. *Techno-economic assessment of HTL integration to the Brazilian sugarcane industry: An evaluation of different scenarios*. Industrial Crops and Products, 173:114139. 2021.